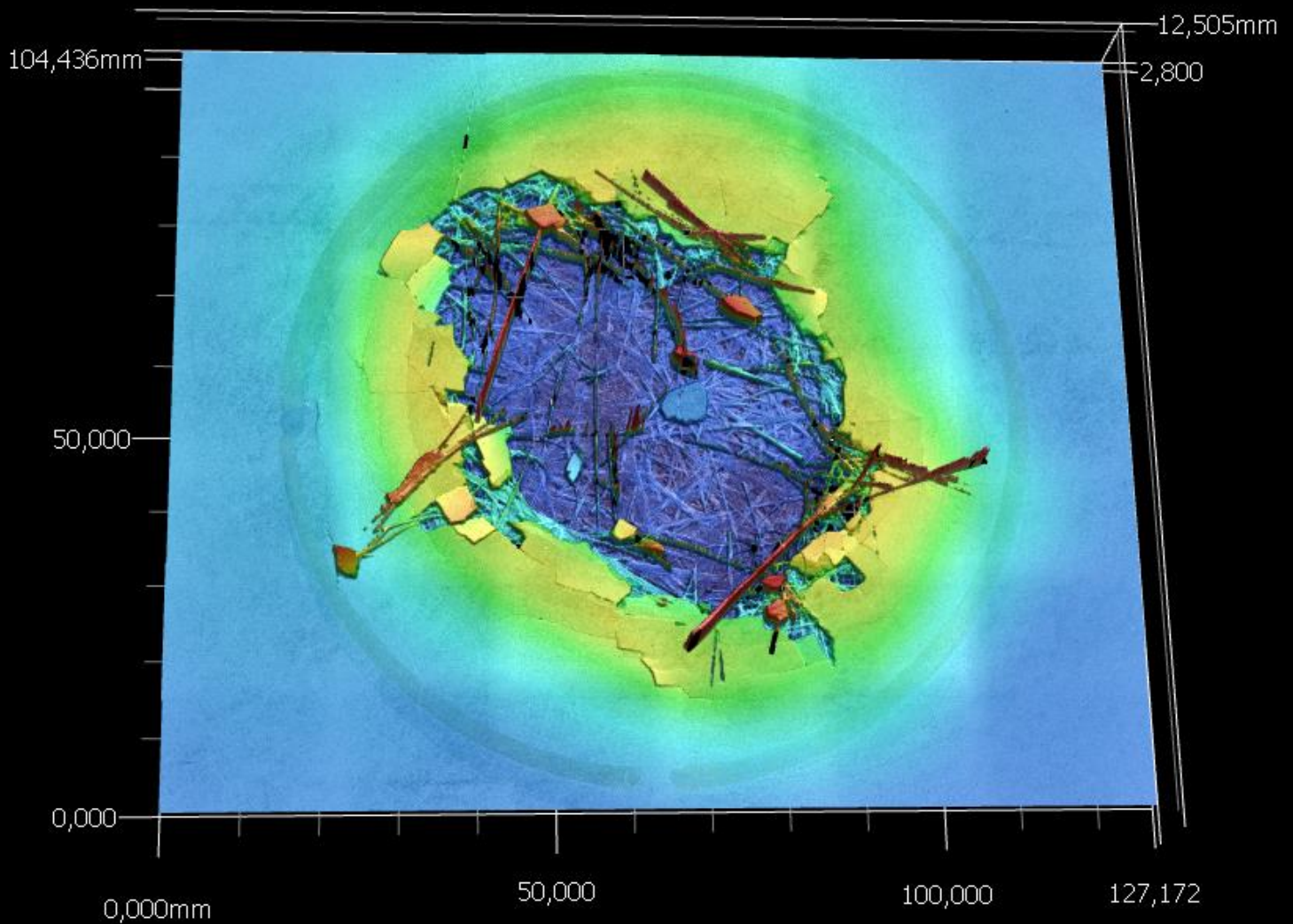


# Effects of gelcoat thickness on damage resistance of leading edge gelcoated glass fibre composite subjected to hailstone impact

Hüseyin Eryörük





# Effects of gelcoat thickness on damage resistance of leading edge gelcoated glass fibre composite subjected to hailstone impact

By

H. Eryoruk

in fulfilment of the requirements for the degree of

**Master of Science**

in Aerospace Engineering

at the Delft University of Technology,

to be defended publicly on Tuesday October 12, 2021 at 10:00 AM.



An electronic version of this thesis is available at <http://repository.tudelft.nl/>.



Delft University of Technology  
Faculty of Aerospace Engineering  
Department of Aerospace Structures and Materials

## **Graduation committee**

Date: 12-10-2021

Chair holder:

---

Dr. Ir. R. Alderliesten

Examiner:

---

Dr. R. M. Groves

Supervisor:

---

Dr. Ir. J.J.E. Teuwen

Supervisor:

---

Dr. Ir. A. Verma



## ACKNOWLEDGEMENTS

---

I began with my master thesis in March 2020, starting with a literature review that took nearly all the way till the end of the master thesis. Reading many articles for someone, who is dyslectic and doesn't like reading, can be difficult. In the phase, where I focused on the process to shoot a hailstone with a gas cannon was the best part of the project. It all took longer than I expected, but it was worth the time, effort and the results I managed to achieve.

During my master thesis, I had weekly or every two weeks meeting with my two supervisors: Dr.Ir. J.J.E. Teuwen and Dr.Ir. A. Verma. Despite that COVID-19 became a problem in the world, nothing changed except that the meetings were done online. In the meeting discussion were done, work progress was shown and help plus feedback was given. I appreciate the support, care and fast response of Dr.Ir. J.J.E. Teuwen. She did this, while she had to spend time on her own work, personal life and many other master students. I appreciate the support of Dr.Ir. A. Verma even when he was not working at the TuDelft anymore, he attended the online meetings. Therefore, I would like to say: thank you Dr.Ir. J.J.E. Teuwen and thank you Dr.Ir. A. Verma!

Other people who helped me during master thesis and who I would like to thank are the technicians in the aerospace lab: Ir. Casper van Dien, Alexander Uithol, Ing. Berthil grashof, Ir. Durga Mainali, Rob van der List, Victor Horbowiec, Fred Bosch and Ing. Dave Ruijtenbeek.

Further, I would like to express my gratitude to my friends from high school, who helped me out if I didn't know what to do at a difficult question from a course or a report that needed to be checked during my bachelor mechanical engineering and master aerospace engineering. Those are Guan-li Liu, Ahmet Güdek and Soma.

Finally, the support and love of my parents, sister and little brother gave me strength to finish VWO at high school. Without their motivation it was not possible to go to this amazing university, where I learned a lot. I am really thankful for making this possible for me: Thank you family! Furthermore, I am grateful for the life I have lived so far: Elhamdülillah.

*Huseyin Eryoruk*

*Delft, 23 of August 2021*

## ABSTRACT

---

Green energy is becoming more important over the years in order to reduce CO<sub>2</sub> emission. One way to obtain green energy is transferring wind energy to electricity with wind turbines. The operation life of wind turbines are commonly between 20 and 25 years, but this is reduced by hail erosion. The goal of the master thesis is to provide the wind turbine community useful information regarding hail impact on a gelcoated leading edge of a wind turbine blade. Performing a literature study showed that there is a gap in literature about the role of gelcoat thickness for wind turbine blades impacted with hailstones. Therefore, three thickness groups are tested on an epoxy/glass fibre composite: 0.65 mm, 0.35 mm and 0.15 mm. Simulated hail ice (SHI) is made by filling a mould with tap water and freezing it. The SHI has a diameter of 20 mm and is shot at 120 m/s for these three coating groups. From literature, it is also noticed that velocity plays a major role in damage mode, so it was included as a test parameter to understand its effect. Samples are made with a 0.15 mm thick coating to see the impact damage at 100 m/s and 90 m/s with SHI having a 20 mm diameter. The SHI is shot with a gas cannon, but before it could be shot it required adjustment, because fracturing and melting of the SHI occurred. Several concepts for ensuring proper test conditions were tested: two concept with sabots (casing around hailstone) proved difficult to realise, while a plastic tube inside the gas cannon barrel with an inner diameter close to the SHI and outer diameter close to the inner diameter of the barrel worked well.

Three different methods are used to analyse the damage on the composite: Optical microscope, C-scan and Laser confocal microscope. The first one takes images from the front and back side of the sample to quantify gelcoat damage and to see visible damage on the back side of the composite. C-scan was used to determine the delamination area in combination with an optical image of delamination from the back side. These two methods are used before impact, at the first, third and fifth impact. The laser confocal microscope is used after the fifth impact whereby the sample is cut into smaller pieces to investigate the damage mechanisms such as; fibre fracture, matrix crack, delamination location and gelcoat thickness measurement.

The coating thickness with the least amount of damage on the gelcoat from the three coating groups (0.65 mm, 0.35 mm and 0.15 mm) tested at 120 m/s is 0.15 mm. The reason for this is that thicker coated samples are observed to be more brittle than samples having a thin coating. It was thought that thickly applied coatings may cure more than thin coatings. To check this, a differential scanning calorimetry was used and it showed that that the three varying coating thicknesses have more or less the same degree of cure.

No conclusion could be drawn about the reduction or increase in damage between glass fibre layers and chopped strand mat as delamination and matrix cracking (interlaminar as well as intralaminar) for varying coating thickness (tested at 120 m/s) due to variation in the (accumulated) kinetic energy. It appears to be that damage between and in the glass fibre layers and chopped strand mat is more sensitive to kinetic energy variation than the gelcoat on top of the composite. Reduction in the velocity decreases damage on the gelcoat and changes the main governing damage mode in the composite from delamination to matrix cracking.



# CONTENT

---

<b>Acknowledgements</b>	<b>7</b>
<b>Abstract</b>	<b>8</b>
<b>Content</b>	<b>9</b>
<b>List of abbreviation</b>	<b>11</b>
<b>List of tables</b>	<b>12</b>
<b>List of figures</b>	<b>13</b>
<b>1 Introduction</b>	<b>16</b>
<b>2 Literature review</b>	<b>17</b>
<b>2.1 Wind turbine blades</b>	<b>17</b>
2.1.1 Materials	17
2.1.2 Structural design	19
2.1.3 Manufacturing	20
<b>2.2 Hail</b>	<b>21</b>
2.2.1 Hail formation	21
2.2.2 Hail fall and size	21
2.2.3 Hailstone speed	22
2.2.4 Behaviour Ice	23
2.2.5 Self-made hailstone and substitution of hailstones	23
<b>2.3 (Hail) impact on composite</b>	<b>24</b>
2.3.1 Carbon fibre composite	24
2.3.2 Glass fibre composite	26
2.3.3 Glass fibre composite with gelcoat	29
<b>2.4 Conclusion</b>	<b>31</b>
2.4.1 Goal	32
2.4.2 Research question:	32
2.4.3 Sub questions:	32
2.4.4 Hypothesis	32
Research question:	32
<b>3 Methodology</b>	<b>33</b>
<b>3.1 Test plan</b>	<b>33</b>
3.1.1 Experiment parameters	33
3.1.2 Analysis	34
<b>3.2 Gas cannon, impact chamber and velocity measurement</b>	<b>35</b>
<b>3.3 Gas cannon challenge</b>	<b>38</b>
3.3.1 Concept one	38
3.3.2 Concept two	40
3.3.3 Concept three	41
<b>3.4 Manufacturing hailstone</b>	<b>43</b>

<b>3.5</b>	<b>Procedure for shooting hailstone</b>	<b>44</b>
<b>3.6</b>	<b>Manufacturing of composite plate</b>	<b>45</b>
3.6.1	Preparation of the mould	45
3.6.2	Applying the gelcoat	46
3.6.3	Stacking and vacuum bagging	47
3.6.4	Processing of the resin	49
3.6.5	Vacuum infusion	49
3.6.6	Debagging	50
3.6.7	Cutting Samples	50
<b>3.7</b>	<b>Analysing method</b>	<b>52</b>
3.7.1	Optical Microscope and visual inspection	52
3.7.2	C-scan	55
3.7.3	Laser confocal microscope	57
3.7.4	Differential scanning calorimetry	60
<b>4</b>	<b><i>Results and discussion</i></b>	<b>61</b>
<b>4.1</b>	<b>Kinetic energy, gelcoat thickness and DSC</b>	<b>61</b>
4.1.1	Kinetic energy	61
4.1.2	Gelcoat thickness	62
4.1.3	DSC	63
<b>4.2</b>	<b>Optical microscope and visual inspection</b>	<b>64</b>
4.2.1	Before impact	64
<b>4.3</b>	<b>C-scan</b>	<b>73</b>
4.3.1	Before impact	73
4.3.2	Damage progression	73
<b>4.4</b>	<b>Laser confocal microscope</b>	<b>77</b>
<b>5</b>	<b><i>Conclusion and recommendation</i></b>	<b>80</b>
<b>5.1</b>	<b>Conclusion</b>	<b>80</b>
<b>5.2</b>	<b>Recommendation</b>	<b>82</b>
	<b><i>References</i></b>	<b>83</b>
	<b><i>Appendices</i></b>	<b>87</b>
	<b>Appendix A</b>	<b>87</b>
	<b>Appendix B</b>	<b>88</b>
	<b>Appendix c</b>	<b>90</b>
	<b>Appendix D</b>	<b>91</b>
	<b>Appendix E</b>	<b>92</b>
	<b>Appendix F</b>	<b>96</b>
	<b>Appendix G</b>	<b>97</b>
	<b>Appendix H</b>	<b>137</b>
	<b>Appendix I</b>	<b>157</b>

## LIST OF ABBREVIATION

---

<i>AGT</i>	Average gelcoat thickness
<i>CG</i>	Coating group
<i>CSM</i>	<i>Chopped strand mat</i>
<i>dB</i>	Decibel
<i>DGA</i>	Damaged gelcoat area
<i>HSC</i>	High Speed Camera
<i>IR</i>	Infrared sensor
<i>LCM</i>	Laser confocal microscope
<i>MPa</i>	Mega pascal
<i>OI</i>	Optical image
<i>RPM</i>	Rounds per minute
<i>S</i>	Sample
<i>SEM</i>	Scanning electron microscope
<i>SHI</i>	Simulated hail ice
<i>SPH</i>	Smooth particle hydrodynamics

# LIST OF TABLES

---

<b>2.1</b>	Protection material with their characteristics [2].	18
<b>2.2</b>	Damages modes in carbon fibre composite for different velocities [33].	24
<b>3.1</b>	Overview of all the samples with their experiment parameters and analysing method.	34
<b>4.1</b>	Kinetic energy per impact and the accumulated kinetic energy.	61
<b>4.2</b>	Average coating thickness with its standard deviation.	62
<b>4.3</b>	All samples divided in three damage conditions, no damage, matrix cracking and delamination	71

## LIST OF FIGURES

---

<b>2.1</b>	Monolithic composite [5].	17
<b>2.2</b>	Sandwich composite [6].	17
<b>2.3</b>	Structural design of a wind turbine blade, modified from [15].	19
<b>2.4</b>	Material layup with gelcoat of a leading edge at the tip of a wind turbine blade [4].	19
<b>2.5</b>	Material layup with flexible coating of a leading edge at the tip of a wind turbine blade [16].	20
<b>2.6</b>	Most common size of hail in the UK [5].	22
<b>2.7</b>	Size of hail for each month in Europe [23].	22
<b>2.8</b>	Terminal velocity of hailstones.	23
<b>2.9</b>	Von-mises stress in the zero layer, which points in the direction of the short axis [41].	25
<b>2.10</b>	Fibre breakage after 50 impacts of 20 mm hailstone at a velocity around 90 m/s [1].	26
<b>2.11</b>	Scattered debris after 10 impacts of 15 mm hailstone at a velocity around 100 m/s [1].	26
<b>2.12</b>	Scaring after 10 impacts of 15 mm hailstone with a velocity around 100 m/s [1].	27
<b>2.13</b>	Matrix removal after 50 impacts of a 20 mm hailstone with a velocity around 50 m/s [1].	27
<b>2.14</b>	Force-deflection curve of a composite (16 layers) impacted with 20 j of energy [45].	27
<b>2.15</b>	Absorbed energy per repeated impact for four different composite. impact energy is 20 j [45].	27
<b>2.16</b>	Picture on the left shows damage on the top surface and picture on the right shows damage on the bottom side [4].	29
<b>3.1</b>	Movable gas cannon.	35
<b>3.2</b>	Impact chamber	36
<b>3.3</b>	location where the samples are placed inside the impact chamber.	36
<b>3.4</b>	Tube with IR sensors.	37
<b>3.5</b>	National instruments Virtual bench VB-8012.	37
<b>3.6</b>	Velocity comparison between IR and HSC.	37
<b>3.7</b>	Impactor cover and impactor head.	38
<b>3.8</b>	Sabot.	38
<b>3.9</b>	Collision plate for the sabots	38
<b>3.10</b>	Collision plate holder	38
<b>3.11</b>	Structure for stopping the sabot.	39
<b>3.12</b>	Robes with springs attached to the impact chamber and gas cannon.	39
<b>3.13</b>	Two parts of the sabot side by side.	40
<b>3.14</b>	Sabot configuration inside the barrel.	40
<b>3.15</b>	Several designs of sabots for concept 2.	40
<b>3.16a</b>	Separation mechanism for concept 2.	41
<b>3.16b</b>	Gap between aluminium plates to let SHI through.	41
<b>3.17</b>	Acrylic tube inside a bigger 3D printed tube.	42
<b>3.18</b>	Small Structure to hold the acrylic tube in place.	42
<b>3.19</b>	Male mould (on the left) and female mould (on the right).	43
<b>3.20</b>	Moulds clamped with two elastics.	43
<b>3.21</b>	Polyethylene bag with SHI.	43
<b>3.22</b>	IR velocity sensor mounted to the barrel via a small structure with a hinge.	44
<b>3.23</b>	Gap leading to the acrylic tube inside the barrel, where the SHI can be loaded.	44
<b>3.24</b>	Aluminium plate undergone a sanding treatment.	45

3.25	Treated aluminium plate with tacky tape.	46
3.26	Wet gauge.	46
3.27	Measurement points on smoothed gelcoat that is between two metal strips with the triangular tool on the right side.	47
3.28	Components of the vacuum infusion process.	48
3.29	Degassing equipment.	49
3.30	Setup for resin supply.	49
3.31	Stage of composite sample after 20 minutes of resin flow.	50
3.32	Water cooled cutting machine (Carate).	51
3.33	Keyence VR-5000, optical microscope.	52
3.34	Volume measurement of sample 1 from CG 0.65 mm for 3 impacts (120 m/s).	53
3.35	Volume measurement of sample 1 from CG 0.65 mm for 5 impacts (120 m/s).	53
3.36	Height plot of sample 1 of CG 0.65 mm after 5 impacts	54
3.37	Optical image from the cross-section of sample 1 of CG 0.65 mm after 5 impacts.	54
3.38	C-scan machine.	55
3.39	C-scan from sample 1 of cg 0.65 after 3 impacts at 120 m/s.	56
3.40	Optical image of the back side from sample 1 of CG 0.65 after 3 impacts at 120 m/s.	56
3.41	Keyence VK-X1000, laser confocal microscope.	57
3.42	Cross-section of sample 5 from CG 0.15 mm including all 6 layers.	57
3.43	Cutting area for coating thickness determination and cross-section analysis.	58
3.44	Samples placed in the mould.	59
3.45	Samples embedded in resin.	59
3.46	Schematic sketch of a gelcoat (black) and the location where line measurement is done (in red).	60
3.47	TA instruments DSC 250.	60
3.48	Heat flow curve of sample 2 from CG 0.15 mm with marked area indicating the area that is going to be measured, which is called reaction enthalpy.	60
4.1	Bar chart of (possible) gelcoat thicknesses for each CG.	63
4.2	Heat flow curve per temperature for sample 2 of CG 0.65 mm, 0.35 mm and 0.15 mm.	63
4.3	Average reaction enthalpy (J/g) for CG 0.65 mm, 0.35 mm and 0.15 mm.	63
4.4	Front side of sample 3 from CG 0.15mm.	64
4.5	Back side of sample 3 from CG 0.15 mm.	64
4.6	Sample 2 of CG 0.35 mm with small scratches	65
4.7	Height plot of sample 2 of CG 0.35 mm.	65
4.8	Sample 3 of CG 0.35 mm containing dry spots	65
4.9	Sample 4 of CG 0.35 mm containing dry spots	65
4.10	Roughness image from sample 8 of CG 0.15 mm after 5 impacts.	66
4.11	OI from sample 1 of CG 0.15 mm after 5 impacts	66
4.12	OI from sample 1 of CG 0.45 mm after 5 impacts.	66
4.13	OI from sample 1 of CG 0.65 mm after 5 impacts.	67
4.14	3D plot from sample 1 of CG 0.65 mm after 5 impacts.	67
4.15	Effective von-Mises stress (Pa) in gelcoat from a 20 mm SHI shot at 100 m/s, modified from [4].	67
4.16	Effective plastic strain in gelcoat from a 20 mm SHI sot at 100 m/s, The black marking show the areas that has been eroded, modified from [4].	67
4.17	Average damaged gelcoat area for the three coating groups impacted at 120 m/s.	68
4.18	Damaged gelcoat area for individual samples of CG 0.15 mm impacted at 120 m/s.	68
4.19	Damaged gelcoat area for individual samples of CG 0.35 mm impacted at 120 m/s.	69
4.20	Damaged gelcoat area for individual samples of CG 0.65 mm impacted at 120 m/s.	69
4.21	Accumulated kinetic energy effect on damaged gelcoat area for the samples tested at a velocity of 120 m/s, without sample 3 from CG 0.65 mm due to missing data. Green	70

	dots are a sample from CG 0.15 mm, orange dots from CG 0.35 mm and blue dots are from CG 0.65 mm.	
<b>4.22</b>	Bart chart of the damaged gelcoat area and all the samples tested with a velocity of 120 m/s.	71
<b>4.23</b>	Minor matrix cracking in sample 5 of CG 0.15 mm after one impact.	71
<b>4.24</b>	Major matrix cracking in sample 5 of CG 0.15 mm after five impacts.	71
<b>4.25</b>	Delamination after 5 impacts on sample 2 of CG 0.15 mm.	72
<b>4.26</b>	Schematic picture of 'peanut' shaped delamination, based on [56].	72
<b>4.27</b>	C-scan from sample 1 of CG 0.65 mm before impact.	73
<b>4.28</b>	C-scan from sample 1 of CG 0.35 mm before impact.	73
<b>4.29</b>	Average delamination area (mm <sup>2</sup> ) for the three coating groups per impact session.	74
<b>4.30</b>	Delamination area (mm <sup>2</sup> ) for samples from CG 0.65 mm per impact session.	75
<b>4.31</b>	Delamination area (mm <sup>2</sup> ) for samples from CG 0.35 mm per impact session.	75
<b>4.32</b>	Delamination area (mm <sup>2</sup> ) for samples from CG 0.15 mm per impact session.	75
<b>4.33</b>	Delamination area (mm <sup>2</sup> ) plotted against the accumulated kinetic energy for samples tested at 120 m/s, without sample 3 from CG 0.65 mm due to missing data. Green dots are a sample from CG 0.15 mm, orange dots from CG 0.35 mm and blue dots are from CG 0.65 mm.	76
<b>4.34</b>	Overview of the 9 samples tested at 120 m/s and their delamination area (mm <sup>2</sup> ).	76
<b>4.35</b>	Cross-section of sample 1 from CG 0.65 mm after 5 impacts at a velocity of 120 m/s.	77
<b>4.36</b>	Cross-section of sample 6 from CG 0.35 mm after 5 impacts at a velocity of 100 m/s.	78
<b>4.37</b>	Cross-section of sample 9 from CG 0.15 mm after 5 impacts at a velocity of 90 m/s.	79

# 1 INTRODUCTION

---

The wind industry underwent rapid growth over the past three decades. Over the years, not only the number of wind turbines increased, but also the (rotor) size of the wind turbine increased. The increase in size is mainly due to higher efficiency and cost-effective considerations that can be achieved with larger wind turbines. However, this brings an important issue for the wind industry; as the wing tips are moving at a higher speed now (about 100 m/s [1]), the leading edge of the blades at these locations are more susceptible to erosion [2]. Erosion caused by rain and/or hail can damage the leading edges of the blades affecting their drag and lift. Depending on the extent of damage caused by erosion, there could be a loss of the annual energy production of wind turbines. According to research by Sareen A. et al. [3], an airfoil (DU 96-W-180) with erosion can result in a loss of energy production by 2 % reaching up to 25 %. Therefore, the reduction of erosion can be seen as an engineering challenge. Among the sources that cause leading edge erosion, hailstones are known to be the most aggressive [4].

Thus, the leading edge erosion issue faced by the wind turbine industry should be taken seriously. Research has to be done in the field of (leading edge) erosion to find ways to reduce the amount of maintenance, cost and repair on wind turbine blades. Therefore, it is important to analyse the top layer of the leading edge. The top layer is usually a protection material to resist surface erosion on the leading edge. For instance, a gelcoat or flexible coating. The focus of the research will be laid on hail erosion, because it is a severe case of precipitation, which makes it interesting to explore.

The aim of the master thesis is to understand the effect of gelcoat thickness with regard the hail erosion and recommend from the gelcoat thicknesses that will be tested, the one that performs the best, which could be possibly used by the wind turbine community.

First, a literature review is performed to know the state-of-the-art of hail erosion on coated glass fibre structures. A literature gap has been found, by which a research question and sub questions are defined. This information can be found in Chapter 2. The next Chapter includes a test plan and methodology to show how it is going to be tested and what is used to give an answer to the research question. Chapter 4, contains the results obtained from the experiment test and a discussion on whether the results answers the research question and sub questions. Important findings will be concluded in chapter 5. Finally, a recommendation for future work will be done in chapter 6.



## 2 LITERATURE REVIEW

In this chapter, the literature review is presented. First information is gathered about wind turbine blades in section 2.1. After that, information is searched about hailstones and summarized in section 2.2. Lastly, articles are searched about wind turbine blades combined with hailstones in section 2.3.

### 2.1 WIND TURBINE BLADES

In this section, information about the materials, structural design and manufacturing of a wind turbine blade are described.

#### 2.1.1 Materials

Five groups of materials are involved in wind turbine blades: Fibres, resin matrix, adhesive, core materials and protection material. The fibres are made out of glass, carbon or an alternation of those two (also called a hybrid material). In the wind turbine industry, glass fibre composites are the most used composite type. It is cheaper than carbon fibre, but less strong and less stiff. The resin matrix is usually a thermoset polymer for instance epoxy, vinyl-ester and polyester [5]. Most composites have a (resin) matrix and (fibre) reinforcement phase. A material is a composite when it has two or more constituents, which are not soluble in each other [5]. The reinforcement provides (tensile) strength and stiffness, while the matrix protects and transfers the load from the fibres. An example of a composite is shown in Figure 2.1, It is called a monolithic composite and it consists of stacks of lamina made out of a resin matrix reinforced with fibres. The fibres in the lamina can be made out of non-crimp fabric material or uni-directional, therefore the properties of the composite can be tailored by changing the orientation of the fibres.

An adhesive is used to connect the different sections of a wind turbine blade. Epoxy or polyester can be used as an adhesive.

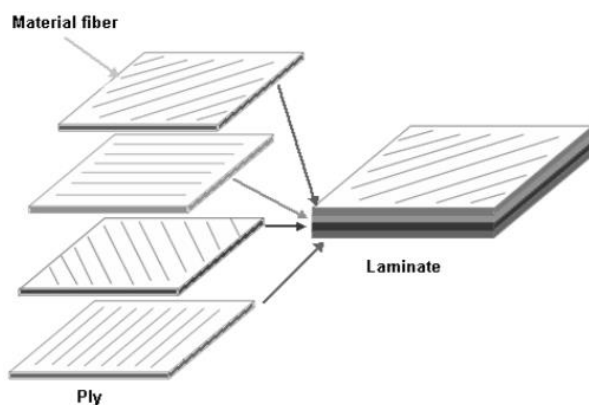


Figure 2.1: Monolithic composite [5].

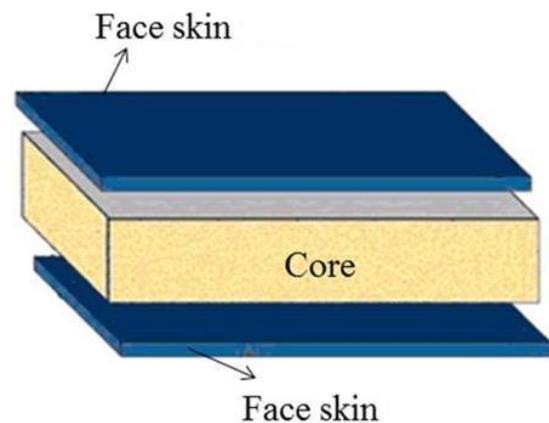


Figure 2.2: Sandwich composite [6].

Core materials are used in sandwich structures, which is a composite type. It consists of face skins (laminate) wrapped around a core material see Figure 2.2. Polymeric foams (PVC or BMI) or balsa wood is used as a core material [7][8][9]. The sandwich composite is made by a vacuum infusion process by which a dry fabric (face skin) is put on the top and bottom of the core material. A resin will flow through the dry fabric and it will flow over the core material. There will be a bond between the face skin and the core material after the resin is cured.

There are several types of protection mechanisms used to protect wind turbine blades against environmental conditions. Five different types will be discussed briefly: Gelcoats, flexible coatings, leading edge tapes, erosion shields and integrated erosion shields. These are also shown in Table 2.1 with their characteristics.

Gelcoats are often applied in-mould, while flexible coatings are applied post-mould with a roller or spray gun in layers. Leading edge tapes are also applied post-mould, a good adhesion of the tape to the substrate is important otherwise it could lead to debonding of the tape. Furthermore, using leading edge tape could lead to an increase in drag of the wind turbine blade by 5 % up to 15 % [10]. Erosion shields can both applied post-mould as well as in-mould and they are either semi-flexible or rigid covers. These covers can be made of metal or polymeric material and the attachment of the cover is done with an adhesive. They provide very good/excellent resistance against erosion. However, since the material of the wind turbine blade and the erosion shield are different, it gives debonding risks due to difference in stiffness [2].

Protection Solution	Application	Susceptible to defects	Susceptible to poor adhesion	Aerodynamic issues	Debonding risk due to stiffness mismatch	Type average erosion resistance
Gelcoats	In-mould	Yes	No	No	No	Poor
Flexible Coatings	Post-mould	Yes	Yes	No	Yes	Medium
Leading Edge Tapes	Post-mould	No	Yes	Slightly	Yes	Good
Erosion Shields	Post-mould	No	Potentially	Potentially	Yes	Very good
Integrated Erosion Shields	In-mould	No	No	No	Yes	Excellent

Table 2.1: Protection material with their characteristics [2].

The two most commonly employed types of protection material in the blade industry are gelcoat and flexible coating [4]. Therefore, the research will be focused more on these two protection materials. Meaning that articles will be searched where gelcoats and/or flexible coatings are used.

Gelcoats are usually made from epoxy or polyester and they are brittle. While flexible coatings are made from polyurethane and they are ductile. But which one is better? In some cases, flexible coatings provide outstanding wear resistance, because of the absorption of hard particles. However, it may be degraded faster by UV light than gelcoats. To determine which one is better will depend on considerations about environmental challenges and material performance [11].

According to Saltz W.T. the gelcoat is usually applied between 0.25 mm and 0.5 mm [12]. These values are close to the coating thickness range from the DNVGL standard (0.3 mm and 0.6 mm) [13]. In the case a gelcoat is applied too thin, it might undercure, while for the case for a too thick applied gelcoat, it could crack easily when applying a force. The flexible coatings are applied in lower quantities than gelcoats. A thinner layer will prove better chemical and mechanical resistance. Flexible coatings should be less than 0.2 mm thick according to Kjærside Storm, B. [11].

Yuhazri M.Y. et al (2015) states that ‘Many current researchers like Gombos, Z. and Summerscales, J. (2014), Landowski m. et al (2014), Salit M.S. (2014) and Raghavendra N. et al (2013) are more to use different gel-coating process or preparation method to fabricate low defect gelcoat in the mould. The main focus is on the performance of gelcoat on their outlined product especially particularly with respect to service period against an harsh environment. The best author’s knowledge stated that there is still no experimental research done about the effect of gelcoat thickness on laminate structure and strength. Thus, this is a very exceptionally topic to be explored in detail to gain deep understanding on roles of different gelcoat thickness affect laminated structure and strength’ [14].

### 2.1.2 Structural design

There are several types of wind turbine blades with different cross-sections depending on the manufacturer. A schematic sketch of a typical structural design can be seen in Figure 2.3. The structure has a shell-like structure, because most of the internal body is hollow. The forefront of the blade is called the leading edge while the rear edge of the blade is called the trailing edge. The blade consists of three main parts: a beam (spar), an aerodynamic shell with surface protection on the suction side and the same shell also on the pressure side. These three parts are separately manufactured and they are at a later stage adhesively joined. The aerodynamic shell on both the suction and pressure side consisted of sandwich structures towards the leading and trailing edge.

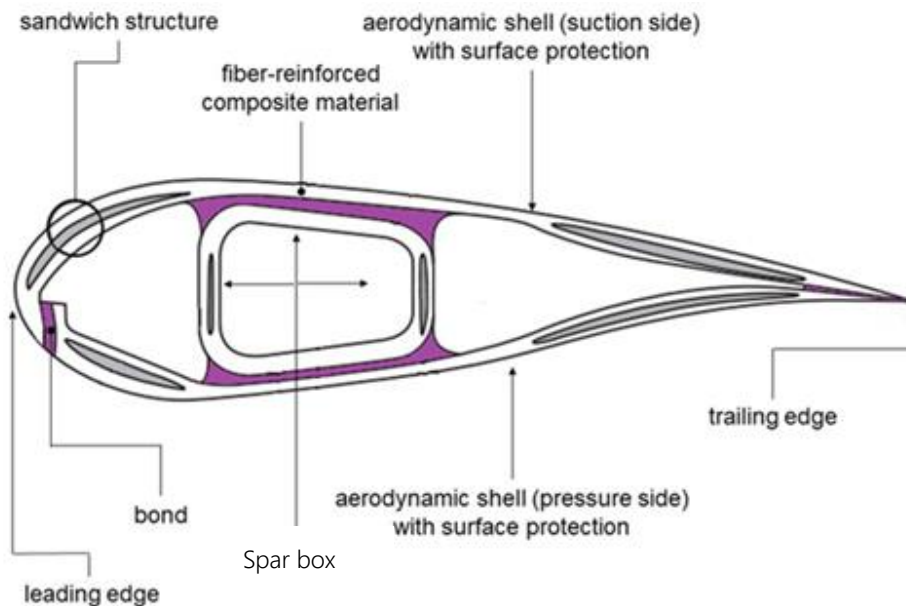


Figure 2.3: Structural design of a wind turbine blade, modified from [15].

The purpose of sandwich structures is to increase buckling resistance. In between, there is a monolithic (single skin) composite. The spar box is the main flap-wise load carrying structure and it transfers blade wise bending load. It has two shear webs consisting of a sandwich structure and two flanges (also known as spar cap) consisting of a monolithic (single skin) composite. The upper spar cap (see Figure 3 where the arrow of the beam is pointing at) will carry compression load, whereas the lower spar cap will mainly carry tension load. The shear webs are designed to cope up with flap-wise shear forces. In some cases, the spar only has one shear web and in other cases, the spar has thin spar caps. In the last case, the exoskeleton (aerodynamic shell) will carry the load with the thick monolithic composite [7][8].

The previous figure did not show a detailed cross sectional layout of the leading edge at the tip of a wind turbine blade. In Figure 2.4 is a detailed and typical cross-sectional layout of a leading edge tip [4]. It shows three layers of biaxial woven glass fibre reinforced polymer (GFRP) each having a thickness of 0.4 mm, a chopped strand mat (CSM) and a gelcoat. The gelcoat is basically a protective resin coating, according to DNVGL standard it should have a thickness between 0.3 mm and 0.6 mm [13]. The CSM is a composite where the short fibres are oriented in every direction, this makes the

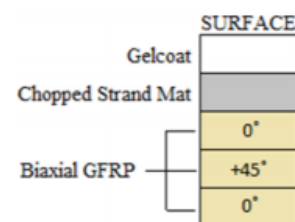


Figure 2.4: Material layout with gelcoat of a leading edge at the tip of a wind turbine blade [4].

material behave nearly as an isotropic material. Furthermore, The CSM (with a thickness around 0.4 mm) provides a smooth and absorbent surface for the gelcoat.

Another detailed cross-section of a leading edge is shown in Figure 2.5. This contains also three layers of glass fabric, but here the fabrics have a different layup sequence. The coating is also different, which is a flexible coating applied in three layers. The putty layer and primer layer replace the chopped strand mat and does have the same function [16]. The composite could also be made without the primer layer, but it provides better adhesion of the coating to the laminate than using only a putty layer [17].

Coating layer 1
Coating layer 2
Coating layer 3
Primer layer
Putty (Filler) layer
GFRP Layer 1 [+45]
GFRP Layer 2 [-45]
GFRP Layer 3 [0]

Figure 2.5: Material layup with flexible coating of a leading edge at the tip of a wind turbine blade [16].

### 2.1.3 Manufacturing

The most common manufacturing technique to make blades is vacuum infusion process (VIP). VIP requires one male or female mould, which will be covered with a thin layer of release agent/wax to remove the product (wind turbine blade) easily after the process is finished. The outer layer of the wind turbine blade is the gelcoat/flexible coating and this will be applied on the mould after the release agent/wax. Flexible coatings are most of the time applied after the product is manufactured.

Applying a gelcoat/flexible coating can be done with a spray gun, brush or a roller [18]. According to BUFA Gelcoat plus Corporation [19] using a brush is easier than a roller and it has the advantage of releasing air very good. But, for large parts, a roller or spray gun is preferred, because they can cover a wide area with coating in a short time [14][20]. According to Saltz W.T., a spray gun is the most suitable method to apply a gelcoat/flexible coating.

On the coating, dry fibre reinforcements are placed, while the coating is in a tacky stage (partly cured). After this step, vacuum bagging of the reinforcement is done to cover all the fibres with resin. Next, the bagging process is explained in steps where the number indicates to order of handling:

1. bagging edge dams are placed next to the part to prevent edge bleeding of resin.
2. peel ply is used to prevent from sticking.
3. The perforated release film is placed, which allows excess resin and entrapped air to escape.
4. The bleeder which is on the top of the perforated release film absorbs all the excessive resin.
5. Release film only allows gas the escape and prevents resin from flowing in the breather.
6. Breather transports all the entrapped air away to the vacuum pump.
7. Sealant tape is placed on the mould where eventually the vacuum bag is stuck to seal the hole composite.
8. On the vacuum bag is a connection point for a tube that is connected to a vacuum pump.

The vacuum bag in this process will be the other half of the mould. When all the fibres are covered with resin it needs to cure. When the resin is cured the process is finished and debagging can be started [17].

## 2.2 HAIL

Particles with a mixture of ice/water/air and a size greater than 5 mm are called hail, if it is smaller than 5 mm it will be called graupel [21]. These two particles are usually opaque and have a spherical or conical shape. The shape can change depending on the diameter, for example, hailstones between 10-50 mm take an ellipsoidal shape.

### 2.2.1 Hail formation

Hailstones in nature are not monolithic ice balls instead, they consist of a spherically layered structure. This structure has a higher toughness than a monolithic ice ball. Monolithic ice balls are made when freezing water in one filling session. The formation of spherically layered ice balls will be explained below. There are different ways to form hailstones in convective storms. One way is when a raindrop freezes during an updraft of a convective storm. The frozen raindrop switches a couple of times from an updraft to a downdraft and the other way around. In a downdraft, the temperature will be slightly above 0° Celsius where it collects supercooled droplets. In an updraft the temperature is lower than 0° Celsius, here the collected droplets are frozen. Most of the mass growth is taking place between -10° and -20° degrees Celsius. The exchange in updraft and downdraft results in a layered spherical structure. Another way of forming hailstone is by the same process as described by the raindrop, but then having an ice crystal instead of a raindrop. The growth of the frozen raindrop or ice crystal can be either 'dry' or 'wet'. This will depend on the speed of heat diffusion to the atmosphere. 'Dry' growth will result in more air bubbles entrapped in the frozen raindrop and ice crystal, whereas for 'wet' growth this will be less. Therefore, hailstones don't have a specific density [21][22].

Researchers performed experiments to determine the density of graupel and hail. The results are put in a table by Field et al [21]. The density range for graupel is between 50 and 700 kg/m<sup>3</sup>, whereas for hail the range is smaller, which is between 810 and 915 kg/m<sup>3</sup>. For simulations involving hail impact, a worst case density of 917 kg/m<sup>3</sup> can be used.

### 2.2.2 Hail fall and size

Macdonald Hamish [5] studied meteorological data that has been collected from the United Kingdom (UK) by a Met Office Integrated Data Archive System (MIDAS). The data from stations are analysed and plotted in Figure 2.6, it shows the most common size of hailstones during precipitation in the UK over a period from 1949 till 2013. Graupel, which is referred to in the figure as ice pellets (have a diameter smaller than 5 mm) is observed the most and hailstone between 5 mm and 9 mm comes next.

The European Severe Storm Laboratory collected reports about hail events in Europe, but only severe hail events. Meaning that the hail from those events will have a size larger than 20 mm. Moreover, 60.79 % of the reports contain the size of the hail; in other reports, it is mentioned that the size could not be determined. In Figure 2.7, a bar chart of the number of hail events is plotted against in which month it occurs. What can be noticed is that most reported hail events are during summer. What else can be noticed is that from the three hail size categories, the smallest hail size (20 to 34 mm) is the most frequent one [23][24].

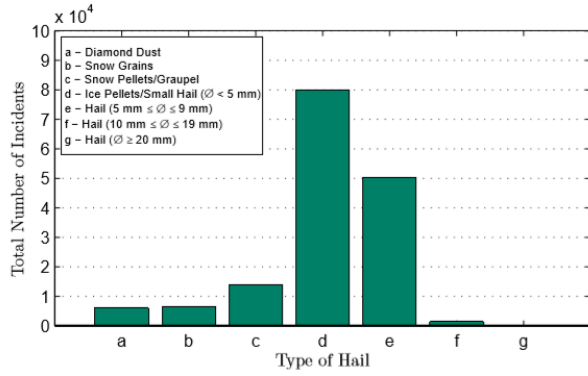


Figure 2.6: Most common size of hail in the UK [5].

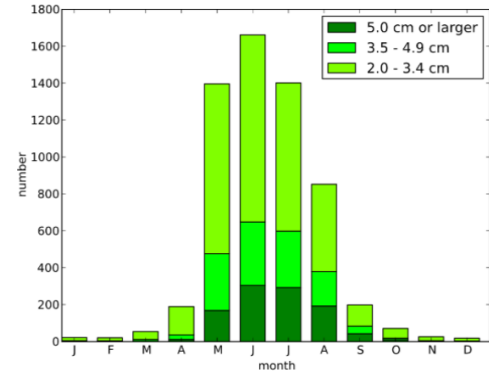


Figure 2.7: Size of hail for each month in Europe [23].

Another country where hailstones are collected is in China at four regions: Guizhou, Heibei, Xuar and Imar. The size of the collected hailstones between 5 and 10 mm are most common [49].

The insurance institute of business and home safety collected hailstones in the period between 2012 till 2017. The hailstones are collected in a couple of states in the U.S.A.: Texas, Oklahoma, Kansas, Nebraska, South Dakota and Minnesota. The diameter of the hailstones are measured with a calliper and it showed that the most common hailstone has a diameter of 15 mm. A diameter of 10 mm and 20 mm for a hailstone is also common, which showed about the same frequency [26].

### 2.2.3 Hailstone speed

When hailstones fall from the sky they reach a maximum speed also called the terminal velocity. This velocity depends on the weight of hailstone ( $w$ ), the drag coefficient ( $c_d$ ), cross-sectional area ( $a$ ) and density of the air ( $\rho_a$ ), which can be calculated with the formula (1) used by Gunn R. and Kinzer G.D [27], and Keegan M.H. et al [28]:

$$v_t = \sqrt{\frac{2w}{c_d \rho_a a}} \quad (1)$$

The density of the air is a function of altitude since the density of air is lower at higher altitudes. The drag coefficient depends not only on the shape of the object, but also on surface roughness and the Reynolds number. For the drag coefficient of hailstones, a value of 0.6 is widely used [29]. However, the shape of hailstones changes for different sizes. A. Heymsfield et al (2014) developed a correlation between the hailstone size and terminal velocity. They did this by collecting the physical properties related to the drag coefficient from 2295 natural hailstones in the US and using a relationship for deriving the terminal velocity from A. Heymsfield and R. Wright (2014). A simplified form to calculate the terminal velocity is shown next (2)(3):

$$v_t = 12.65 D_{max}^{0.65} \quad \text{For } D_{max} < 2.05 \text{ cm} \quad (2)$$

$$v_t = 15.69 D_{max}^{0.35} \quad \text{For } D_{max} > 2.05 \text{ cm} \quad (3)$$

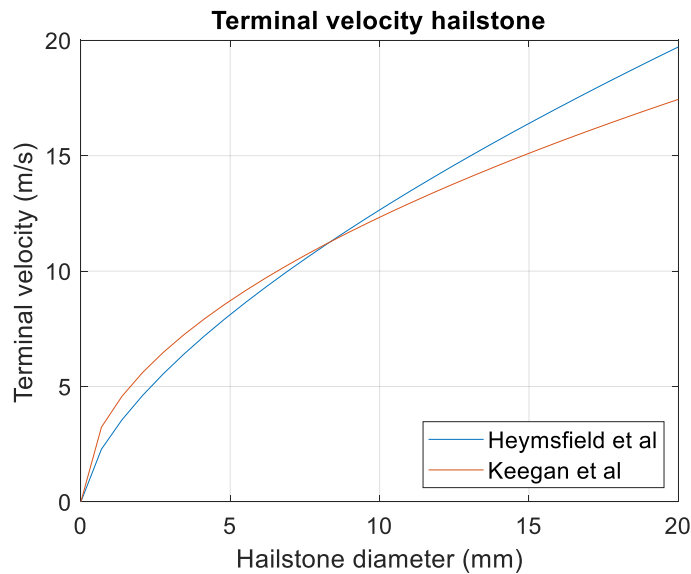


Figure 2.8: Terminal velocity of hailstones.

The  $D_{max}$  stands for the maximum diameter of the hailstone. These formulas are valid at a pressure level of 1 bar. The first formula does change for hailstones larger than 2.05 cm into the second formula due to shape changes of the hailstone [30]. A plot of the first and second formula can be seen in Figure 2.8, where the parameters for the first formula are chosen from article the of Keegan M.H. et al [28]. These graphs are meant to give you an idea of what terminal velocity a hailstone could have. A hailstone with a diameter of 10 mm and 20 mm does have terminal velocity of ~12 m/s and ~18 m/s, respectively.

#### 2.2.4 Behaviour Ice

Schulson, E.M. (1990) performed compression tests with cylindrical ice to know more about the behaviour of ice. In this test, he observed for ice specimens kept at -10 degrees Celsius that the lower the strain rate is, the higher the compression strength is. Ice also behaves differently for a lower strain rate, it behaves more ductile rather than brittle. In another test, he measured the compression test for ice with different temperatures. It turns out that the lower the temperature is, the higher the compression strength is [31]. Further, in the event of an impact pressure waves are formed at a SHI, it starts from the point of contact and travels to the back of the hailstone. This results in micro-cracks, which shatters the hailstone to smaller ice particles [32].

#### 2.2.5 Self-made hailstone and substitution of hailstones

Making a hailstone such that it nearly represents a hailstone created by nature can be done in several ways. As mentioned before hailstones consist of a spherically layered structure. Making this layered structure can be quite difficult and time consuming. Therefore, it is easier to make a monolithic hailstone or a flat-wise layered hailstone. However, a spherically layered structure is significantly tougher than a monolithic hailstone [33]. In the standard test method for hail impact resistance of aerospace transparent enclosures (ASTM F320-05), cotton fibre is added to a hailstone to make it tougher [34].

Metal spheres do not represent a hailstone well according to the EASE [21]. Also, ceramic beads with the same diameter and impact energy result in more damage [4].

## 2.3 (HAIL) IMPACT ON COMPOSITE

This section contains information about experimental tests and simulations that have been carried out to see what kind of damage a composite plate has after being (repeatedly) shot with an object, mainly a simulated hail ice (SHI). It consists out of three subsections: experimental tests on carbon fibre composite, glass fibre composite and glass fibre composite with gelcoat.

### 2.3.1 Carbon fibre composite

Tang, Z. et al. used LS-DYNA combined with smooth particle hydrodynamics (SPH) to simulate hail impact (SHI diameter of 42.7 mm) on carbon fibre composite. Different parameters are investigated to see what kind of effect that had on the failure mode and energy absorbing capacity, those are the initial angle of impact, impact velocity, different layup and different composite material. Different velocities of 100, 120, 140 and 160 m/s are tested on the same angle of impact (90°). The higher the velocity is, the more delamination there is and also a higher peak force. At velocities around 140 m/s and higher, failure of carbon bundles is observed. In a simulation of Fiore G. et al. [35] delamination is observed at a lower velocity (83.28 m/s) with a SHI diameter of 50.8 mm.

Variation in an angle of impact is tested at a velocity of 120 m/s. The lower the angle is, the lower the amount of delamination and peak force is observed, because less energy is absorbed by the composite panel. The influence of layup is tested with a velocity of 120 m/s and an impact angle of 90°. Four different layups are tested:  $[0^\circ/45^\circ]_{4S}$ ,  $[0^\circ/90^\circ]_{4S}$ ,  $[-45^\circ/45^\circ]_{4S}$  and  $[0^\circ/45^\circ/-45^\circ/90^\circ]_{2S}$ . The simulation shows that  $[0^\circ/45^\circ]_{4S}$  layup has the least amount of delamination. It is capable of absorbing more energy compared to the other composites layups [36].

The results found for a varying velocity in this research are not the same as in the research of Kim H. and Kedward K.T. [33], who investigated the failure modes in carbon fibre composite that could occur by conducting experiments (by using a nitrogen gas cannon). Moreover, when impacting a SHI with varying velocities, different types of damage occur. But in order to start the initiation of damage, a certain amount of kinetic energy is needed to create damage in a composite panel. This is called failure threshold energy and it depends on the panel thickness and SHI diameter. After this threshold, different damage modes occur depending on the velocity see Table 2.2.

Low velocity <span style="float: right;">→ High velocity</span>				
1 Delamination	2 Backside fibre failure with minor delamination	3 through-thickness cracks in recurring diamond shape pattern	4 extensive through-thickness cracks	5 clean hole

Table 2.2: Damages modes in carbon fibre composite for different velocities [33].

These same damage types are used by Appleby-Thomas G. J. et al during their research about multiple ice impacts on two commercially important carbon fibre reinforced polymers. The impacting object is a hemispherically-fronted ice with a diameter of 22 mm (kept at -20° Celsius before shooting), shot at a velocity between 81 m/s and 268 m/s. It is shot with a single-stage gas gun using air as a driving gas. The damage is analysed with visual inspection and ultrasonic inspection, whereby a C-scan showed the area of delamination in the composite [37]. Mahinfalah M. and Skordahl R.A. performed a similar impact test, but with lower velocities. The diameter of the SHI are 25.4 mm and 38.1 mm, tested with a velocity of 43 m/s and 45.9 m/s, respectively. Internal and external damage is assessed by ultrasonic inspection and there is no form of damage found in the composite [38].



In contrast to the damage modes at varying velocities used by the previous authors in this subsection, Azouaoui, K. [39] and Choi H. Y. and Chang F. K. [40] states that the initial damage mode after an impact is matrix cracking, which can lead to interface delamination. The matrix cracks are small and cannot be seen with the naked eye just like delamination and back side fibre failure. However, since the velocity for the damage modes is not specified by Kim H. and Kedward K.T and Appleby-Thomas G. J. et al it is difficult to argue, whether delamination starts first or matrix cracking, because it depends on the velocity (and laminate thickness).

Another simulation with low velocity impacts on carbon fibre reinforced polymer (CFRP) is done by Guo Z. et al with the numerical simulation software Abaqus in combination with the subroutine VUMAT, which is used to model the low-velocity impact damage. The impacted object, a punch, is modelled with three-dimensional solid element (C3D8R), a mass of 0.42 kg and a velocity of 7 m/s. The composite panel itself is 100 mm long and 100 mm wide with a layup of  $[0^\circ/90^\circ/0/90^\circ/0^\circ]_s$ . The Von-Mises stresses are analysed for In the composite panel and the first layer ( $0^\circ$ ) showed stresses in a 'peanut' shape see Figure 2.9 [41].

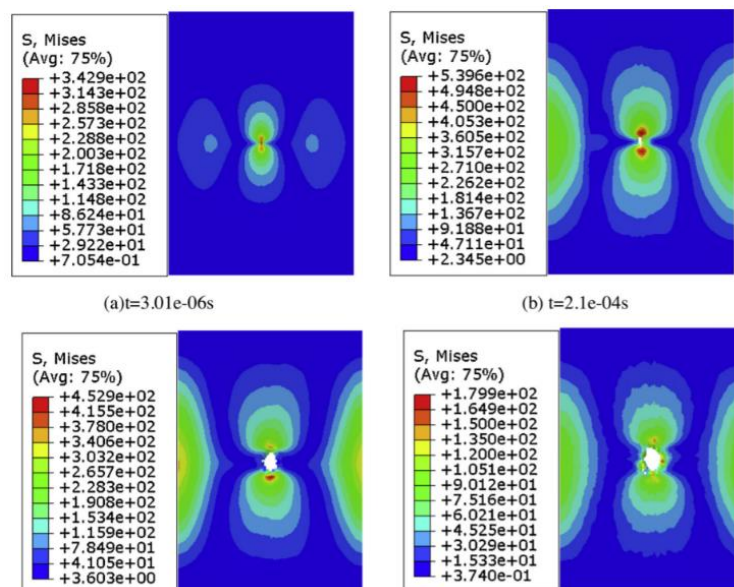


Figure 2.9: Von-Mises stress in the zero layer, which points in the direction of the short axis [41].

Additionally, A bolted composite structure is also simulated with the same impact object. Different boundary conditions are applied. The six-sided simply supported composite is strengthened more than the two-sided simply supported composite. The ability to absorb energy became lower for the composite which was fixed at six sides. Therefore, the impact resistance is better than the two sided simply supported structure [41]. For high velocity impacts (about 80 m/s or higher) Kim H. and Kedward K.T [33] came to the conclusion that the boundary condition does not affect the damage mode or failure threshold energy, because of localized deformation at the time of damage initiation, Before  $100 \mu s$ .

### 2.3.2 Glass fibre composite

In 2017, Macdonald H. performed SHI impacts on glass fibre composite, since there is not much known about this [5]. Two years later Macdonald H. and his colleagues performed similar tests and published an article about repeated impact tests of SHI with a diameter of 5 mm, 10 mm, 15 mm and 20 mm at target velocities of 50 m/s, 60 m/s, 75 m/s and 90 m/s for five different numbers of simultaneous impacts: 1, 5, 10, 25, 50. A meteorological study from Macdonald H. [5] showed that the common hailstone size during precipitation in the UK over a period over 65 years is lower than 20 mm. The size of the SHIs is based on this study and also because of a gap in research about the repeated impact of small SHIs. The SHI is made with a PTFE polymer mould consisting of two hemispherical halves in which distilled water is injected. There is no reason given why distilled water is used and not tap water. Rainwater contains minerals and salts, like sodium, potassium, calcium, magnesium, chloride, sulphate, nitrate and ammonia [42]. These minerals and salts can be found in tap water too [43], while distilled water contains no salts and minerals.

The mould was stored in a chest freezer at minus 24 degrees Celsius. The apparatus used is a pressure vessel with detachable barrels for different hailstone types. At the end of the barrel was a light gate to measure the velocity of the SHI. For better detection, a black dye was added during the manufacturing of the SHI.

After the SHIs left the barrel, they were recorded with a high speed camera at 5000 fps to see whether hailstones shattered before impacting the material. The material that was impacted consisted of five layers E-glass covered in epoxy which represents the skin of a wind turbine, each layer is triaxial stitched with an orientation of  $[0^\circ/-45^\circ/45^\circ]$ . The damage was analysed with mass loss measurement, optical microscopy and scanning electron microscope (SEM). The mass loss measurements are not adequate to derive a conclusion, because of moisture absorption of the composite during impact. They recommended non-contact profilometry to further quantify damage such as a confocal microscope [44]. Data from the optical microscope showed pictures of the surface with damage on the bottom side in the form of whitening of the matrix and also along with the fibre at an angle of 45 degrees. This was only the case for the 15 mm and 20 mm SHI shot at a high velocity (about 90 m/s). For the same case, the SEM showed that fibres were sticking out of the resin see Figure 2.10. Also, scattered debris and localised scarring were observed see Figure 2.11 and 2.12. Large-scale matrix removal occurred only for SHIs with a diameter of 20 mm for large numbers of impacts at the lowest speed of impact see Figure 2.13.

The 5 mm and 10 mm SHIs showed minimal damage for large numbers of impact, compared to the larger SHI at small numbers of impact. An important finding here is that velocity plays a major role in the severity of surface damage. It is more important than the diameter or number of impacts [1].

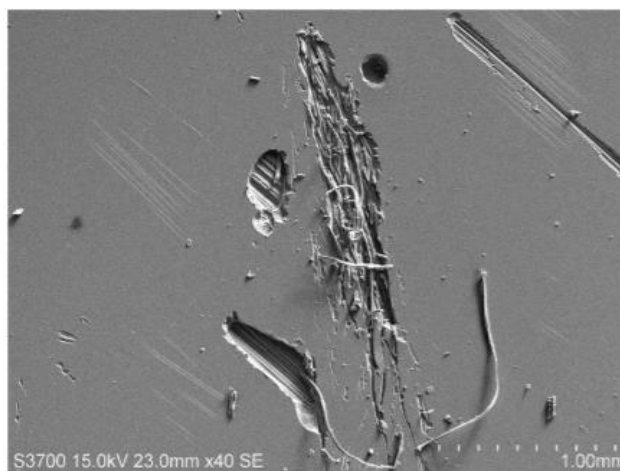


Figure 2.10: Fibre breakage after 50 impacts of 20 mm hailstone at a velocity around 90 m/s [1].

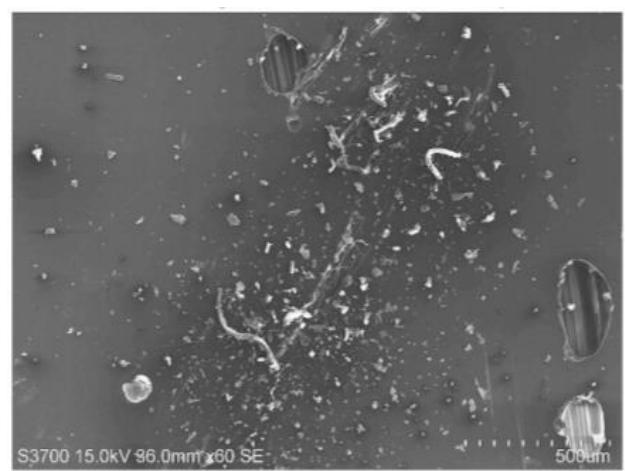


Figure 2.11: Scattered debris after 10 impacts of 15 mm hailstone at a velocity around 100 m/s [1].

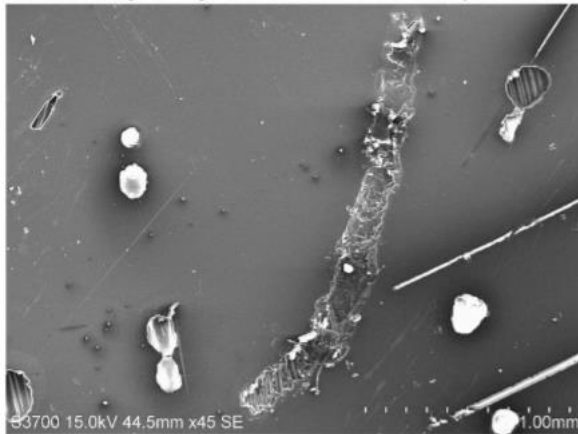


Figure 2.12: Scarring after 10 impacts of 15 mm hailstone with a velocity around 100 m/s [1].

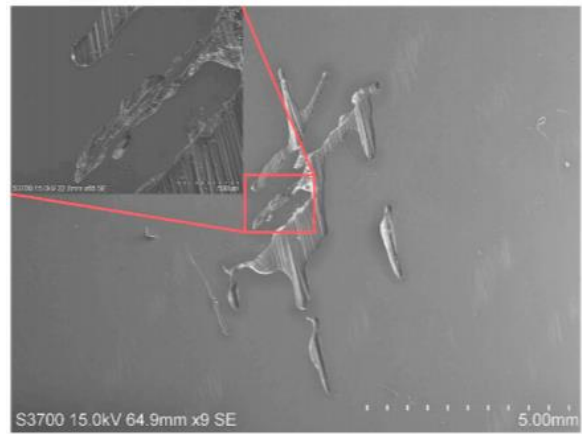


Figure 2.13: Matrix removal after 50 impacts of a 20 mm hailstone with a velocity around 50 m/s [1].

Five years earlier, Atas C. and his colleagues performed also a repeated impact test on glass fibre composite, where the composite is tested with various thicknesses to investigate what kind of effect that had. Also instead of SHI, they used a drop weight impact testing machine, CEAST-Fractovis Plus. The weight used for the impact had a hemispherical nose with a diameter of 12.7 mm. The total mass of the weight is 5.02 kg. Five woven E-glass/epoxy composites are made with different thicknesses: 2.70 mm, 3.35 mm, 4.05 mm, 5.05 mm and 5.75 mm. An advanced data acquisition system is needed and a piezoelectric force sensor to measure the relevant quantities such as the amount of energy absorbed. The absorbed energy is obtained from integrating the area of the force-deflection curve, see Figure 2.14. It is observed that thinner composite panels absorb more energy than thicker composite panels for the same amount of impact energy till the maximum number of impacts for the thinner composite panel has been reached see Figure 2.15. This is due to more deflection of thinner beams since they are less stiff. For every thickness, a spike in the amount of absorbed energy is noticed and an increase of the absorbed energy is also observed before each panel is perforated [45]. The absorption of energy is in the form of damage. There are several types of damage that can occur in composites such as delamination, matrix crack and fibre breakage. The increase of energy absorption should indicate more damage before the perforation of the panel.

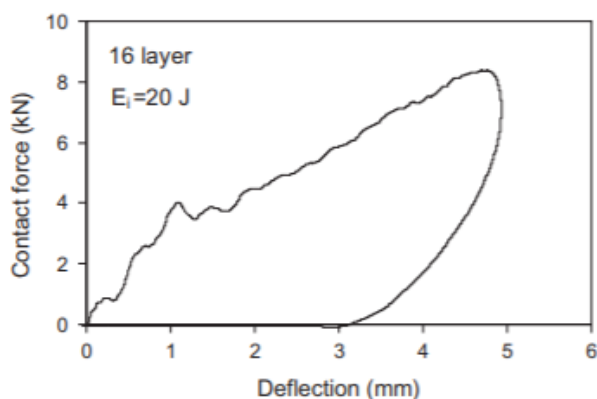


Figure 2.14. Force-deflection curve of a composite (16 layers) impacted with 20 J of energy [45].

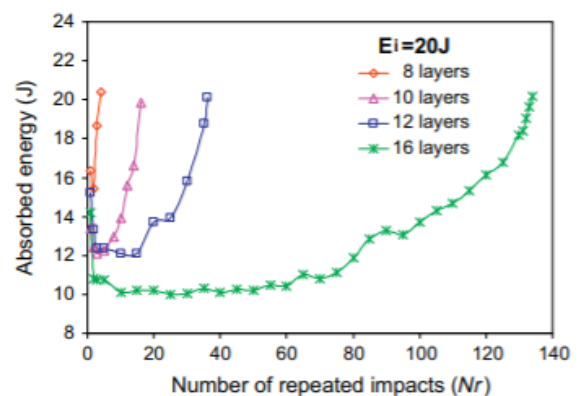


Figure 2.15. Absorbed energy per repeated impact for four different composite. Impact energy is 20 J [45].

Azouaoui K. investigated a similar topic as Atas C., which is fatigue impact on an epoxy resin (R368) reinforced with E-glass fibre. This laminate consists of eight layers of 'Tafetta' woven fabric. The plate itself was 280 mm long and 180 mm wide with a thickness of 5.4 mm. The apparatus that he used for his experiments is self-made in the laboratory. It consists out of a crank-connection rod mechanism, by which the rotational movement is provided by an asynchronous motor and then is transferred to a cyclic translation. This will cause a hemispherical head (with a diameter of 35 mm and mass of 5 kg) to impact the composite panel with a determined frequency. The composite panels were clamped at two edges and on the back of the composite panel were strain gauges attached to measure the strain. The amount of damage is measured in forms of stiffness reduction in two ways: the first one is measuring the stiffness difference of the specimen by performing a flexing test on a conventional tensile test machine. The second one is by calculating a parameter, which is based on the ratio of the load to the displacement. The type of damage is analysed by using photomicrography. The results show that there are three different zones with increasing impact numbers: The first zone is initiation and multiplication of delamination, which initially occurs in the last interface of the laminate (furthest away from the impact point). The second zone is a saturation of delamination, where no extra damage is added. The third zone is ply cracking with fibre breaking, but this happened only when adding 50 percent extra impact energy [39].

The damage resistance of glass fibre composites can be improved by adding clay particles to the composite. Dolati, S et al. researched this topic by conducting an impact test on a glass fibre/epoxy composite with varying amounts of clay particles. SHIs with a diameter of 20.5 mm are shot with a velocity in the range of 130-140 m/s. This was done on a gas gun by using a rupture disk in the breech unit where the SHI is loaded, if a certain pressure has been reached, the rupture disk will break and the SHI will be fired. The damage resistance of the composite is afterwards analysed with X-ray diffraction and transmission electron microscope. Single and repeated impact showed a change in damage mode where matrix cracks were almost disappeared [46].

Glass fibre composite is not only used for wind turbines it is also used in other applications, such as airplanes and helicopters. Impact on helicopter blades has been researched by Tawk I. et al. They performed experiments with a helicopter blade where the leading edge is made of a glass fibre epoxy composite skin, a polymeric foam and a stainless steel coating. The blade is impacted with a steel ball of 125 g at speeds ranging from 30 to 130 m/s by using a gas cannon. The damage is analysed by a high speed camera (using 30000 fps) during the impact and afterwards, the blade is cut to see internal damage. The important findings are that first the stainless steel coating undergoes damage and increasing the velocity results in plastic deformation of the steel coating. This also leads to the separation of the foam with the glass fibre composite skin [47].

### 2.3.3 Glass fibre composite with gelcoat

Keegan M.H. performed a repeated impact test with a gas cannon for SHIs with a diameter of 10 mm. The gas cannon consists of a barrel with an inner diameter of 63.5 mm and a nitrogen gas reservoir. A high speed camera (FASTCAM Super10KC) with 10,000 fps is used to capture the SHI motion. The repeated impact has been done 20 times with a speed of 100 m/s. An epoxy gelcoat, CSM and three layers of bi-axially reinforced glass fibre composite with the next orientations  $[0^\circ/45^\circ/0^\circ]$  are used, respectively from top to bottom where the SHI is hit on the top side. So there are five layers and each layer here is 0.4 mm thick. The width and length of all the layers are 120 mm by 120 mm. After the impact test, he performed a visual inspection, but no form of damage could be seen. He suggests the use of microscopy or other methods, because maybe there is damage, which could not be seen with the naked eye [4]. Another test Keegan M.H. performed is impact with a 10 mm ceramic bead with a velocity of 87.5 m/s. A single impact leads to formation of ring-like cracking distribution on the gelcoat. Throughout the sample, there is lots of whitening in the matrix material, which indicates matrix cracking and interlaminar damage. Even on the bottom side of the composite, damage is observed along the fibre orientation see Figure 2.16. Results of his simulation for a single impact of a 10 mm and 20 mm SHI show that they did not have enough amount of impact energy that could lead to rapid erosion. The impact of the 10 mm and 20 mm SHI caused an interface pressure between the gelcoat and the chopped strand matt of 23 MPa and 64 MPa, respectively. The damage is formed in a ring shape for all SHI. In conclusion, the bigger the diameter of a hailstone the higher the stress in the surface coating and substrate material [4].

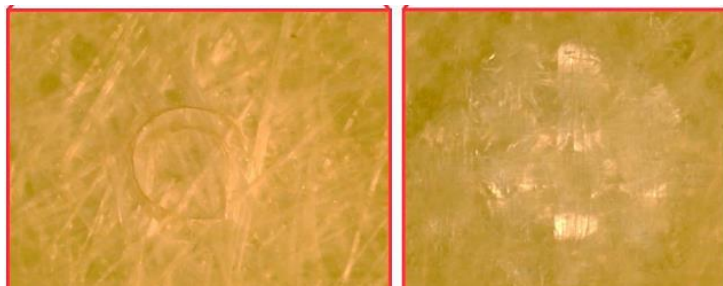


Figure 2.16: Picture on the left shows damage on the top surface and picture on the right shows damage on the bottom side [4].

In 2013 Nash D.H., Keegan M.H. and Stack M. performed simulations with LS-DYNA (using SPH) for a SHI of 5 mm, 10 mm and 15 mm in diameter with velocities from 70 m/s till 120 m/s in steps of 10 m/s. The material that they used is an epoxy gelcoat, CSM and three layers of bi-axially reinforced glass fibre composite with the next orientations  $[45^\circ/0^\circ/45^\circ]$ . The curvature of the leading edge has a radius of 9 mm and the information is retrieved from a large wind turbine manufacturer. Damage on the gelcoat is based on Von-Mises stress exceeding the yield strength (80 MPa) of the gelcoat. The 5 mm SHI simulation resulted in no damage for all velocities. While the 10 mm SHI with a velocity of 90 m/s and higher resulted in damage and for the 15 mm SHI damage already starts at 80 m/s. Impact simulation also showed that a SHI of 10 mm diameter with a velocity of 100 m/s showed maximum stress around 80 MPa, which is not enough to cause failure in the composite substrate material, but is large enough to cause potential delamination across the laminate interfaces [48].

In summary, the articles shown previously some authors used metal or ceramic balls as an impacting object. The advantage of this is the reusability. However, most of the authors used a SHI as an impacting object, this is not reusable, but it is more representative as hail in nature. The diameter of SHI used during the experiments does range from 5 mm to 50.8 mm. According to meteorological data in the literature review, hail size differs per country, but in general, hailstone sizes smaller than 20 mm are commonly precipitated. The velocity of the SHIs in the experimental tests does range from 30 m/s to 268 m/s. As mentioned before, the tip speed of a wind turbine blade is about 100 m/s, adding the terminal velocity of a hailstone with a 10 and 20 mm in diameter, gives an impact velocity of 112 and 118 m/s, respectively. Most impacts are done with a gun/cannon using compressed air or nitrogen. The gas cannon can be used in two ways, the first one is shooting a SHI (with a sabot) by releasing the pressure manually. The second one is by putting the SHI in a breech unit containing a rupture disk. The rupture disk fractures at a certain pressure level and the SHI will be shot then. A drop tower is also used, but this is more for low velocity impacts. Damage caused by impact was analysed with several methods. Surface damage was analysed with visual inspection and mass loss measurement, but these methods are more useful for extreme impact cases that result in severe damage. Otherwise, it is better to use a profilometry, which is recommended by Macdonald H. et al. [1] instead of mass loss measurement. Internal damage was analysed by using a SEM, optical microscope, ultrasonic inspection and mechanical testing. SEM will analyse damage on a small case, while optical microscope on a larger scale. Ultrasonic inspection with a C-scan can give information about the delamination area. Mechanical testing can be used, if you are interested in the mechanical properties and damage tolerance of a material.

## 2.4 CONCLUSION

The impact of hail (and rain) erosion on the leading edge can result in loss of energy production by 2 % reaching up to 25 % [3]. The amount of energy loss is significant, which makes it important to find a way to reduce this amount. A literature review is done to look for what is already used to protect a wind turbine blade against hail erosion. The two most common protection materials on a wind turbine blade are gelcoats and flexible coatings [4]. Each of them performs differently depending on the environment.

The two protection materials are applied in a different thickness range. According to the DNVGL standard, a gelcoat should be applied in a thickness range between 0.3 mm and 0.6 mm [13], while a flexible coating is usually applied till a maximum thickness of 0.2 mm [11].

It is noticeable that both protection materials are not specified with an optimum gelcoat thickness. No articles were found with regard to hail impact on varying coating thicknesses. Therefore, this research gap was chosen to be explored further in order to come up with an optimal coating thickness that could possibly be used by the wind turbine community.

A gelcoat was chosen as the protection material for research, because the range in which it can be applied is bigger.

From articles about impact on composite materials, it is shown that parameters such as, velocity of the impacting object, mass of the impacting object, material of the impacting object, shooting angle of the impacting object, laminate thickness, laminate material and ply orientation are important for the type and the amount of damage you get. It was decided to do the research as similar to the real life problem to a certain extent. Meaning that the same laminate will be used as in the leading edge, but in a simple shape like a plate instead of a curved beam. The velocity plays a major role in terms of damage mode compared to the mass of an impacting object. Minor research is done about simulated hail ice impact at different velocities on a gelcoated glass fibre composite. This could be useful information for researches and the wind turbine blade community.

Research could be done with an experimental setup and/or a simulation. The chosen method is experimental, because with this method it is possible to play around with the materials ( hailstone and composite) and apparatus (gas cannon) to gain experience how the materials behave and apparatus works.

#### 2.4.1 Goal

Understanding the effect of gelcoat thickness with regard the hail erosion and provide useful information to the wind turbine community, by which one way to do this is to provide an optimal gelcoat thickness, from the ones that are tested.

#### 2.4.2 Research question:

What are the effects of gelcoat thickness and impact velocity on the damage mode in leading edge gelcoated glass fibre composites subjected to hailstone impact?

#### 2.4.3 Sub questions:

1. How could a hailstone be shot with the available gas cannon in the lab of the university?
2. What is the main governing damage mode in the composite: delamination, matrix cracks on the gelcoat, matrix cracks in the substrate or fibre breakage?
  - A. How does the main governing damage mode change for different velocities?
  - B. How will the main governing damage mode change for different coating thicknesses?

#### 2.4.4 Hypothesis

##### Research question:

A thicker coating will have less damage in the substrate and interface, because the impact energy will be transferred better due to the thick coating, while the surface damage will be the same for both a thin or thick coating, since this is more material dependent. To elaborate more on the last part, the same amount of coating will be removed for both a thin and thick coating. Meaning that the thicker coating will last longer, since it will take more time to degrade the surface.

##### Sub questions:

1. It should be shot with a sabot, because other researchers used it too and probably with a stopping mechanism for the sabot.
2. It is expected that the gelcoat will undergo the most amount of damage, because that is also what happens in real life on wind turbine blades.
  - A. It is expected that the main governing damage mode will not change for different velocities.
  - B. It is expected that the main governing damage mode will not change for different coating thicknesses.



## 3 METHODOLOGY

---

Chapter 3, contains a test plan of the project first, then a description is given from the gas cannon with its corresponding instruments. After that, challenges of the gas cannon by which one of the sub questions is answered. Next, the manufacturing of a SHI is explained before the section 'Procedure for shooting a hailstone'. Lastly, the manufacturing of the samples will be explained.

### 3.1 TEST PLAN

In this section, details are given on how the research question and sub questions are going to be answered. The parameters involved in the project are explained, the way of making the panels and which method are used to analyse the damage.

#### 3.1.1 Experiment parameters

In order to answer the research question, samples with three different coating thicknesses will be tested: 0.15 mm, 0.35 mm and 0.65 mm. The 0.35 mm and 0.65 mm coating values are based on the gelcoat range advised by the DNVGL standard [13], whereas 0.15 mm is tested out of curiosity. A SHI with a 20 mm diameter will be shot 5 times with a velocity of 120 m/s to each panel. To verify the data, each panel with a different coating thickness will be repeated three times. The coating thickness, diameter and velocity are based on the values found in real life, except the diameter. A SHI with a 10 mm diameter is more common than a SHI with a 20 mm diameter. However, a big SHI (20 mm) is needed to create damage (in a short time), without damage the research question could not be answered. It will be repeated five times to see the damage progression for the first impact, third impact and fifth impact. After five impacts, the samples are already badly damaged so performing more impacts is not necessary .

One coating thickness is chosen to check how the main governing damage modes change for different velocities. These samples will have a gelcoat thickness of 0.15 mm and will be tested with three different velocities: 120 m/s, 100 m/s and 90 m/s. These velocities represent the wind turbine blade tip speed in different wind conditions from windy to less windy, respectively. These samples will be shot 5 times with a SHI have a 20 mm diameter. Each velocity will be tested on a different panel and the test will be repeated three times to verify the data.

The samples will have a dimension of 200 mm by 200 mm, the reason for this is to make sure that it absorbs all the impact from the SHI, but small enough that it can be scanned by the optical microscope. The thickness of the panels is about 2 mm thick and the layup looks as follows (starting from impact side (top) to bottom side): epoxy gelcoat layer (Rengel SW 5200 with hardener Ren HY5212), e-glass fibre chopped strand mat and two fabrics of woven e-glass fibre. One glass fabric contains two layers of glass fibre, these are orientated in the next symmetric orientation, [45/-45/-45/45]. Epoxy (Araldite LY 1564 with hardener Aradur 3487) is used to infuse the dry fibre reinforcement, because it has the same properties as a resin required for a wind turbine blade, such as low viscosity and long pot life. Moreover, the composite layup and thickness are close as much to what is found in the literature to represent a leading edge see section 2.1.2.

The shape is simplified to a flat square plate, because otherwise manufacturing and analysing damage will take more time. The same is done with the hailstone, it doesn't consist of a layered structure like a natural hailstone instead, it has a monolithic structure. Both the composite plate and hailstone are reduced in toughness by doing this. The main reason for this simplification is that there is no experience in making hailstone, shooting hailstones and making a gelcoated glass fibre composite. Therefore, time is needed to understand and handle the basics first.

The boundary condition for all the panels is that two opposing edges are clamped/fixed. According to literature, in the case of a high velocity impact, the boundary condition is less important, because of local deformation from the impact [33].

### 3.1.2 Analysis

Every sample will be analysed the same way. Analysing will be done before impact, after one impact, at three impacts and five impacts. The methods used for analysing the damage progression are the optical microscope (plus smartphone camera) and C-scan machine both non-destructive-methods. The optical microscope is used to scan the damage on the gelcoat and also to get an optical view of the back side of the sample for possible matrix cracks and fibre breakage, also delamination can be seen and these will be compared with the C-scan. The C-scan data is used for detecting delamination between glass fibre layers (including CSM), so not between the CSM and gelcoat.

After the fifth impact, the samples are cut to investigate matrix cracks and fibre breakage with a laser confocal microscope (LCM). This device is chosen because it gives a detailed picture of the cross-section and the scanning doesn't take much time. Moreover, the coating thickness is going to be measured by using the laser confocal microscope as well. More details about that can be found in the analysing method section. Furthermore, a differential scanning calorimetry (DSC) is used to check if a varying coating thickness has an effect on gelcoat curing. An overview of all samples with their experiment parameter and analysing methods can be found in Table 3.1.

Samples name (s=sample)	Velocity	Diameter	Coating thickness	Amount of impacts	Optical microscope	C-scan	LCM	DSC
					Used after number of impact:			
<b>S1 of 0.65 mm</b>	120 m/s	20 mm	0.65 mm	5	0, 1, 3 and 5	0, 1, 3 and 5	5	5
<b>S2 of 0.65 mm</b>	120 m/s	20 mm	0.65 mm	5	0, 1, 3 and 5	0, 1, 3 and 5	5	5
<b>S3 of 0.65 mm</b>	120 m/s	20 mm	0.65 mm	5	0, 1, 3 and 5	0, 1, 3 and 5	5	5
<b>S4 of 0.65 mm</b>	= Extra	sample	0.65 mm	-	-	-	-	-
<b>S1 of 0.35 mm</b>	120 m/s	20 mm	0.35 mm	5	0, 1, 3 and 5	0, 1, 3 and 5	5	5
<b>S2 of 0.35 mm</b>	120 m/s	20 mm	0.35 mm	5	0, 1, 3 and 5	0, 1, 3 and 5	5	5
<b>S3 of 0.35 mm</b>	120 m/s	20 mm	0.35 mm	5	0, 1, 3 and 5	0, 1, 3 and 5	5	5
<b>S4 of 0.35 mm</b>	= Extra	sample	0.35 mm	-	-	-	-	-
<b>S1 of 0.15 mm</b>	120 m/s	20 mm	0.15 mm	5	0, 1, 3 and 5	0, 1, 3 and 5	5	5
<b>S2 of 0.15 mm</b>	120 m/s	20 mm	0.15 mm	5	0, 1, 3 and 5	0, 1, 3 and 5	5	5
<b>S3 of 0.15 mm</b>	120 m/s	20 mm	0.15 mm	5	0, 1, 3 and 5	0, 1, 3 and 5	5	5
<b>S4 of 0.15 mm</b>	= Extra	sample	0.15 mm	-	-	-	-	-
<b>S5 of 0.15 mm</b>	100 m/s	20 mm	0.15 mm	5	0, 1, 3 and 5	0, 1, 3 and 5	5	-
<b>S6 of 0.15 mm</b>	100 m/s	20 mm	0.15 mm	5	0, 1, 3 and 5	0, 1, 3 and 5	5	-
<b>S7 of 0.15 mm</b>	100 m/s	20 mm	0.15 mm	5	0, 1, 3 and 5	0, 1, 3 and 5	5	-
<b>S8 of 0.15 mm</b>	90 m/s	20 mm	0.15 mm	5	0, 1, 3 and 5	0, 1, 3 and 5	5	-
<b>S9 of 0.15 mm</b>	90 m/s	20 mm	0.15 mm	5	0, 1, 3 and 5	0, 1, 3 and 5	5	-
<b>S10 of 0.15 mm</b>	90 m/s	20 mm	0.15 mm	5	0, 1, 3 and 5	0, 1, 3 and 5	5	-

Table 3.1. Overview of all the samples with their experiment parameters and analysing method.

### 3.2 GAS CANNON, IMPACT CHAMBER AND VELOCITY MEASUREMENT

The gas cannon is used to shoot a SHI to a composite plate. It consists out of three main components a barrel, pressure vessel and pressure regulating system see Figure 3.1, where the parts are marked and numbered. The barrel (1) and pressure vessel (3) form a substructure and are connected to each other with a yellowish connection part (2), this is a switch to release the pressure from the pressure vessel. This substructure is mounted to a rigid red frame, which has wheels underneath so that it can be moved around. The height of the substructure can also be adjusted.

In the lab of the Aerospace faculty of TuDelft there is a tube system with circa 8 bar of pressure. A hose is connected to this system and to the pressure vessel. A pressure regulating system (4) determines the pressure inside the pressure vessel. This pressure is measured with a sensor and is shown on a display, where it can be set to a value between 1 and 8 bar. The pressure can also be decreased with a push of a button. Besides, the pressure is also decreasing slowly due to a leakage, therefore when the pressure is in range at the desired pressure it should be shot as soon as possible.

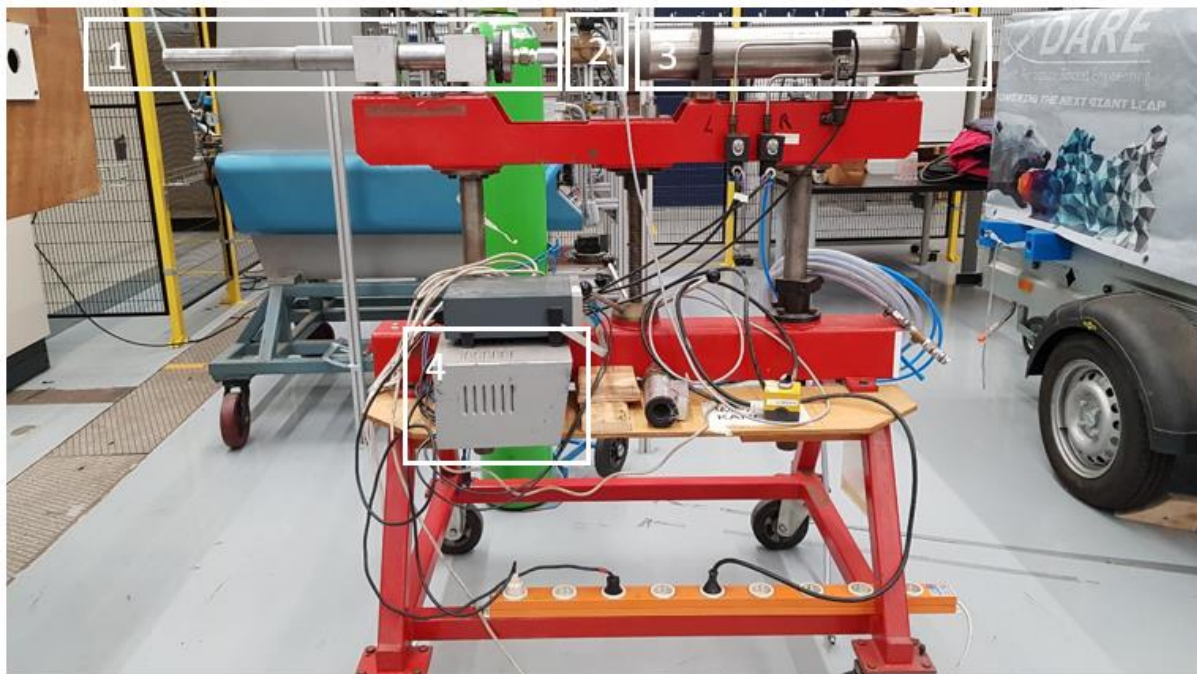


Figure 3.1: Movable gas cannon.

The barrel of the gas cannon will be placed inside an impact chamber see Figure 3.2. This chamber is mounted to a frame underneath and has on four sides an 18 mm thick multiplex wood and about 100 mm thick foam to absorb flying debris from the impact. The other two sides have a polycarbonate panel, by which one can be opened.

The impact chamber has two compartments as can be seen in the figure. The compartment on the left is meant to store stuff like foam or small devices. The one on the right is where the impact happens. It contains two holes, one on the left and one on the right side. The hole on the right side is meant to put the barrel through and the hole on the left is meant for modification to test-setup, but this is not used for the experiment.



Figure 3.2: Impact chamber.

On the left side, the composite panels will be clamped at two edges see Figure 3.3. The composite plate will be clamped between the wood and the metal bracket. The wood gives a space of about 20 mm between the composite sample and aluminium backing structure. Each clamp has two bolts going through the bracket and wood, the edge of the composite plate will touch the bolt. Touching the bolt will indicate that the composite plate is clamped at an even distance upward as well as downward.

On the left side of the left bracket are two triangle metal parts, similar metal parts can be found between the left and right bracket at the bottom side. These triangle metals parts are used to ensure the same fixation location for each sample during the experimental tests.

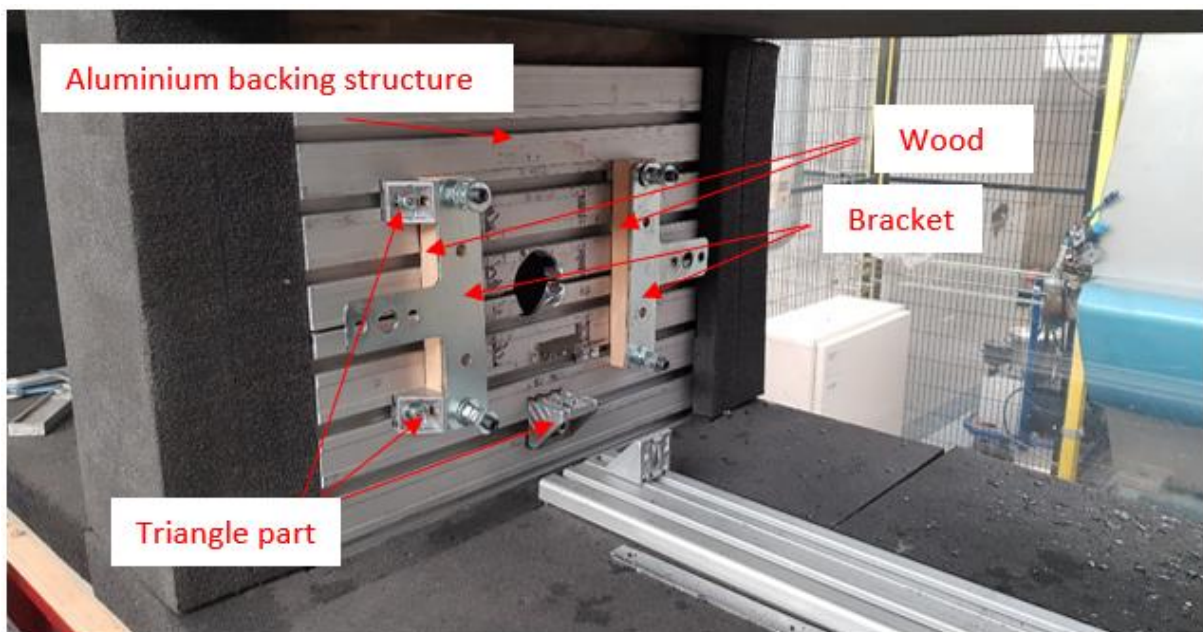


Figure 3.3: location where the samples are placed inside the impact chamber.

The velocity of the SHI will be measured with two infrared sensors, OPV302 cavity surface emitting laser, and two silicon phototransistors, OP800 series. These are mounted to an aluminium tube with holes for the sensor see Figure 3.4. The wires from the sensor are connected to an electric circuit and to an oscilloscope, National instruments Virtual bench VB-8012 see Figure 3.5. This is used in combination with a software called Labview to detected pulses for the two sensors. The pulses are generated by the SHI travelling through the tube and blocking the infrared light. The time between two pulses can be measured in the software, while the distance between the two sensors is 30 mm and with this known the velocity can be calculated by dividing the distance by the time. The way of mounting the aluminium tube with sensors to the barrel can only be understood after reading section 3.3 gas cannon challenge and further explained in section 3.6.



Figure 3.4: Tube with IR sensors.



Figure 3.5: National instruments Virtual bench VB-8012.

A comparison of the velocity of a 20 mm SHI between the infrared sensor (IR) and high speed camera (HSC), Photron Fastcam Mini AX200, can be seen In Figure 3.6. Two measurements of each method are done and it can be seen that both methods result in more or less the same velocity per pressure. Except at about 5 bar, where the second measurement of HSC gave a much lower reading, but in general, the data points are close to each other. It takes less time to know the velocity of the SHI with the IR method than with the HSC method, therefore the IR method is chosen over the HSC method. The raw data of the 4 measurements are present in Appendix A.

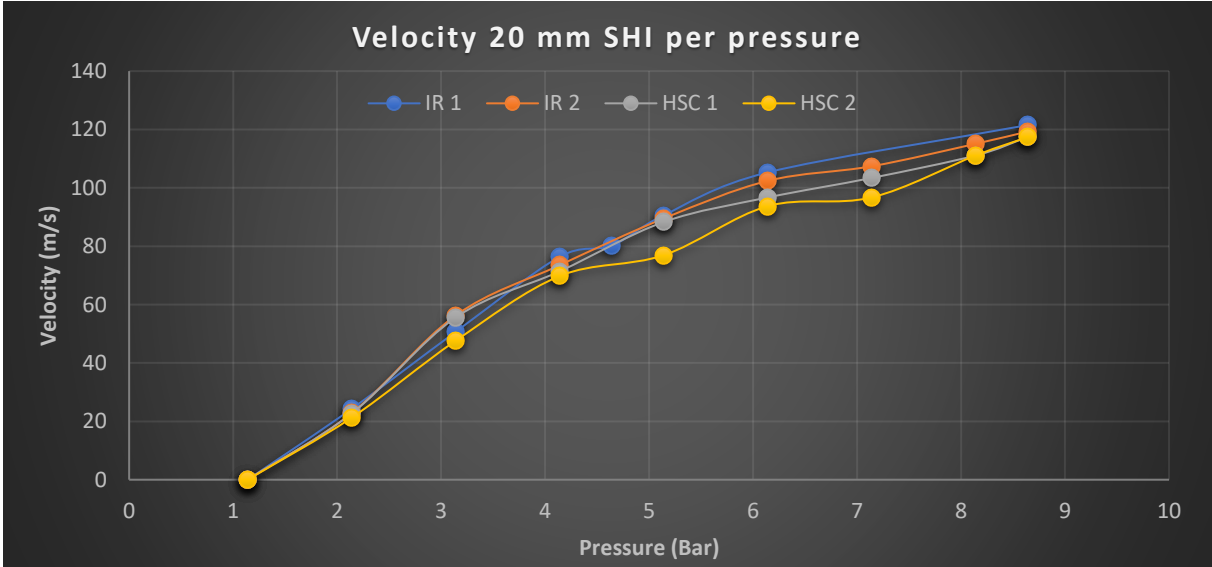


Figure 3.6: Velocity comparison between IR and HSC.

### 3.3 GAS CANNON CHALLENGE

A SHI could not be placed in the barrel itself, because the SHI was melting fast within 10 seconds there was no (10 mm) SHI anymore due to the high conductivity of the metal barrel. Three concepts are tried and only the third one worked. These concepts are tested with a 10 mm SHI, except the third one which is also tested with a 20 mm SHI.

#### 3.3.1 Concept one

In concept one a sabot (SHI carrying casing) is used to prevent the SHI from melting. The sabot consists out of an impactor cover and an impactor head indicated with number 1 and 2 see Figure 3.7, respectively. These parts can be connected to each other which is shown in Figure 3.8. The impactor cover is made of plastic (POM), which has a low friction coefficient with the metal barrel. Its main function is to provide a high speed and smooth travel of the sabot through the barrel. The impactor head is 3D printed from the material PLA and is used to place the SHI inside.



Figure 3.7: Impactor cover and impactor head.



Figure 3.8: Sabot.

When the sabot has reached the tip of the barrel it is travelling at its highest speed. At this point, it will collide with a thick aluminium plate with a hole in the centre see Figure 3.9. This hole coincide with the hole in the impactor head and is slightly larger. There are also eight smaller holes with plain bearings, a steel rod will go through this (the half hole on the edge is just for orientation). The rods are fixed to a frame, which can be seen in Figure 3.10. Around the rod is a spring, during a collision of the sabot to the aluminium plate will move around the rod and will be stopped by the springs.



Figure 3.9: Collision plate for the sabots.



Figure 3.10: Collision plate holder.

A picture of the whole structure with the frames in the impact chamber can be seen in Figure 3.11. The sabot will hit the aluminium plate. The sabot will be decelerated at this point, while the SHI will move through the hole in the plate. The impactor head will be crushed during the impact, but the impactor cover will stay intact, which does partly leave the barrel. The reason that the impactor head is 3D printed is, because of the fast and high amount of production with this process. For repeated impacts, this will be a requirement. Another reason is the low mass that can be achieved by choosing a low value for the infill setting.



Figure 3.11: Structure for stopping the sabot.

After shooting, the sabot is still pushing against the aluminium plate due to the pressure in the barrel, which cannot escape. The springs are pushing the aluminium plate back. There is so much energy that the gas cannon was rolling backwards. Therefore, a rope with tensions springs is attached to the gas cannon and impact chamber see Figure 3.12. Shooting one SHI with this concept took five minutes, which allows the SHI to melt more than when it is done faster. The impact energy of the sabot plus the pressure in the barrel after shooting, which could not escape due to the sabot, made the experiment a little bit dangerous. Stronger springs are required to shoot at a higher pressure level than 8 bars. With this in mind, it was decided to better go for concept two.

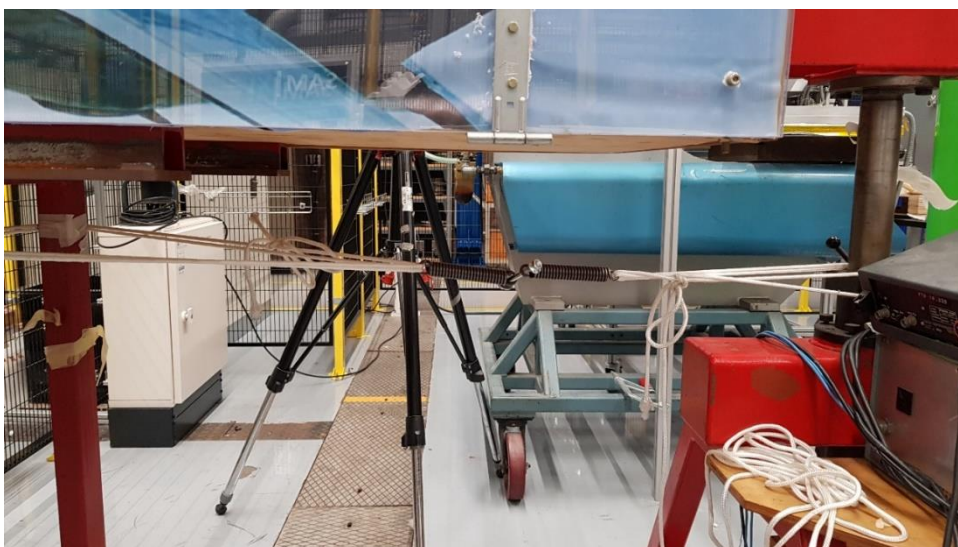


Figure 3.12: Robes with springs attached to the impact chamber and gas cannon.

### 3.3.2 Concept two

Also for this concept, a sabot is used, but with a different design. The design is based on the sabot used by a standard test method (ASTM F320-16) for hail impact resistance of aerospace transparent enclosure. This design was not used in the first place, because the firing range should be between 3-6 meters, while the compartment of the impact chamber where the impact happens is about 1 meter. The sabot design is 3D printed and consists of two halves see Figure 3.13. The sabot is designed to separate after leaving the barrel, but on the inside, it needs to be stuck together see Figure 3.14. The two half spheres on the sabot and two holes in the other half of the sabot maintain a connection with each other inside the barrel. After leaving the barrel, it could still separate, the two halves will rotate away from each other due to a lift force generated by the oblique shape. All sabot designs are shown in Figure 3.15, where the first design is indicated with number 1 and the last design is indicated with number 4. It was believed that by reducing the mass of the sabot, that this concept perhaps could work, but even sabot number 4 with a shell-like structure was not light/good enough.



Figure 3.13: Two parts of the sabot side by side.



Figure 3.14: Sabot configuration inside the barrel.

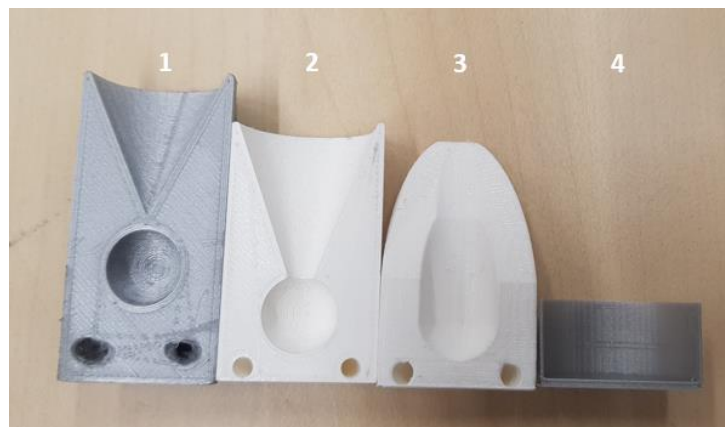


Figure 3.15: Several designs of sabots for concept 2.

On the opposite side of the tip of the barrel will be the composite plate. There are two aluminium plates placed at an angle to divert the sabots away from the composite plate. The aluminium plates have a gap in between so that the SHI will go through it and hit the composite plate see Figure 3.16a and 3.16b. This design is also optimized, the aluminium plates are placed closer to the composite plate to make the travel length for the sabots longer, the aluminium plates are constructed in a stiffer way and the gap between the aluminium plates are clamped with a bolt and nut to fix the size of the gap.





Figure 3.16a: Separation mechanism for concept 2.

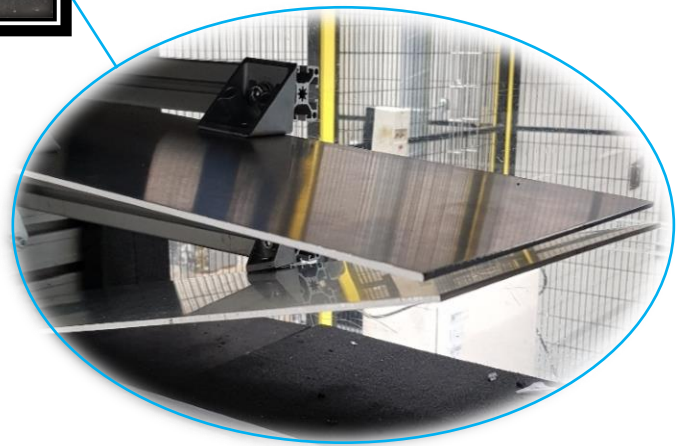


Figure 3.16b: Gap between aluminium plates to let SHI through.

Different sabots are tested as mention before, but it did not work even with the optimized version of the structure and sabots. The sabot did separate a small amount, but this was not enough. It crushed against the edge of the aluminium plate and small debris travelled with the SHI through the gab and collided with the composite plate. This could lead to extra damage and that's why this concept was not used anymore. The distance between the aluminium plates and the tip of the barrel should be indeed bigger.

### 3.3.3 Concept three

In this concept, an acrylic tube will be put in the barrel. The outer diameter will be around 24.9 mm, since the inner diameter of the barrel is about 25 mm. The acrylic tube for the 10 mm hailstone required an extra 3D printed casing around it to hold the tube at the centre of the barrel see Figure 3.17. The acrylic tube for the 20 mm SHI does not require a 3D printed casing, but needs to be made smaller in the outer diameter, since the outer diameter is 25.6 mm. This is done with the machining process called 'turning' till a diameter of 24.9 mm is reached. The outer surface is sanded with a fine scotch brite to put/take the tube easily in/out.



*Figure 3.17: Acrylic tube inside a bigger 3D printed tube.*

The acrylic tube required a fixation at the end of the barrel otherwise it could be shot together with the SHI out of the barrel. To prevent any acceleration of the acrylic tube, an aluminium plate with a hole slightly bigger than the hole of the acrylic tube, but smaller than the outer diameter of the acrylic tube is placed at the tip of the barrel. This plate is connected with four bolts to another aluminium plate around the barrel. Between these two aluminium plates is a rubber, which is wrapped around the barrel and tightened with two hose clamps see Figure 3.18. This small structure is custom made meaning that the aluminium plates are cut and drilled and the metal threads were also cut in size.

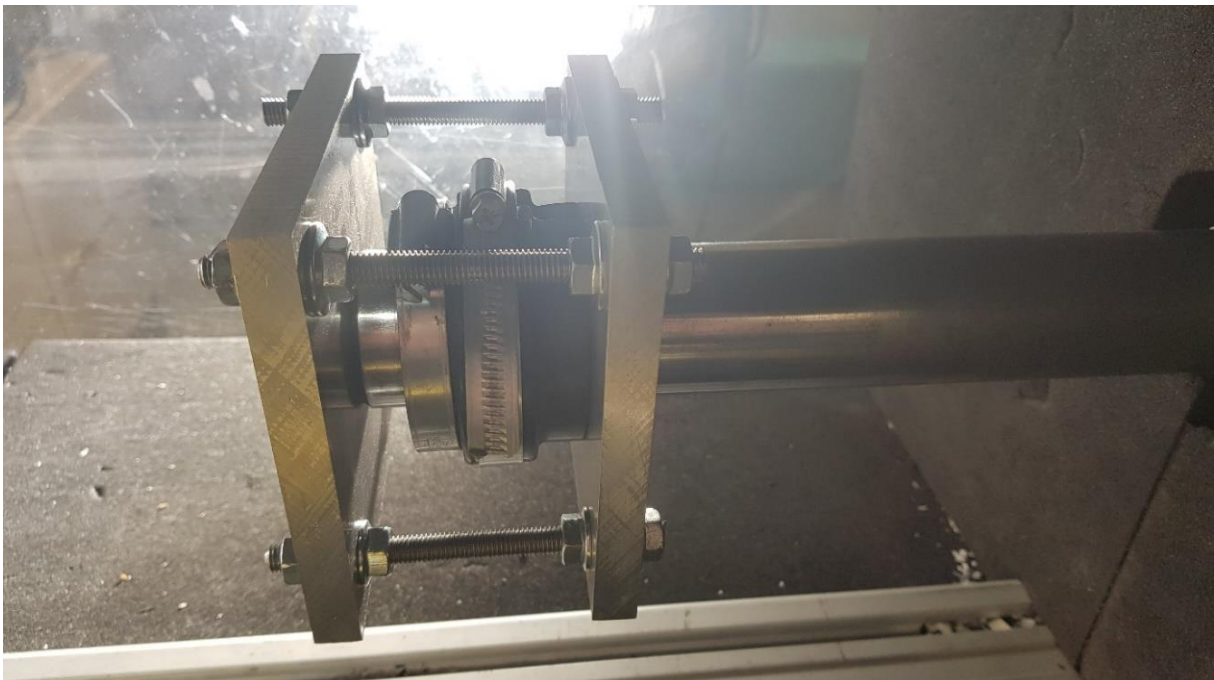


*Figure 3.18: Small Structure to hold the acrylic tube in place.*

### 3.4 MANUFACTURING HAILSTONE

The 20 mm SHI will be made with a female and male mould see Figure 3.19. The moulds are 3D printed (PLA material) with an extra fine profile and a thickness layer of 0.05 mm is used. This is a cheap, fast and easy method to produce several moulds for a repeated impact. Tap water is used for the SHI and it is injected into the mould through a little gap in the male mould with a syringe to reduce the number of voids. The female and male moulds are clamped to each other with two elastics see Figure 3.20. The fit is still not watertight, so water can pour out of the gaps between the male and female mould, that is why the gaps are lubricated with grease/Vaseline to make a seal.



Figure 3.19: Male mould (on the left) and female mould (on the right). Figure 3.20: Moulds clamped with two elastics.

After injecting water into the mould, the mould is stored in the freezer for 5 hours at  $-22^{\circ} \pm 5^{\circ} \text{C}$ . The water is frozen after 5 hours and the SHI can be removed. Removing the SHI is done after keeping the mould for 6 minutes at room temperature. This makes it easier to remove the SHI, because the bond between the SHI and mould is getting weaker. Besides, the possibility to damage the surface of the SHI is also reduced. After 6 minutes, the SHI is pushed from the mould with a plastic rod in a polyethylene bag see Figure 3.21. Subsequently, it is checked for any cracks, if there are no cracks it is put back in the freezer to use it later for the impact test. Otherwise, it is thrown away, because cracks can reduce the strength of the SHI. The plastic rod and polyethylene bag are first put in the freezer for about 15 minutes before contact is made with the SHI to prevent melting.



Figure 3.21: Polyethylene bag with SHI.

### 3.5 PROCEDURE FOR SHOOTING HAILSTONE

Once the acrylic tube is placed inside the barrel of the gas cannon, the barrel can be moved inside the impact chamber. A large try square is placed on the barrel and aluminium backing structure to make sure that the hailstone is shot perpendicular to the composite plate. Next, a laser is mounted on the barrel before impact testing to make sure that SHIs are shot in the centre of the sample. For this, a test-composite-sample with a marking at the centre is used to align the laser pointer and the marking. The test-composite-sample was made early in the master thesis to gain knowledge about manufacturing and has the same dimensions as the composite samples used for answering the research question and sub questions.

Alignment of the barrel can be done by increasing or decreasing the height of the barrel. If the gas cannon needs to be positioned to the left or right it is simply pushed towards that direction.

Afterwards, the try square is used again to check if the angle between the barrel and aluminium backing structure has changed or not. Wooden wedges are placed under the wheels of the gas cannon to make sure that it is locked in place. Now, the small structure with the aluminium plates containing holes at the centre is mounted at the tip of the barrel to stop the acrylic tube from moving. To this small structure, the IR velocity sensor is connected via a hinge see Figure 3.22.

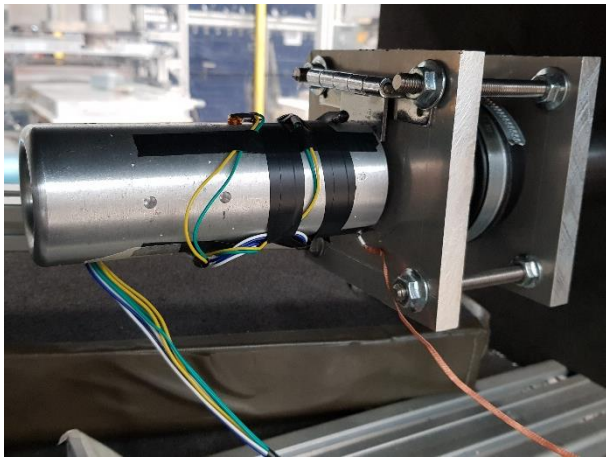


Figure 3.22: IR velocity sensor mounted to the barrel via a small structure with a hinge.

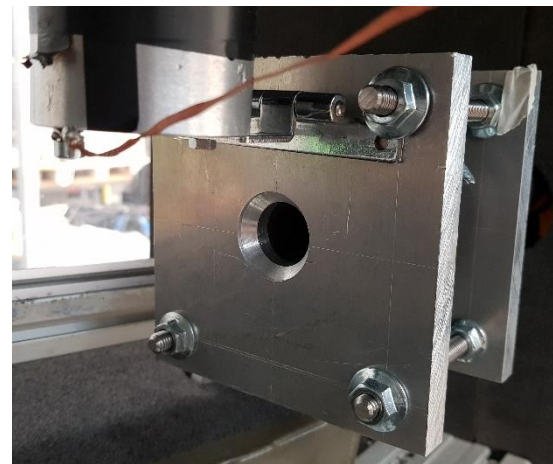


Figure 3.23: Gap leading to the acrylic tube inside the barrel, where the SHI can be loaded.

The IR velocity sensor can be turned upward to make loading of the SHIs easier see Figure 3.23. The electricity and pressure hose can be connected to the gas cannon now. Further, the composite sample can be clamped at the before mentioned location.

The mass of the SHIs is measured on a weighing balance before the test day. This is done while it is still in the bag, the mass of the bag is later subtracted. All the bags are numbered and each bag has therefore a specific mass.

The SHIs from the freezer are placed on a cold paper from the plastic bag they were in. From the cold paper, it is put in the barrel via the hole in the aluminium plate see Figure 3.23. It is pushed deep (about 50 mm) in the barrel with a 3d printed rod. The velocity sensor can be turned downwards now, the impact chamber can be closed and the SHI can be shot by raising the pressure first. Before shooting on the composite samples, a test composite sample is shot first to really make sure that everything works well and has been aligned correctly.

### 3.6 MANUFACTURING OF COMPOSITE PLATE

The manufacturing of the composite plates is done with four sessions of vacuum infusion. Two sessions are done at the same time on one plate. Meaning that a manufacturing step is done for both sessions in order to go to the next step. When two sessions are done at the same time, nothing is shared for example the vacuum pump, resin and vacuum bag. Except for the aluminium plate and epoxy gelcoat.

#### 3.6.1 Preparation of the mould

Since the composite will have a plate shape, the mould is also a flat plate. First a thick and large aluminium plate is needed to make a lot of samples in one go, otherwise, it will take a lot of time to perform vacuum infusion every time just for one sample. The aluminium plate needs a surface treatment to make the surface less rough than it was before in case of deep scratches. It is sanded with an air pressured sanding machine using the grit sizes: P80, P120, P180, P240, P320 and P400. Then it is sanded with scotch brite to reduce the roughness even more, see Figure 3.24 for the result.

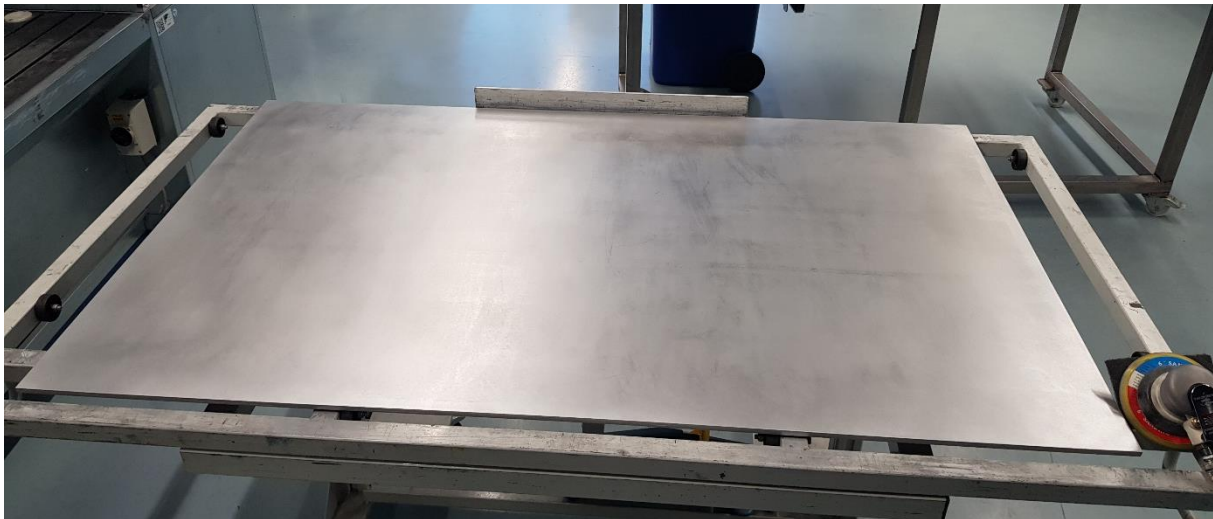


Figure 3.24: Aluminium plate undergone a sanding treatment.

The surface is then cleaned with isopropanol to get rid of dirt such as aluminium oxide. This is done by pouring isopropanol on a paper towel and cleaning the plate three times. Afterwards, it was also cleaned with acetone only one time, which is a more aggressive liquid to get rid of obstinate particles. The next phase is marking the areas with paper tape where the vacuum bag will come. The purpose of this is actually protect the area against liquids, which will be used next. The plate will be covered in three layers of release agent, Marbocote 227CEE. It is applied alternately in the horizontal and vertical direction, whenever you swap from one direction to the other direction you will have to wait five minutes to let it dry. The release agent is used to easily remove the product from the aluminium plate otherwise it will stick to it, because resins are used to make the composite plates. After applying the release agent, the paper tape can be removed to place tacky tape on the same areas where the paper tape was, see Figure 3.25. The tacky tape can stick to aluminium plate since there is no release agent on the paper taped area. The tacky tape makes an air tight seal with the vacuum bag, which will be used at a later stage of the vacuum infusion process.

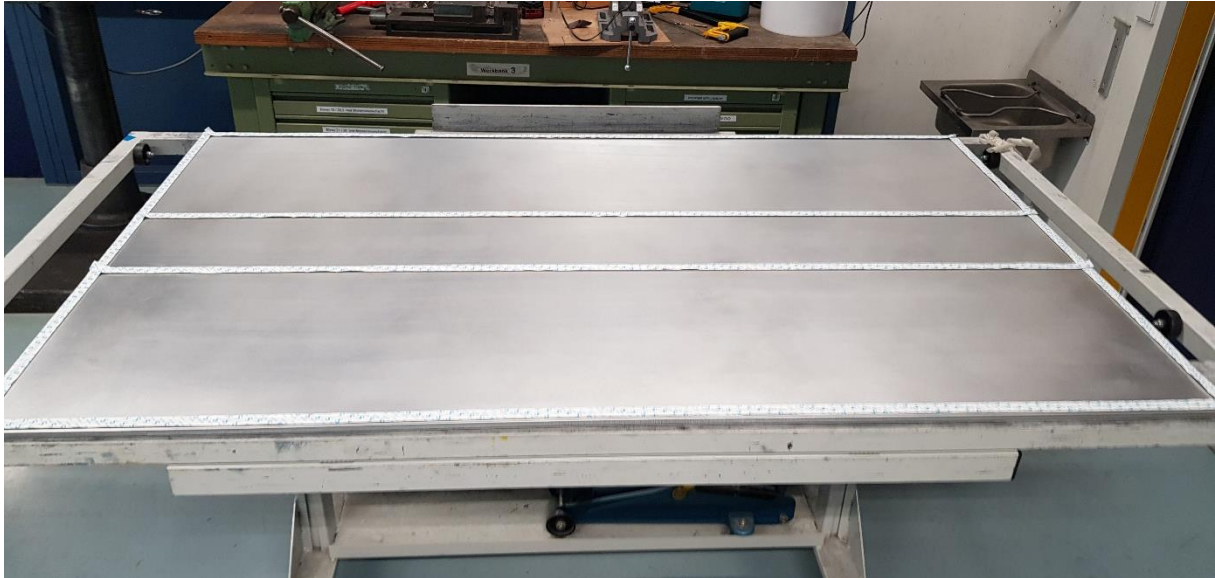


Figure 3.25: Treated aluminium plate with tacky tape.

Figure 3.25 shows two big rectangular areas and one small rectangular tacky taped area. Each big rectangular shows the area of vacuum infusion. In this area, smaller areas will be taped with paper tape where each specimen is manufactured individually till the infusion starts. Thus there won't be a big plate in one go, but smaller plates instead, because of the documentation required for the gelcoat to see at which spot the gelcoat is measured in the thickness. The measuring points should not be on the impact site otherwise, it can affect the results of the test.

### 3.6.2 Applying the gelcoat

The aluminium plate is now prepared to apply the epoxy gelcoat. The epoxy gelcoat will be measured and mixed before it is applied. This is done in a fume cabinet wearing protective clothing, safety goggles and chemical resistant gloves. A measuring cup is first put on a weighing balance, Weegschaaldirect WPS 4000/C/1, the mass of the cup is set to zero and then the gelcoat consisting of a base agent (Rengel SW 5200) and accelerator (Ren HY 5212) are put in a measuring cup in the ratio 100:20 (parts by weight), respectively. The ventilation system in the cabinet influence the measured mass by  $0.1 \pm g$  and the human mistake by not adding the exact quantity of the base agent and accelerator is  $0.2 \pm g$ . After the right quantity is measured, it is stirred for five minutes with a wooden stick. The aluminium plate is placed on a table with a ventilation system above. A plastic foil is wrapped around the table to improve ventilation efficiency. Now a small amount of gelcoat is put from the cup to the aluminium plate with a wooden stick. It is then spread out over the marked area with a foam roller. The thickness of the gelcoat is measured with a wet gauge see Figure 3.26. This tool is made out of stainless steel and has teeth, where each tooth is extended more than the next teeth or the other way around. It is then pressed against the coating and the last teeth that has been submerged in the coating will tell the thickness of the coating. Since the gelcoat has a rough surface it is difficult the measure the thickness. Due to the roughness, some teethes are partly marked and sometimes the teeth which is more extended towards the coating is

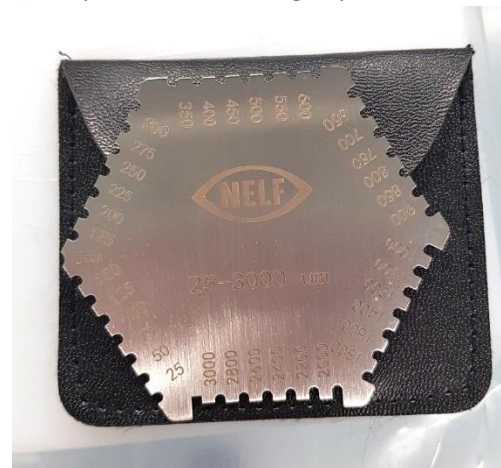


Figure 3.26: Wet gauge.

not covered, while the teeth which is less extended toward the coating is covered. To have a better idea of the coating thickness, the surface of the coating was smoothed out. There are two stainless steel strips put parallel to each other between the coating. A rectangular tool is placed on these strips and moved from the right side of the coating to the left in order to make the top surface smooth. The strips (filler gauges) come in different thicknesses and can be stacked on each other. The amount and thickness of the strips are chosen such that when the tool is moved over these strips, that the coating thickness should be closed to the desired coating thickness. It is then measured with a wet gauge at four locations. The indentation of the wet gauge at these four locations can be seen in Figure 3.27 also the strips and the triangular tool. The wet gauges need to be cleaned with Acetone and a cloth after a measurement is done to prevent any misreading by the next measurement. During cleaning, a gas is smelled and it is preferred to do the cleaning with Acetone close to the ventilation system or wearing a gas mask with APEK1 filters.



Figure 3.27: measurement points on smoothed gelcoat that is between two metal strips with the triangular tool on the right side.

After measuring at these four locations, the roller is moved slowly from left to right over the coating without pressure, just with the own weight of the roller. The coating will have about the same thickness as before and also the same roughness. The thickness now is likewise measured as when the coating was smooth. The location of the thickness measurement is marked with a red marker on the paper tape. This is repeated for the other samples that are needed to be made. The coating has to become tacky before the backing structure can be applied, which happens after 24 hours when the resin is mixed.

### 3.6.3 Stacking and vacuum bagging

The next day, the reinforcement can be laid starting with the chopped strand mat (CSM) (240 by 240 mm in dimension), which is a randomly orientated glass fibre layer for better bonding of the coating to the composite. On top of the CSM are two glass fabrics laid with the next layup [45/-45/-45/45] in the same dimension as the CSM. It is bigger than the dimensions used for testing, which is 200 by 200 mm, because at the edges are imperfections and these need to be removed by cutting away the edges. Airtech non-coated Peel ply is used on top of the glass fabric to texture the back side of the composite. It is 250 mm in width and 300 mm in length to make sure it is in contact with the bleeder.

In this way, it can be ensured that there is vacuum applied on the composite. Furthermore, a perforated Release film from Airtech Wrightlon 3900 blue is added on top with a dimension of 250 by 250 mm to guarantee easy removal of the vacuum bag elements and also for resin flow to the composite. To distribute the resin over the composite equally a flow mesh is added on top of the perforated release film, Airtech greenflow 75. It is 220 mm in the width and 210 mm in the length. It is smaller than the composite in order to force the resin to flow through the composite and not directly flow to the bleeder (Airweave N10), which is placed between the composite and the outlet tube to absorb excessive resin. The required dimension of the flow mesh can change for different resins and fibre reinforcement, if it is too short, then it will take more time to flow through the reinforcement and there could be a chance that not all the fibre are wetted with resin. The infusion mesh is wrapped around and fastened with staples to the infusion line, which is connected to a T-assembly in the inlet tube see Figure 3.28. The resin will flow from the inlet tube and T-assembly to the infusion line. The infusion line makes it possible for the resin to flow to the infusion mesh. The resin can now flow with the same speed over the width.

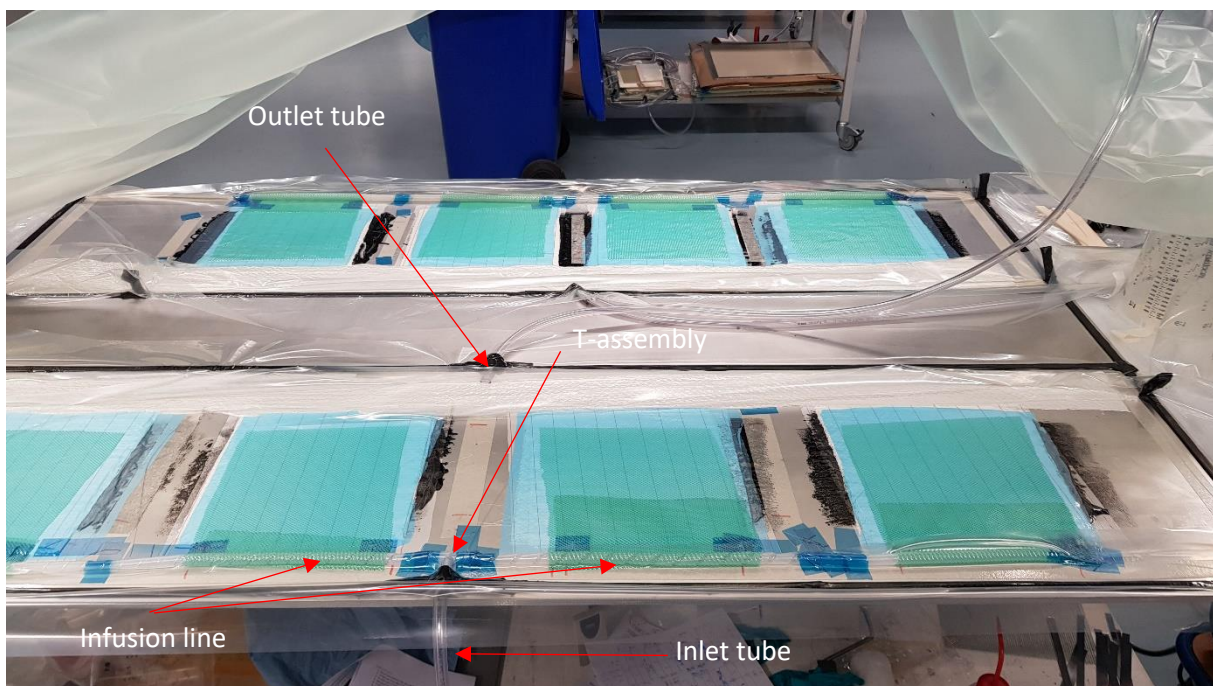


Figure 3.28: Components of the vacuum infusion process.

The inlet and outlet tube (Rehau Rauclar-E) face each other on the opposite side. Tacky tape is rolled around the inlet and outlet tube and stuck to the tacky tape which was already on the aluminium plate. Another strip of tacky tape with a length of 200 mm is laid over the inlet and outlet tube to hold it in position. A piece of bleeder is also placed in the outlet tube to make sure that the outlet tube is not closed during vacuum and also to reduce the resin flow to the outlet tube.

One of the final steps before putting the vacuum bag is to tape everything that is sharp with Kapton tape to prevent any leakage in the vacuum bag. The end of the infusion line is cut with scissors and might contain sharp edges so that must be taped. The edge of the infusion mesh can also be taped, but it is done partly during the manufacturing process to save time. In addition, the staples in the infusion mesh are also taped. Furthermore, other parts such as the peel ply, perforated release film, infusion mesh and infusion line is also taped to hold it in position. The reason for this is when putting the vacuum foil on the infusion area, the other parts might move and it will be difficult to reposition these parts, since the vacuum foil is stuck to the tacky tape. The vacuum bag used here is the Airtech



WL7400. It is cut in the size 800 by 2000 mm, which overlaps the infusion area to be sure that is more than enough. Pleats of tacky tape can be used to reduce the amount of wrinkles in the vacuum bag.

The final step of the vacuum bagging process is to perform a leakage test. The inlet hose is clamped so that air cannot enter and escape the inside of the vacuum bag. The outlet tube is connected to a vacuum pump. The pressure inside the vacuum bag is reduced to 50 hPa, then the pump is turned off. If the pressure increases with 1 hPa every 10 seconds or longer it should be alright. However, this is the case if there is a small leakage on the outlet tube side. If the leakage is somewhere in the inlet tube side, then the air bubbles could travel through the composite, which can lower the quality of one or more samples. In the case that leakage is spotted in the form of a gap between the vacuum bag and tacky tape, it can be sealed by pressing the vacuum bag firmly to the tacky tape or adding more tacky tape to this area.

### 3.6.4 Processing of the resin

Since the vacuum bagging is done the resin can be mixed for the infusion process. The same weighing balance is used as for the epoxy gelcoat. The resin for the composite is a two component epoxy: base agent (Araldite LY1564) and accelerator (Aradur 3487). They are put in a white bucket and mixed in the ratio 100 gr Araldite with 34 gr Aradur. It is stirred for five minutes to mix the two components good. After this, scotch brite is put in the resin and hold in place with a wooden stick that is clamped to the bucket. It is used for the degassing process to reduce the number of air bubbles in the resin. The resin is degassed for 15 minutes in a special vacuum chamber see Figure 3.29. The time for stirring and degassing is kept up with a timer. The processing of the resin is done twice, when one is in the degassing phase the other one is in the mixing and stirring phase.



Figure 3.29: Degassing equipment.

### 3.6.5 Vacuum infusion

The white bucket with the degassed resin is then placed in a larger bucket with water. The purpose of this is to cool down the bucket with resin, because after mixing the resin components, an exothermic reaction happens, which can generate heat. Next, the tip of the inlet tube is cut at an angle so when the tube is put in the bucket with resin, the tube doesn't get stuck with the bucket during vacuum infusion. The tube is taped around a wooden stick to make it more rigid. The stick is then clamped to the resin bucket to fix the tube in place. Before the inlet tube is placed in the bucket of resin, the inlet tube is clamped. Additionally, the resin bucket is also stuck to the water bucket with a clamp to fix it in place. A weight is put under the edge of the water bucket making the resin bucket lean on an angle. The reason for this is to accumulate more resin to the spot

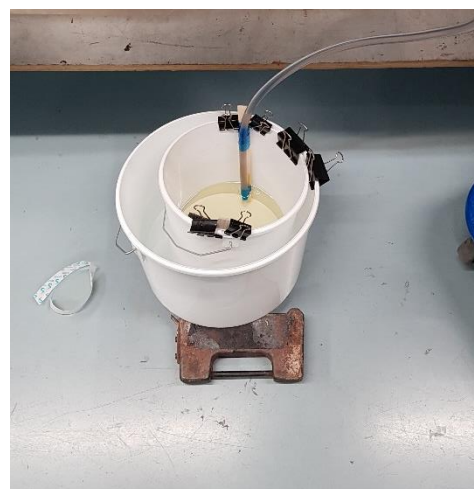


Figure 3.30: Setup for resin supply.

where the tube is placed in the resin bucket. More resin can be taken from the resin bucket during vacuum infusion now, see Figure 3.30 for the whole resin supply setup. The outlet tube was already connected to a vacuum pump for a leakage test. The next step is setting the pressure to 70 hPa on both pumps. The final step to let the resin flow through the laminate is unclamping the inlet tubes on both sides at the same time, so opening one and within seconds the other one. The resin contacts the epoxy gelcoat after 5 hours when it became tacky. The resin starts to flow through the composite and it takes about 20 minutes to reach the end of the composite plate see Figure 3.31 for this moment.

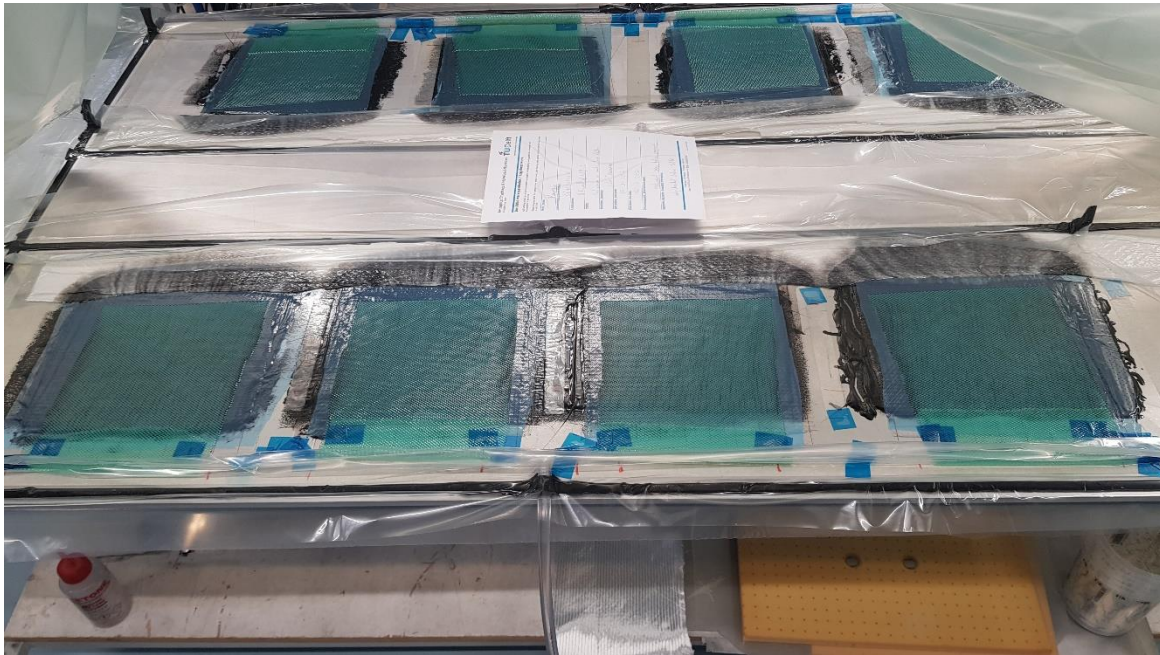


Figure 3.31: Stage of composite sample after 20 minutes of resin flow.

A pressure of 70 hPa is maintained for 2 hours after this, the pressure is changed to 500 hPa to create a laminate with a balanced resin-fibre content. After 15 minutes from the moment that the pressure was changed, the inlet tube is clamped again. This is done to have an equal pressure over the laminate and thus creating a laminate with an equal thickness. The composite samples are cured at room temperature (22° C) for seven days.

### 3.6.6 Debugging

After the composite samples have been cured, the debugging process can start. The elements used for vacuum bagging can be removed starting with the vacuum bag and tacky tape. The other parts are removed by peeling the peel ply. When the peel ply is almost removed, the sample is marked on the spots where the thickness was measured and also the sample thickness and number are written. Most of the materials used for vacuum bagging and infusion can be thrown away except the aluminium plate, weight, clamps and large bucket with water. These can be reused for the next vacuum infusion process.

### 3.6.7 Cutting Samples

The composite samples will have imperfections on the edge, which can be seen after debugging. They need to be cut in size so areas are marked with a red marker. The composite itself is about 240 by 240 mm before cutting and after cutting it should be 200 by 200 mm. They are cut in size with a diamond water-cooled cutting machine from Carat see Figure 3.32. Protective gear such as plastic gloves, safety goggles, lab coat, dust mask and protection ear muffs must be used during this process.

On the table of the cutting machine, a paper towel is laid first, before putting the composite plate on top of it. The gelcoated side will face the paper towel, if the paper towel was not there the coating might be scratched by the table. The backside will face upward, because the stitches are showing how the fibres are aligned. The cutting is done by looking at the marked areas, alignment of the fibres and a line laser beam pointing at the composite, showing the location where the cut will take place. During cutting, the sample is held in place by applying force with hand on the composite plate. The width and length of the composite plate are also measured after each cut with a tape measure. When all four edges are cut, the composite plate will be dried off with a paper towel, because the water used for cooling the blade will make the samples wet. After cutting, measurements such as the length and width of the samples are written down. These can be found back in Appendix B, like the many other information that has been recorded in the manufacturing process of the sample.

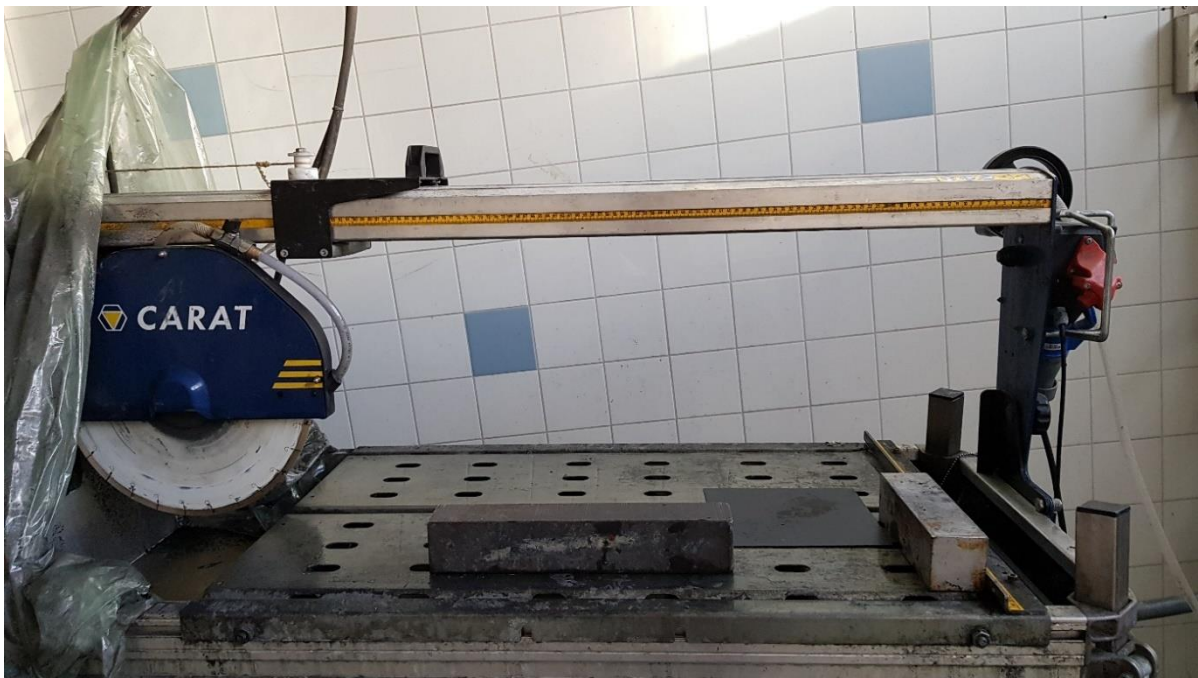


*Figure 3.32: Water cooled cutting machine (Carate).*

### 3.7 ANALYSING METHOD

In this section, methods will be explained to measure the thickness of the coating and analyse the damage caused by the impact such as, optical microscope, C-scan and laser confocal microscope.

#### 3.7.1 Optical Microscope and visual inspection

A photo camera from a smartphone, Samsung galaxy s8, is used for capturing pictures from the top and bottom sides of the whole sample. These pictures are then used to visualize the samples before and after the impact. The samples are placed on a white A3 paper and a light source is used to capture a good picture. After the samples are impacted, a measuring line will be placed along the damaged area to have an idea how big the damage is. This is done for each panel and impact session in case the damages area is bigger than that the optical microscope can capture.

In order to scan the surface damage on the sample an optical microscope is used, Keyence VR-5000, for wide area surface measurement see Figure 3.33. The samples are placed on the platform and oriented in the right position using a 3D printed block hook. Low magnification (12x) is used to capture more area in a short amount of time. Autofocus is used, before mapping the area of interest in high resolution. This area cannot be taken in one scan, therefore a couple of small areas are scanned and stitched together. After scanning, an image is shown of the top surface of the sample. This image and the measurement data is then saved so that it can be analysed further. Information can be retrieved by looking at height plots and 3d plots of the scanned surface. Calculations can also be done to determine the roughness, damaged area and volume of the selected area.



Figure 3.33: Keyence VR-5000, optical microscope.

Besides, the optical microscope is also used to capture an image from visible damage on the bottom side. The visible damage could be fibre matrix cracking and delamination, which results in whitening of the matrix material another damage that could be found is fibre breakage. The Delamination area (white area) will be compared with the delamination area found from the C-scan.

The amount of volume removal from the top surface of the composite sample could not be measured after the impact. The reason for this is that the fibres from the CSM after impact are bulging out. This interferes with the height measurement and therefore resulting in an inaccurate volume measurement, see Figure 3.34 for the volume measurement of sample 1 of CG 0.65 mm impacted 3 times with a velocity of 120 m/s. It does have a volume of 838,26 mm<sup>2</sup>, while the same sample for undergone 5 impacts has a volume of 796,23 mm<sup>2</sup>, see Figure 3.35.

Therefore, the damaged gelcoat area (DGA) is mainly compared, which is the area where the gelcoat is completely removed and the area where the gelcoat is separated from the composite plate. This information was retrieved from the optical image (OI), height plot or 3d plot. Besides the DGA, cracks and no damage in some samples are also observed. These three categories are used to characterize all samples after impact(s).

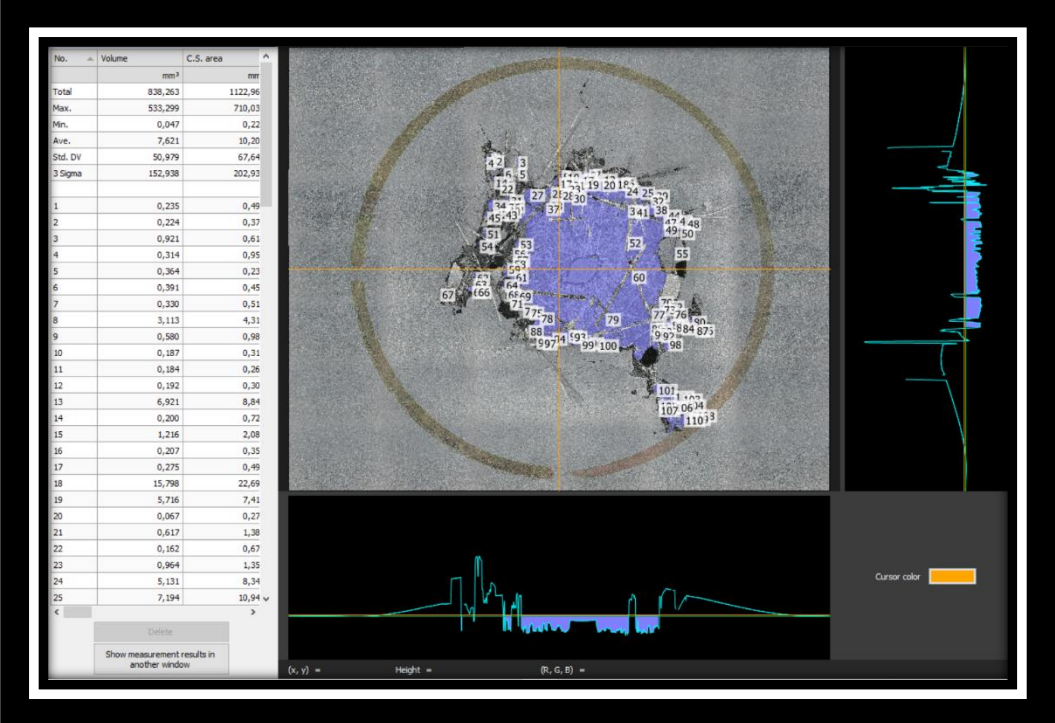


Figure 3.34: Volume measurement of sample 1 from CG 0.65 mm for 3 impacts (120 m/s).

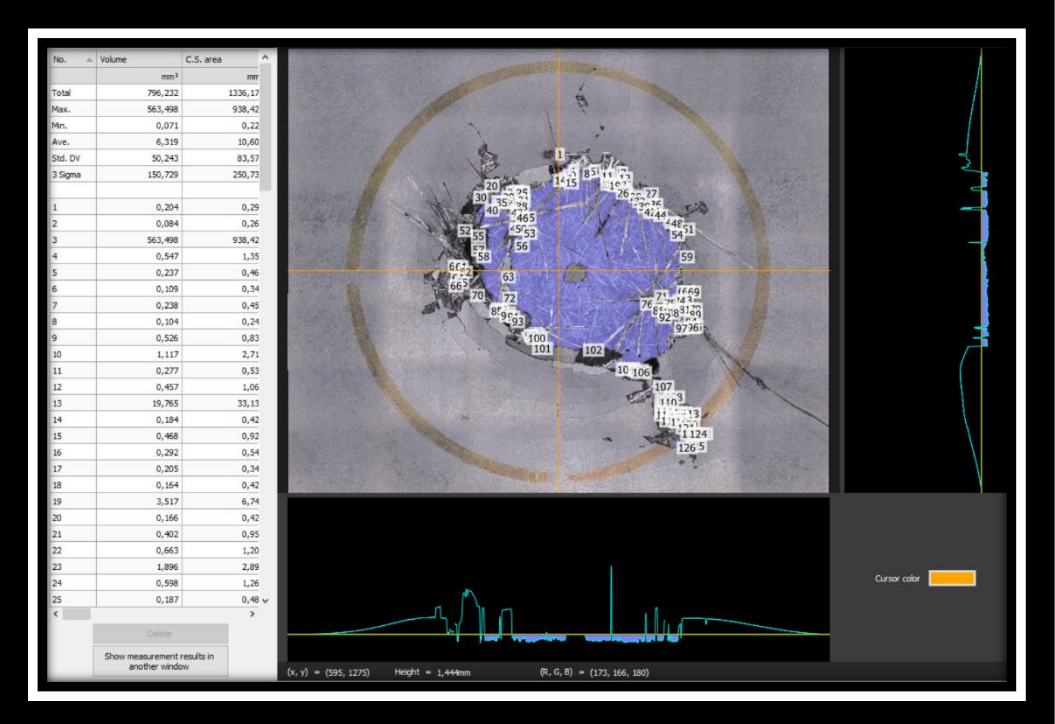


Figure 3.35: Volume measurement of sample 1 from CG 0.65 mm for 5 impacts (120 m/s).

An example of how the DGA is determined can be seen in Figure 3.36. A height plot can be seen of sample number 1 from CG 0.65 mm after 5 impacts. The area where the gelcoat is removed is in the centre having a dark blue colour (reduction in height). Blue indicates where the gelcoat is intact and all the other colours indicates an increase in height meaning that the gelcoat is separated from the composite panel. The area where an increase in height is detected has been circled around with a black marking and the area inside is known as the damaged gelcoat area, which is measured with ImageJ. When the sample had to be cut for the LSM, a picture of the cross-section was taken during that process, at the moment where the samples were cut in a smaller size. The cross-section can be seen in Figure 3.37, from the optical image it can be seen at which location the gelcoat is separated from the panel. This location is highlighted with the red line and the location where no separation is seen, is highlighted with a green line. These lines can be found back in Figure 3.36, which also shows the location where the cut is made for that cross-section.

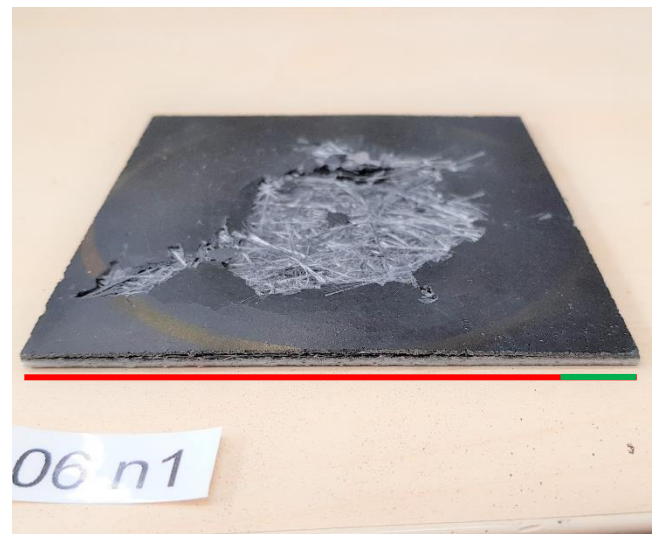
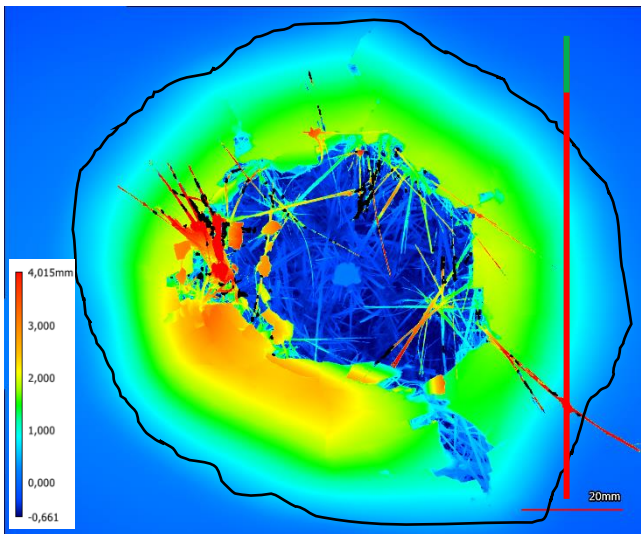


Figure 3.36: Height plot of sample 1 of CG 0.65 mm after 5 impacts. Figure 3.37: Optical image from the cross-section of sample 1 of CG 0.65 mm after 5 impacts.

The location of the black marking and the red vertical line in Figure 3.36 are compared with each other. Since they both represent the separation of the gelcoat with the CSM, the black marking should have an intersection at both tips of the red line. It can be seen that the intersection is close to the tip, but not exactly on the tip of the red line. A reason for this could be that the impact induced bending in the panel and that the height plot is slightly affected by this bending.

### 3.7.2 C-scan

An ultrasonic scanner will be used for scanning porosity and delamination in the samples see Figure 3.38. The ultrasonic scanner used here is the Olympus Epoch 650. A pulse-echo transducer sends a sound wave from one probe through the other. The samples will be clamped to a 3D printed part, which is placed over an aluminium beam. The 3D printed part is partly submerged underwater, while the samples are fully submerged underwater like the probes, because a medium (water) is needed for a good energy transfer of the sound waves from one probe to the other.

The output data of the C-scan is an excel file with dB (signal strength) values that needs to be corrected for thickness difference between the samples, because of the varying coating thickness. The correction is done in Matlab and the programming code can be found in Appendix C. After correction, the output data from the C-scan of the samples will be transformed to a coloured image starting from 2 dB (a strong signal) shown with a dark blue colour and ending with -12 dB (a weak signal) shown with a red colour. Besides the sample, a part of the sample holders and the water itself are scanned. This can be distinguished by colour change and shape. The composite does block the signal more than the water that's why the water is dark blue and undamaged composite blue and/or light blue. If there is delamination, then a red colour will be seen. The sample holder is also red due to its porosity. Delamination area represents delamination between the glass fibre layers (including the CSM), but not delamination between the gelcoat and CSM. The delamination area is then measured with ImageJ by drawing a line around the red area. The delamination area of the samples is then compared with each other.



Figure 3.38: C-scan machine.

Scanning the samples after impact brought some challenges. One challenge is that due to the impact the first layer on the back (see subsection 3.7.3 for a cross-section of a sample) is bulging out sometimes, especially coating group of 0.65 mm and 0.35 mm shot with a velocity of 120 m/s. The consequence is that when the sample is put in the water for a C-scan, water is leaking inside the composite. A disturbance of the delamination area was the effect, so a solution was needed. The first layer on the back needed to be sealed, a tape could not be used since the surface is rough through the peel ply from the vacuum infusion. Therefore, the back side of the panel where the gaps are, is lubricated with Vaseline. The solution worked, but the disadvantage is that the Vaseline is reducing the strength of the signal on the lubricated area resulting in a green colour on the C-scan image. However, the reduction is minor compared to a delamination which can be distinguished with a red colour.

Another challenge was that during the impact session the gelcoat was getting damaged and separated from the composite. When the samples are put in the water for a C-scan, air is entrapped between the gelcoat and composite. The C-scan was meant to focus on delamination only between de glass fibre layers and CSM, not between the CSM and gelcoat, because this was already looked into with the optical microscope. This problem is discovered after scanning for the third impact, the samples for the fifth impact are put longer underwater to get rid of entrapped air bubbles.

The entrapped air bubbles between the gelcoat and CSM create a red colour in the scan, similar to a delamination. Therefore, the C-scan images from the first and third impact are compared with the optical images of the bottom side of the sample. Delamination in transparent epoxy/glass fibre composites can be seen as a whitening of the epoxy-matrix. So a red area should coincide with a white area as mentioned in the methodology section.

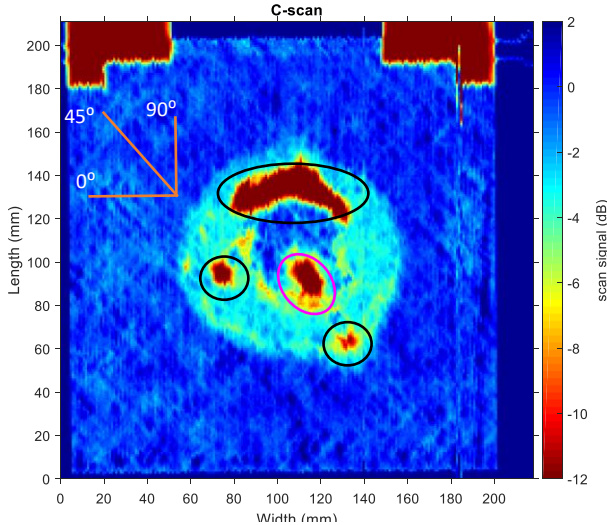


Figure 3.39: C-scan from sample 1 of CG 0.65 after 3 impacts at 120 m/s.

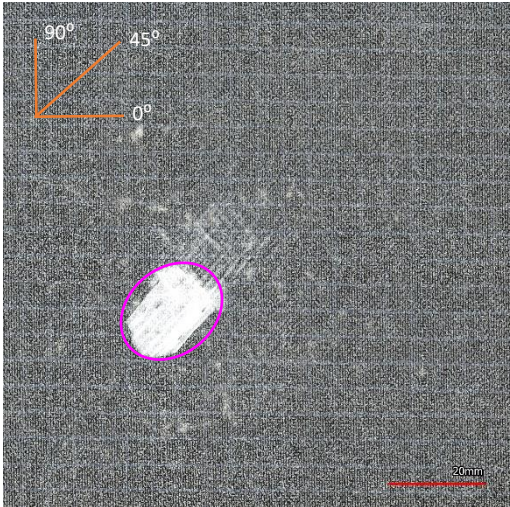


Figure 3.40: Optical image of the back side from sample 1 of CG 0.65 after 3 impacts at 120 m/s.

Figure 4.39 is a C-scan for sample 1 from group coating 0.65 mm after 3 impacts with a velocity of 120 m/s. An optical image from the backside for the same panel and test condition can be seen in Figure 4.40. The C-scan is flipped around a vertical axis at the centre, giving a different view than the optical image. Yet, similarities can be found such as the pink marked area on both figures. This is a delamination that can be found in both images. According to the C-scan image, there should also be delamination in the black circled areas, but these cannot be found back from the optical image. Additionally, the black encircled red area in the C-scan is away from the impact site (the centre), which is another reason for excluding this area in calculating the delamination area.



### 3.7.3 Laser confocal microscope

A laser confocal microscope, Keyence VK-X1000 see Figure 3.41, is used to scan the cross-section of the samples. The scans of the cross-section will give information of fibre fracture, matrix cracking, location of the delamination and coating thickness. The laser confocal microscope works the same as the optical microscope mentioned before, except that it has also a laser to scan samples. Some advantages compared to the other microscope is that the laser confocal microscope can take a more detailed scan of the surface and it can zoom in more. Disadvantages are that small objects can be scanned and it takes a longer time to scan the same area as with the optical microscope (Keyence VR-5000).

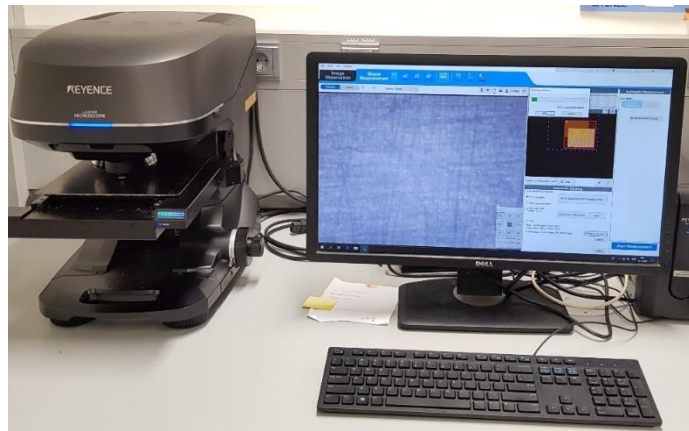


Figure 3.41: Keyence VK-X1000, laser confocal microscope.

A typical picture from the laser confocal microscope containing all the layers is shown in Figure 3.42. This is sample 5 from CG 0.15 mm after five impacts (shot with a velocity of 100 m/s). Four layers of glass fibre can be seen plus the CSM and gelcoat. The gelcoat has a black colour with white particles attached to the CSM. The bond appears to be good between those two since the gelcoat can be found in the CSM. Moreover, the resin to infuse the fibres seem to be distributed well. Previously, it was observed that fibres of the CSM were sticking out after multiple impacts. It was thought that it could be a manufacturing error, but that is not the case by looking at Figure 3.42. The gelcoat itself is brittle and it is believed that when it is combined with fibres it is more prone to damage.

The samples are cut in such a way that the first layer is in a lateral position so that if there is fibre fracture, it would be more visible to see. The first layer is more likely to have fibre fracture than the other layers due to higher tension stress on the bottom of the panel during impact. The disadvantage is that the matrix cracks at the first layer (and fourth layer) are less/not visible.

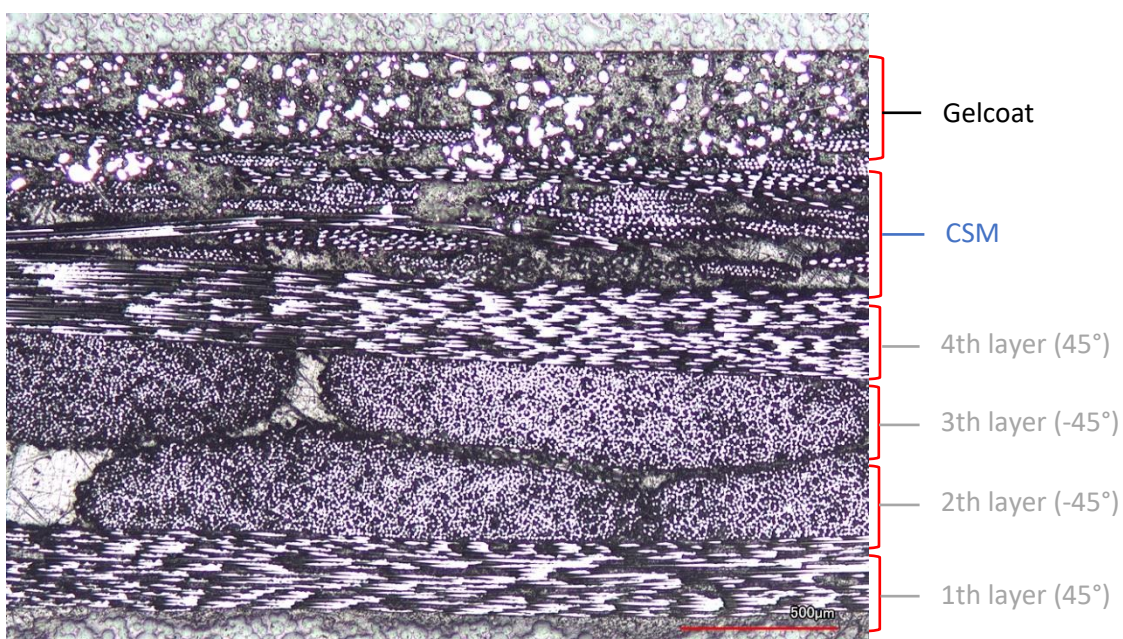


Figure 3.42: cross-section of sample 5 from CG 0.15 mm including all 6 layers.

### 3.7.3.1 Sample preparation

To gain useful information from the laser confocal microscope, the samples (200 mm by 200 mm) need to be prepared. From each sample, a small sample (20 mm by 24 mm) will be cut from the centre to scan for fibre fracture, matrix cracking and delamination depth. Furthermore, four other small samples (10 mm by 10 mm) will be cut to measure the coating thickness see Figure 3.43. First each sample (200 mm by 200 mm) will be cut in a smaller size (100 mm by 100 mm) with the same diamond cutting machine as used in section ‘cutting samples’ it is indicated with a blue square in the Figure. After the blue square area has been cut, small samples from the leftover parts are cut for determining the coating thickness see Figure 3.43, where the green squares (10 mm by 10 mm) show the areas where the small samples are going to be cut. This location is chosen because close to the centre there is most of the time no coating. However, the location should also be close to the centre of the sample (200 mm by 200 mm) in order to give a good indication of the coating thickness on the impact site.

The blue square in Figure 3.43 is cut, because the sample in the centre will be cut with another cutting machine, where only small samples fit. For this, the Struers Secotom-10 cutting machine is used with a diamond cutting wheel from the brand Stuers, M1D20. The rounds per minute (RPM) is set to 3000 and the feed rate is 1 mm per second. The reason for using another cutting machine is that the last mention machine doesn’t leave damage or just minor damage. It is important to leave no damage on the sample cut from the centre otherwise, it will be unknown if it happened from the impact or from the cutting. This was less important for the other four samples (10 mm by 10 mm) since only the coating thickness is going to be measured. Any form of damage is also removed in the sanding and polish step, which will be explained later. In Figure 3.43, it can be seen that the sample in the centre is marked green with also a red marking. The red marking indicates the area that will be lost during sanding and polishing. Lengthwise it will be approximately 4 mm and it is taken into account that after loss of material, the to be scanned cross-section is still the centre.

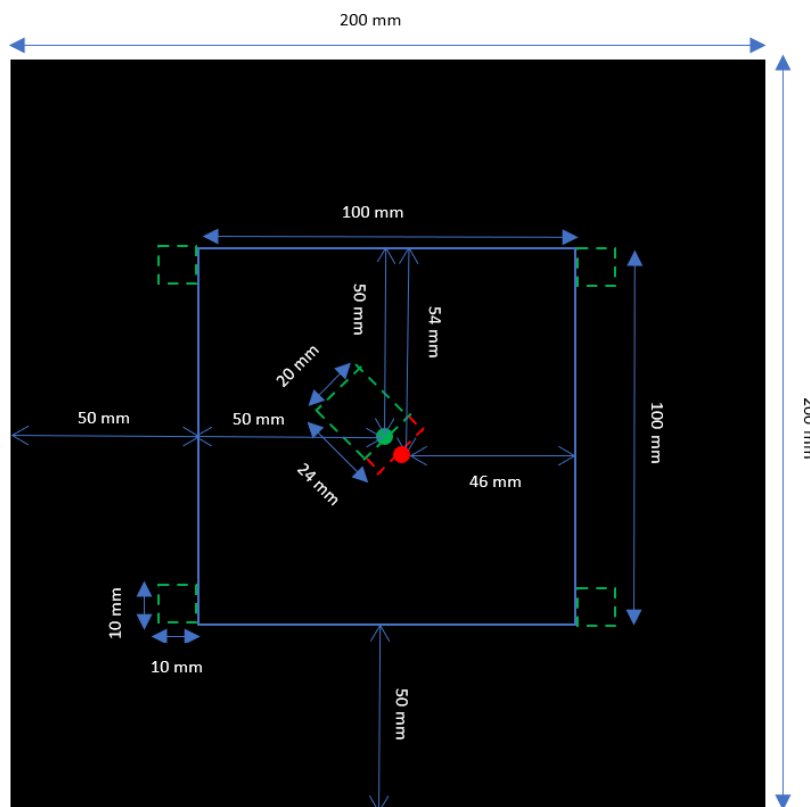


Figure 3.43: Cutting area for coating thickness determination and cross-section analysis.

There are 60 small samples in total (10 mm by 10 mm) for determining the coating thickness and 15 small samples in total (20 mm by 24 mm) for analysing damage from the impact. The width of the last mention samples, which is 20 mm, can be bigger for some samples in order to capture more information from one side of the centre.

The samples are laid in a row of 5 or 6 perpendicular on a table and stuck to each other with a small aluminium plate containing double-sided tape on both sides. This stack of small samples is then put in a mould with two openings, in which one can be closed see Figure 3.44. Further, the mould will be filled with a resin to fix the samples in a certain position. For the resin, two spoons of Technovit 47 powder (hardener) and one spoon of Technovit 47 Liquid (base agent) are mixed in a cup and then later poured into the mould. The resin cures fast, after five minutes the samples can be removed from the mould.



Figure 3.44: Samples placed in the mould.



Figure 3.45: Samples embedded in resin.

To get a good view of the cross-section of the composite panels, the samples should be sanded first. A Struers DAP-7 machine is used in combination with a silicon carbide sanding paper, it will be done in five different grain sizes. Starting with an 82  $\mu\text{m}$  sanding paper and continue the process with 36  $\mu\text{m}$ , 18  $\mu\text{m}$ , 8  $\mu\text{m}$  and lastly 5  $\mu\text{m}$ . These sanding papers are clamped first and then turned with 250 rounds per minute (RPM). Moreover, the DAP-7 machine contains a water tap, which is turned on during the process. Each sanding step takes two minutes and a timer is used during sanding to keep track of the time. After sanding, Polishing is needed to finish the process. This is done on the same machine as with sanding, besides the same RPM is used. The grain sizes of the polishing cloths are 6  $\mu\text{m}$ , 3  $\mu\text{m}$  and 1  $\mu\text{m}$ . starting from the high grain size to the smallest one. In each polishing step, the samples are cleaned with ethanol and polished for 1 minute with their corresponding paste. Cleaning with ethanol is done to prevent contamination from one cloth to the other. The end results of preparing the samples for the laser confocal microscope can be seen in Figure 3.45.

### 3.7.3.2 Dry coating thickness measurement

From each sample, four smaller samples (10 mm by 10 mm) are collected as mention before in subsection 3.7.3.1. Each small sample is scanned in the width at 5 locations meaning that there are 20 thickness measurements per sample to determine its average coating thickness (ACT) and the corresponding standard deviation. Thickness measurement at a location is done with line measurement via the Keyence software.

A schematic example of the gelcoat (black) is given in Figure 3.46. The two red lines show how the line measurement is done. The top side of the gelcoat is smooth so that could be easily aligned. The bottom side of the gelcoat showed sometimes a skew so the red line is placed at the same angle. Besides that it is skewed, it is also locally thick, the red line is placed in the middle of the local thick areas. The software forms a line in the middle of the two red lines shown as an orange dotted line in the figure. The length of this line will be the coating thickness of that location.

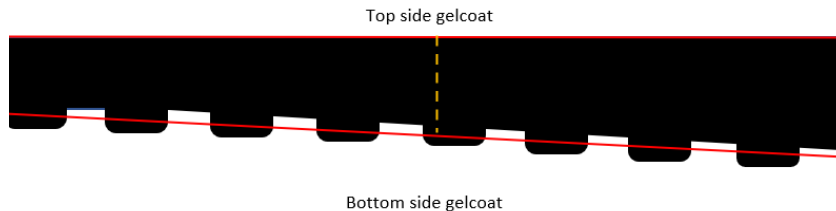


Figure 3.46: Schematic sketch of a gelcoat (black) and the location where line measurement is done (in red).

### 3.7.4 Differential scanning calorimetry

The gelcoat is partially cured on the sample at room temperature. According to Saltz W.T. [12] small coating thicknesses tend to undercure (low degree of cure). The gelcoat itself is forming an exothermic reaction when mixed, it is expected that more gelcoat mass is going to induce more heat resulting in a difference of curing between the varying gelcoat thicknesses. To check if all varying gelcoat thicknesses have the same degree of cure, a heat analysis is performed after the last (fifth) impact. To do this, a small quantity of the gelcoat is scraped of the samples (6 per coating group) with a chisel. This is put in a small glass bottle before testing it with the differential scanning calorimetry (DSC). The TA instruments DSC 250 is used for a thermal analysis see Figure 3.47. 3.5 mg of gelcoat is put in an aluminium pan, which is closed afterwards. The DSC compares the heat flow per temperature with this pan and empty reference aluminium pan. The samples are heated from room temperature to 350 °C with a ramp of 10 °C per minute. During heating, a coating that is not fully cured should cure during the process. Curing of the epoxy gelcoat results in an exothermic reaction, which should show an increase in the heat flow curve. An example of a heat flow curve can be seen in Figures 3.48, which shows a decrease in heat flow between 25 °C and 50 °C (endothermic reaction), then it starts to increase with one small peak and a second bigger peak, which are exothermic reactions. The area underneath the first small peak, reaction enthalpy (J/g), is compared between the varying gelcoat thicknesses. After 260 °C, there is another exothermic reaction going on, but the area underneath could not be calculated because the temperature range is chosen too short.



Figure 3.47: TA instruments DSC 250.

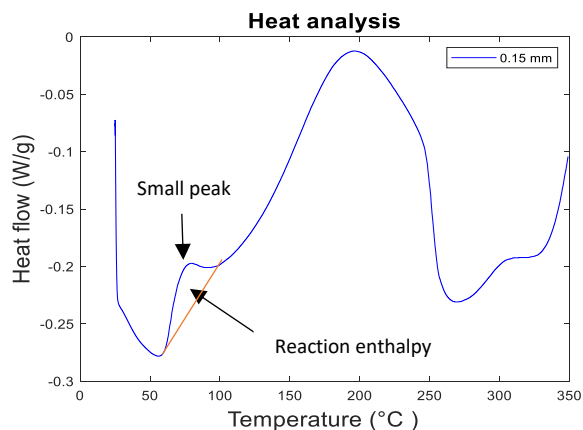


Figure 3.48: Heat flow curve of sample 2 from CG 0.15 mm with marked area indicating the area that is going to be measured, which is called reaction enthalpy.

## 4 RESULTS AND DISCUSSION

In chapter 4, the results from the performed analysis are shown, which is also discussed. The chapter is divided into 4 sections in the same order as mentioned: First the kinetic energy, gelcoat thickness and DSC, then optical microscope and visual inspection, afterwards C-scan and finally laser confocal microscope.

### 4.1 KINETIC ENERGY, GELCOAT THICKNESS AND DSC

There are two subsection as written in the title section: one is about kinetic energy of the SHI just before it hits a sample and the other subsection is about the gelcoat thickness.

#### 4.1.1 Kinetic energy

The mass and velocity of the SHIs can be found in Appendix D, they are used to calculate the kinetic energy. The kinetic energy is used as a measure of how much impact energy the sample is subjected to. The next formula is used to calculate the kinetic energy where M is the mass in kg and V is the velocity in m/s:

$$E_k = 0.5 * M * V^2 \quad (1)$$

The kinetic energy is calculated for each impact and summed for all five impacts. This is called the accumulated kinetic energy. The kinetic energy for each impact and the accumulated energy can be found in Table 4.1. It happened twice that the velocity of the SHIs was not detected by the IR sensor during the second impact. Calculation of the kinetic energy was not possible anymore, leaving no value for the accumulated kinetic energy for those specific samples (marked in yellow in Table 4.1).

Kinetic energy							
Speed	S = sample	First impact	Second impact	Third impact	Fourth impact	Fifth impact	Accumulated
120 m/s	S1 of 0.65 mm	33.0 ± 1.6 J	31.8 ± 1.6 J	30.9 ± 1.6 J	29.0 ± 1.5 J	30.0 ± 1.5 J	154.7 ± 3.5 J
	S2 of 0.65 mm	28.0 ± 1.5 J	28.4 ± 1.5 J	27.0 ± 1.4 J	29.1 ± 1.5 J	27.8 ± 1.5 J	140.3 ± 3.3 J
	S3 of 0.65 mm	26.7 ± 1.4 J	-	31.1 ± 1.6 J	28.4 ± 1.5 J	27.2 ± 1.4 J	-
100 m/s	S1 of 0.35 mm	29.8 ± 1.5 J	29.1 ± 1.5 J	29.1 ± 1.5 J	30.0 ± 1.5 J	29.9 ± 1.5 J	147.9 ± 3.4 J
	S2 of 0.35 mm	26.0 ± 1.6 J	26.9 ± 1.6 J	30.6 ± 1.5 J	29.4 ± 1.5 J	28.3 ± 1.6 J	141.2 ± 3.4 J
	S3 of 0.35 mm	29.4 ± 1.6 J	30.7 ± 1.5 J	28.2 ± 1.6 J	28.7 ± 1.5 J	29.3 ± 1.5 J	146.2 ± 3.4 J
90 m/s	S1 of 0.15 mm	34.6 ± 1.7 J	32.4 ± 1.6 J	29.1 ± 1.5 J	31.1 ± 1.5 J	30.4 ± 1.5 J	157.6 ± 3.5 J
	S2 of 0.15 mm	32.9 ± 1.6 J	31.3 ± 1.6 J	29.5 ± 1.5 J	28.4 ± 1.5 J	31.5 ± 1.6 J	153.6 ± 3.4 J
	S3 of 0.15 mm	31.6 ± 1.6 J	29.9 ± 1.5 J	31.6 ± 1.6 J	29.1 ± 1.5 J	30.5 ± 1.5 J	152.7 ± 3.4 J
	S5 of 0.15 mm	18.9 ± 1.2 J	20.0 ± 1.2 J	15.3 ± 1.1 J	21.4 ± 1.3 J	21.6 ± 1.3 J	97.2 ± 2.7 J
	S6 of 0.15 mm	23.4 ± 1.3 J	-	23.0 ± 1.3 J	22.3 ± 1.3 J	22.5 ± 1.3 J	-
	S7 of 0.15 mm	21.8 ± 1.3 J	22.7 ± 1.3 J	21.3 ± 1.3 J	22.1 ± 1.3 J	21.0 ± 1.3 J	108.9 ± 2.9 J
	S8 of 0.15 mm	15.5 ± 1.1 J	16.6 ± 1.1 J	17.4 ± 1.2 J	16.3 ± 1.1 J	16.8 ± 1.1 J	82.6 ± 2.5 J
	S9 of 0.15 mm	13.4 ± 1.0 J	16.5 ± 1.1 J	17.2 ± 1.1 J	17.1 ± 1.1 J	16.0 ± 1.1 J	80.2 ± 2.5 J
S10 of 0.15 mm	18.3 ± 1.2 J	16.7 ± 1.1 J	17.0 ± 1.1 J	16.8 ± 1.1 J	15.3 ± 1.1 J	84.2 ± 2.5 J	

Table 4.1: Kinetic energy per impact and the accumulated kinetic energy.

The standard deviation for the kinetic energy is also included in Table 4.1 to have an idea if the data values are overlapping each other, it is calculated with the next formula:

$$\sigma_{Ek} = \sqrt{(0.5 * V^2)^2 * \sigma_m + (M * V)^2 * \sigma_v^2} \quad (2)$$

$\sigma_m$  = standard deviation of the mass, which is 0.00005 kg. and  $\sigma_v$ = standard deviation of the IR sensor is 3 m/s. The standard deviation for the accumulated kinetic energy can be calculated by using the next formula:

$$\sigma_{Ekacc} = \sqrt{\sigma_{Ek1}^2 + \sigma_{Ek2}^2 + \sigma_{Ek3}^2 + \sigma_{Ek4}^2 + \sigma_{Ek5}^2} \quad (3)$$

#### 4.1.2 Gelcoat thickness

The average coating thickness with its standard deviation of each sample is shown in Table 4.2. The individual samples of the three coating groups (0.65 mm, 0.35 mm and 0.15 mm) are compared with each other by their average coating thickness (ACT). Variation in the coating thickness was expected. It can be seen that sample 2 of CG 0.65 mm has 0.082 mm thicker coating than it should have (marked in a red colour in the table). The standard deviation is also about 2-3 times higher than all the other samples. CG 0.35 mm on the other hand, has not such high deviations in ACT. Sample 3 of this group deviates to most of the targeted thickness, 0.021 mm, which is 4 times less than sample 2 of CG 0.65 mm. In addition, the sample with the highest deviation in ACT from CG 0.15 mm is sample 5 with 0.033 mm, still about 2.5 times less than sample 2 of CG 0.65 mm.

Samples name	Average coating thickness
Sample 1 of 0.65 mm	0.612 ± 0.069 mm
Sample 2 of 0.65 mm	0.732 ± 0.12 mm
Sample 3 of 0.65 mm	0.642 ± 0.039 mm
Sample 1 of 0.35 mm	0.343 ± 0.067 mm
Sample 2 of 0.35 mm	0.352 ± 0.044 mm
Sample 3 of 0.35 mm	0.329 ± 0.040 mm
Sample 1 of 0.15 mm	0.150 ± 0.040 mm
Sample 2 of 0.15 mm	0.121 ± 0.026 mm
Sample 3 of 0.15 mm	0.129 ± 0.040 mm
Sample 5 of 0.15 mm	0.183 ± 0.047 mm
Sample 6 of 0.15 mm	0.140 ± 0.027 mm
Sample 7 of 0.15 mm	0.152 ± 0.031 mm
Sample 8 of 0.15 mm	0.180 ± 0.049 mm
Sample 9 of 0.15 mm	0.145 ± 0.039 mm
Sample 10 of 0.15 mm	0.135 ± 0.042 mm

Table 4.2: Average coating thickness with its standard deviation.

The minimum and maximum average coating thickness (ACT) measured per coating group (CG) is plotted in Figure 4.1 in a bar chart (orange rectangle). Note that CG of 0.15 mm has more samples taken to form a bar chart. The error bars represent the lowest and highest value of gelcoat thickness. It can be noticed that the range of the standard deviation for the three coating thicknesses does not overlap each other, meaning that there is enough difference in thickness.

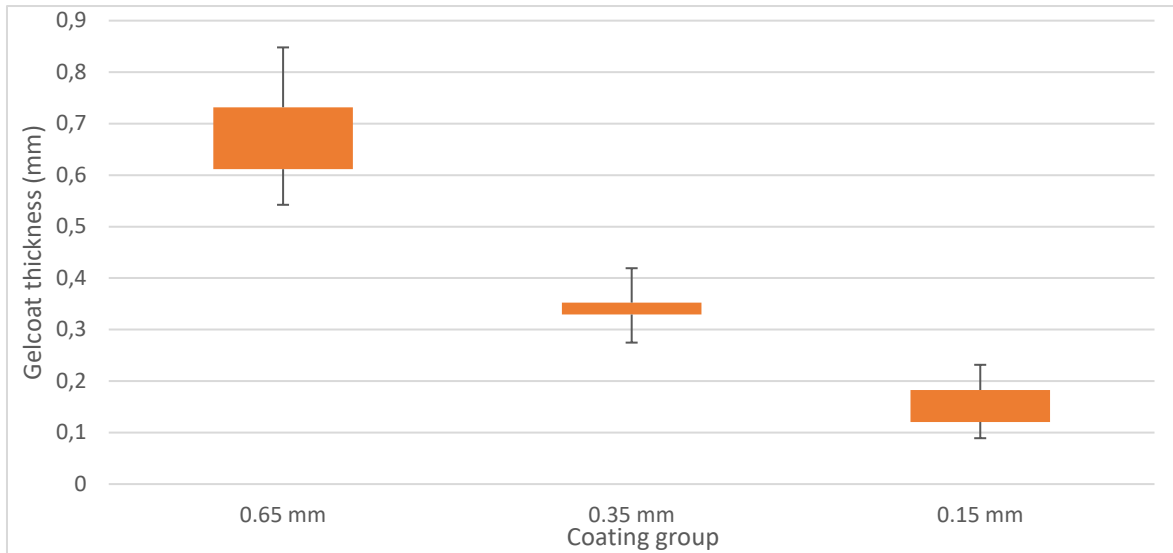


Figure 4.1: Bar chart of (possible) gelcoat thicknesses for each CG.

#### 4.1.3 DSC

There are 18 heat flow curves in total, but only one is plotted from each CG in Figure 4.2 to have a clear view. All curves have a similar shape and the average reaction enthalpy is taken for each CG, these values are shown in Figure 4.3. It was expected that the smaller coating groups would have more undercure (low degree of cure) in the gelcoat. Therefore, a higher average reaction enthalpy was expected for the thinner CGs, but it can be seen that the average reaction enthalpy becomes higher for a thicker coating thickness. However, the average reaction enthalpy between the coating groups is close to each other -7.5 J/g for CG 0.15 mm and -8 J/g for CG 0.65 mm. The standard deviation is also overlapping each other so it is difficult to say that a thicker coating thickness results in more reaction enthalpy. From the results, it can be concluded that the CGs have almost the same amount of undercure (low degree of cure).

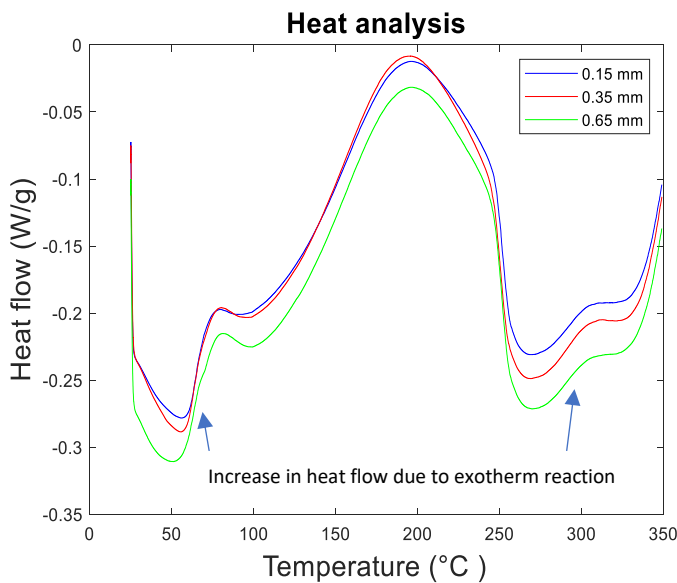


Figure 4.2: Heat flow curve per temperature for sample 2 of CG 0.65 mm, 0.35 mm and 0.15 mm.

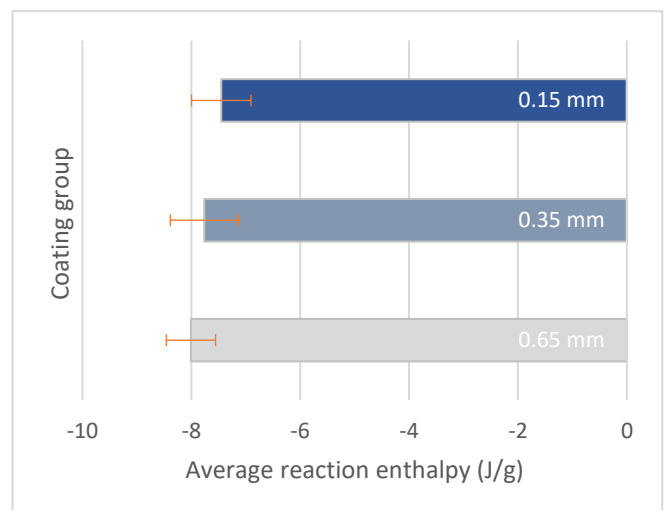


Figure 4.3: Average reaction enthalpy (J/g) for CG 0.65 mm, 0.35 mm and 0.15 mm.

## 4.2 OPTICAL MICROSCOPE AND VISUAL INSPECTION

The section is divided into two subsections: Before impact and damage progression. The first will focus if there is any damage before shooting a SHI. The second one explains first that the amount of volume removal of the sample could not be compared. Subsequently, the method that is used to compare the sample is criticized, after which the results are shown. Next, a discussion is made about the results and the factors that could influence that. And finally, optical images from the back side of the samples are shown. The delamination that can be seen will be discussed about its shape. A size comparison will be made in the C-scan section.

### 4.2.1 Before impact

A visual inspection was performed after manufacturing the composite panels to make sure that the process went well. An example of a good manufactured composite plate is sample 3 of CG 0.15 mm, see Figure 4.4 for an image of the front side and Figure 4.5 an image of the back side. On the front side (coating) no scratches are found. The black circle around the centre has a radius of 50 mm and is only meant to provide extra perspective in the case of damage. On the back side of the sample are no defects. The horizontal and vertical white lines on the back of the sample are stitches to hold the fibre bundles in place, which can be seen due to the transparency of the matrix material. To check for porosity/delamination the C-scan is used see section 4.5. The delamination can also be seen with the naked eye as a whitening of the matrix material.

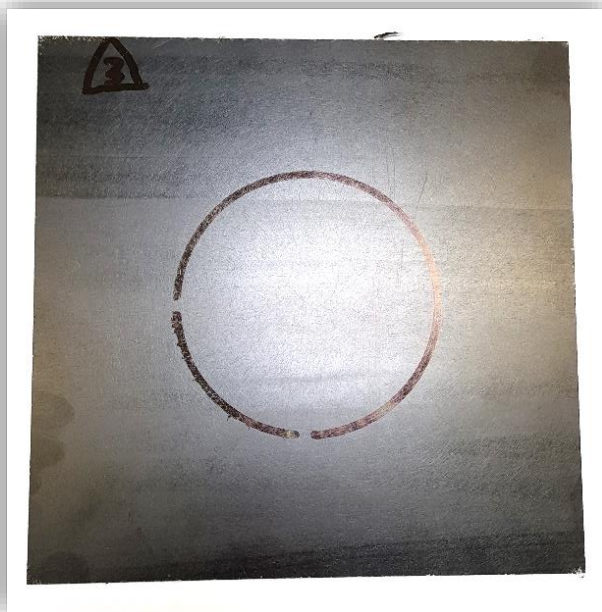


Figure 4.4: Front side of sample 3 from CG 0.15mm.



Figure 4.5: Back side of sample 3 from CG 0.15 mm.

Sample number 2 of CG 0.35 mm has small scratches on the coating, which happened during debagging see Figure 4.6. During debagging the sample is moved around to loosen it from the peel ply and the infusion mesh. If dirt or parts of the coating fall between the coating and the aluminium plate, it can damage the coating when this is moved around. The scratches are small and cannot be seen in the height plot see Figure 4.7. The scratches are also more on the right bottom corner, so the influence of the scratches on the test is minimal since the SHIs are shot in the centre.



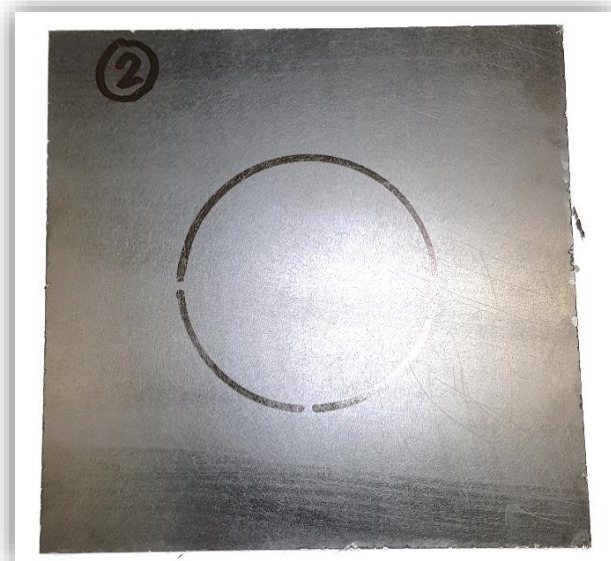


Figure 4.6: Sample 2 of CG 0.35 mm with small scratches.

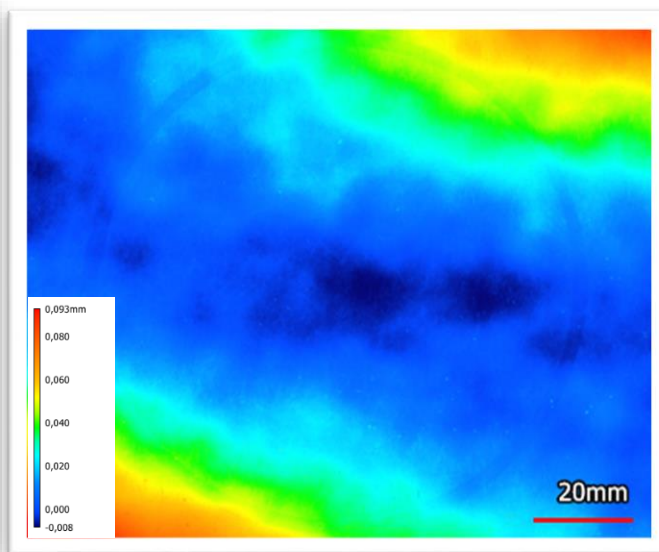


Figure 4.7: Height plot of sample 2 of CG 0.35 mm.

Some of the samples do have a white spot on the back side, see Figure 4.8 for sample 3 of CG 0.35 mm and Figure 4.7 for sample 4 from the same CG. These white spots are dry spots, which indicate that at these locations the fibres are less or not merged with resin. The other samples have fewer dry spots and are further away from the impact area. The dry spots are not excluded from the factors having an influence on the damage resistance of the samples. Therefore, it will be taken into account when there is a variation in damage between samples. Sample 4 from CG 0.35 mm (in Figure 4.9) is discarded since this was an extra sample and it did contain dry spots. This is also done for sample number 4 of the other CGs.

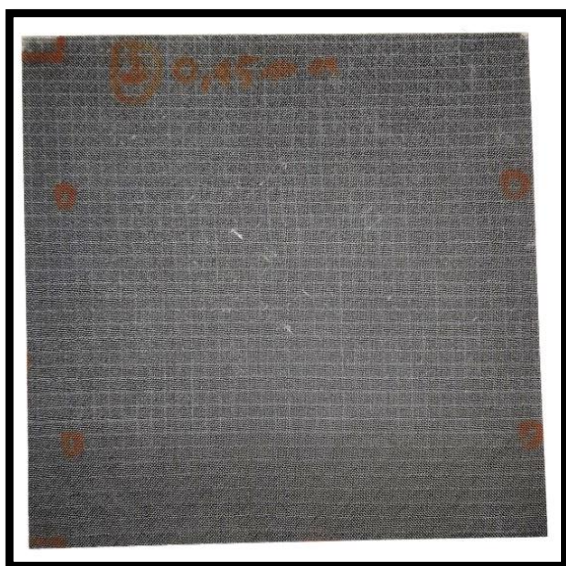


Figure 4.8: Sample 3 of CG 0.35 mm containing dry spots.



Figure 4.9: Sample 4 of CG 0.35 mm containing dry spots.

Notable from the impact test is that the separation of the gelcoat from the panels happens in the CSM. This indicates that the bond there is the weakest. Furthermore, it was observed that the glass fibre from the CSM was sticking out. A reason for this could be that the resin might have a low content in the CSM. This could explain the weak bonding in the CSM. And will be further investigated in the laser microscope section.

The samples from CG 0.15 mm that are shot with 90 m/s showed no damage on the coating except for sample 8, which showed cracks after five impacts see Figure 4.10. These cracks are observed by moving a red line along the optical or height image in the microscope software, which measured the roughness at that location, see Appendix E for roughness images of other samples. When samples with the same coating thickness are shot with 100 m/s, cracks are more observed on these samples, even at the first impact. In addition, sample five even showed 14.28 mm<sup>2</sup> damaged area of the gelcoat after five impacts.

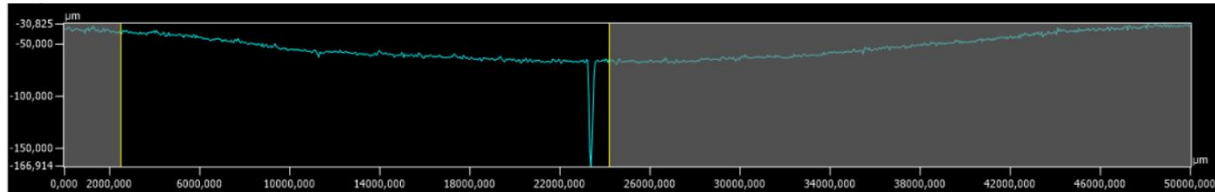


Figure 4.10: Roughness image from sample 8 of CG 0.15 mm after 5 impacts.

Increasing the velocity to 120 m/s for the same coating thickness, showed more cracks and more damaged gelcoat area (DGA). All three samples (with gelcoat thickness 0.15 mm) tested with this velocity showed a DGA after five impacts, by which the lowest one is 20.24 mm<sup>2</sup> and the highest one is 475.11 mm<sup>2</sup>. For the same impact conditions, the 0.35 mm and 0.65 coated panels showed less variation in DGA for the samples with the same thickness. The 0.35 mm and 0.65 mm coated samples showed a DGA 5 and 13 times higher than the highest value of the 0.15 mm coated samples, respectively, see Appendix F for a full overview of the type and amount of damage on the gelcoat.

With only looking at coating removal it can also be noticed that a thicker coating has more coating removal. An example is given in Figure 4.11 with sample 1 of CG 0.15 mm after 5 impacts with a velocity of 120 m/s and in Figure 4.12, for the same test parameters, sample 1 of CG 0.45 mm is shown which has clearly more damage. Another optical image from sample 3 of CG 0.65 mm is also included with the same previously mentioned test parameters to make the picture complete, see Figure 4.13. Comparing these three images with each other shows that indeed the thicker the CG is, the more gelcoat removal there is.

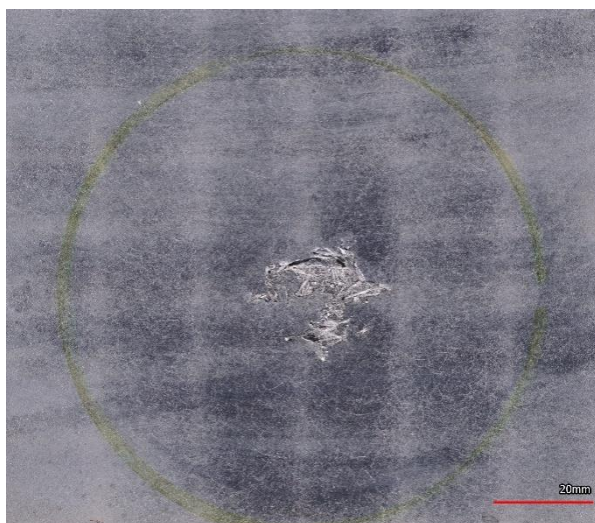


Figure 4.11: OI from sample 1 of CG 0.15 mm after 5 impacts. Figure 4.12: OI from sample 1 of CG 0.45 mm after 5 impacts.

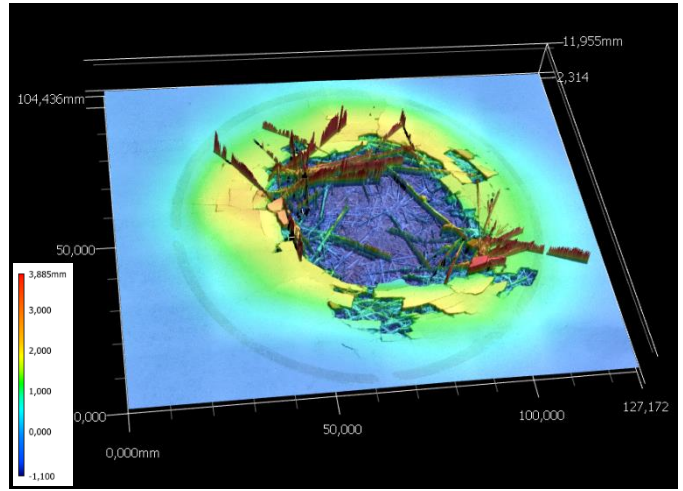
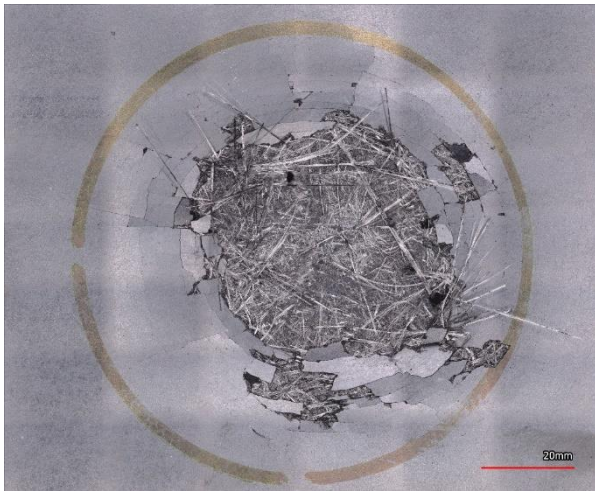


Figure 4.13: OI from sample 1 of CG 0.65 mm after 5 impacts. Figure 4.14: 3D plot from sample 1 of CG 0.65 mm after 5 impacts.

It is less noticeable on samples with a small coating thickness, but for samples from coating group 0.65 mm, ring-shaped cracks could be seen like in Figure 4.14, where a 3D plot of sample 1 of CG 0.65 mm is shown after 5 impacts. There are multiple formations of ring-shaped cracks in the gelcoat. Furthermore, most of the time a part of the gelcoat is left at the centre, exact at the location where the SHI is shot. This phenomenon can be explained from the research that Keegan M. H. [4] did. He performed simulations with a 20 mm SHI on a stand-alone epoxy gelcoat. The SHI is shot with a velocity of 100 m/s. The effective von-Mises stress (Pa) and plastic strain from the impact is shown in Figure 4.15 and 4.16, respectively. Both Figures show their highest value in rings away from the centre, whereas the centre shows a relatively low value for the effective von-Mises stress and plastic strain. This gives confirmation that the process for shooting a SHI on a gelcoated composite plate went well.

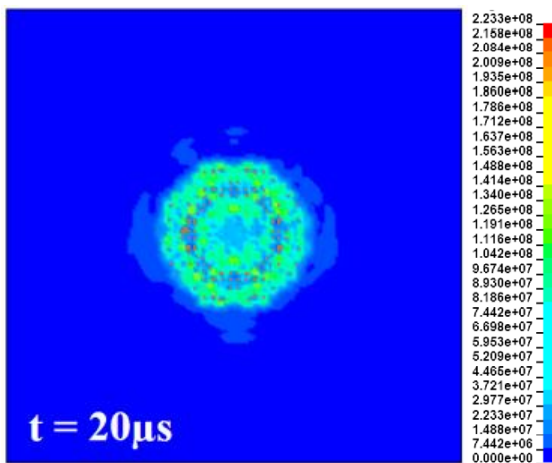


Figure 4.15: Effective von-Mises stress (Pa) in gelcoat from a 20 mm SHI shot at 100 m/s, modified from [4].

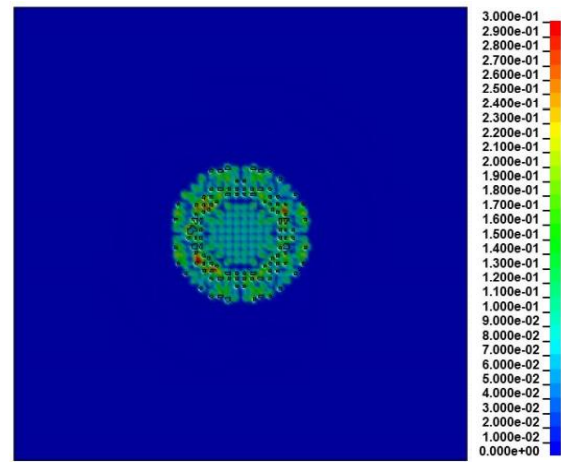


Figure 4.16: Effective plastic strain in gelcoat from a 20 mm SHI shot at 100 m/s, The black marking show the areas that has been eroded, modified from [4].

The progression of the DGA for the three different coating thicknesses test at 120 m/s is shown in Figure 4.17 clustered per number of impacts. The average of the DGA is plotted since each coating thickness has three samples for a test at 120 m/s. Further, the error bars show the lowest and highest amount of area removal from all the samples tested from a coating thickness. A value of zero for DGA means either no damage or cracks. From Figure 4.17, it can be seen that a 0.15 mm coated sample has the lowest amount of DGA and 0.65 mm coated sample the highest. Further, all samples are showing more or less a linear increasing DGA. The error bars from the CGs are not overlapping each other.

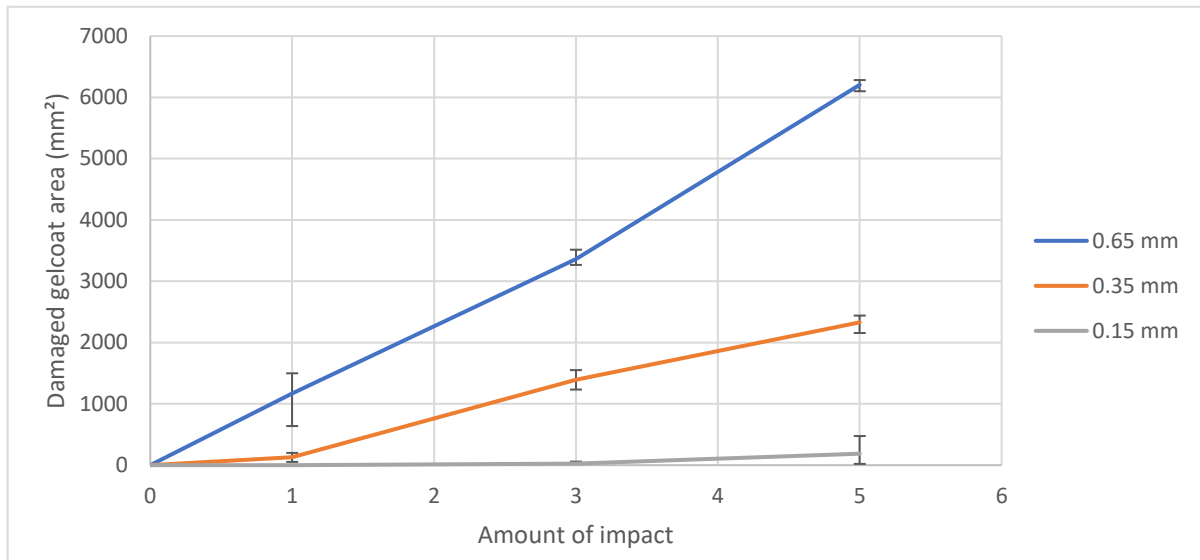


Figure 4.17: Average damaged gelcoat area for the three coating groups impacted at 120 m/s.

New plots of the DGA for individual samples were made to check if the previously shown graphs show a similar damage progression. In Figure 4.18, the DGA for the individual panels of 0.15 mm coated samples is given. It can be seen that panel 1 deviates more in DGA than the other two panels between the third and fifth impact. Looking at Table 4.1 for the kinetic energy gives about 8 % (2-3 J) higher kinetic energy for panel 1 at the fourth impact compared to the other two samples. The fifth impact for sample 1 has no higher kinetic energy than the other two samples. Further, the accumulated kinetic energy is only 2 % (6-7 J) higher than the other two panels. From the optical images, no dry spots could be seen on these three panels. That means that only 2 % (6-7 J) difference of kinetic energy should have led to 800 % more DGA. The 2 % higher accumulated kinetic energy is on the low side, a higher percentage would be more realistic for 800 % extra damage. Besides, there is also a possibility that the accumulated kinetic energy for all three samples is the same by looking at its standard deviation. One reason could be due to a thicker coating thickness, because sample 1 has an ACT of 0.150 mm, while panel 2 and 3 have an ACT of 0.121 mm and 0.129 mm, respectively. This is difficult to say, because the ACT is overlapping due to a high standard deviation.

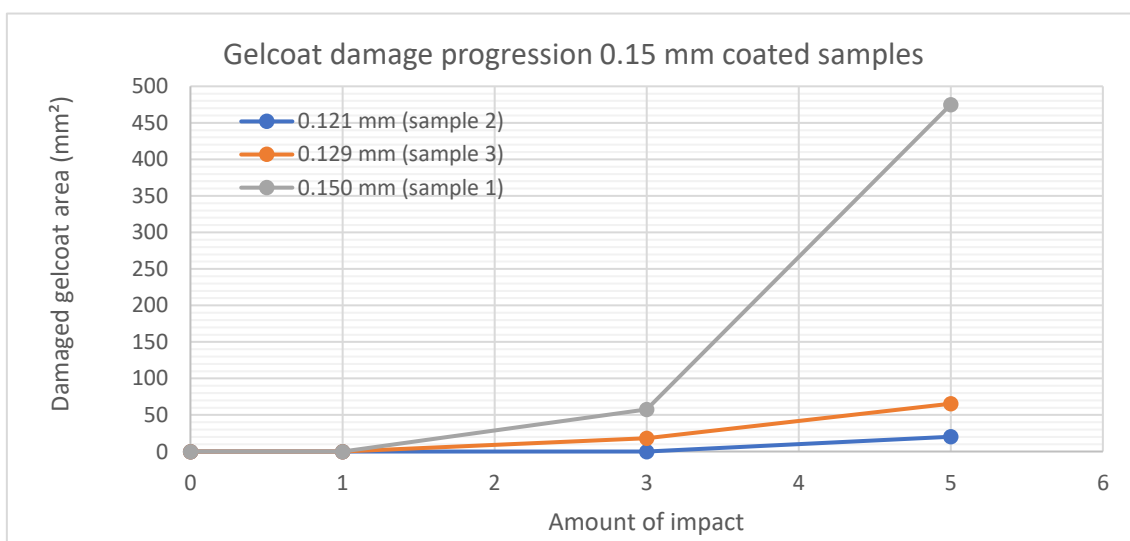


Figure 4.18: Damaged gelcoat area for individual samples of CG 0.15 mm impacted at 120 m/s.

In Figure 4.19, is the DGA for the individual samples of 0.35 mm coated sampled. The graphs of these three panels look the same, no outliers can be seen. However, this can be seen for one of the samples in CG 0.65 mm see Figure 4.20. Sample 3 has definitely a lower DGA than the other two samples for the first impact. These samples are also checked for defects, but none was found. Further, sample 3 had 5 % lower kinetic energy than sample 2 for the first impact, the last mention sample is also 15 % (0.090 mm) thicker, than sample 3 having a ACT of 0.642 mm. Therefore, these two should have a difference in DGA, which is the case, so now samples 3 and 1 will be compared. Sample 1 has 24 % more kinetic energy than sample 3, but a slightly thinner ACT, 5 % (0.030 mm) thinner. The ACT of both panels could overlap each other, but it has a relatively higher kinetic energy, which could be an explanation for the difference in DGA for samples 3 and 1.

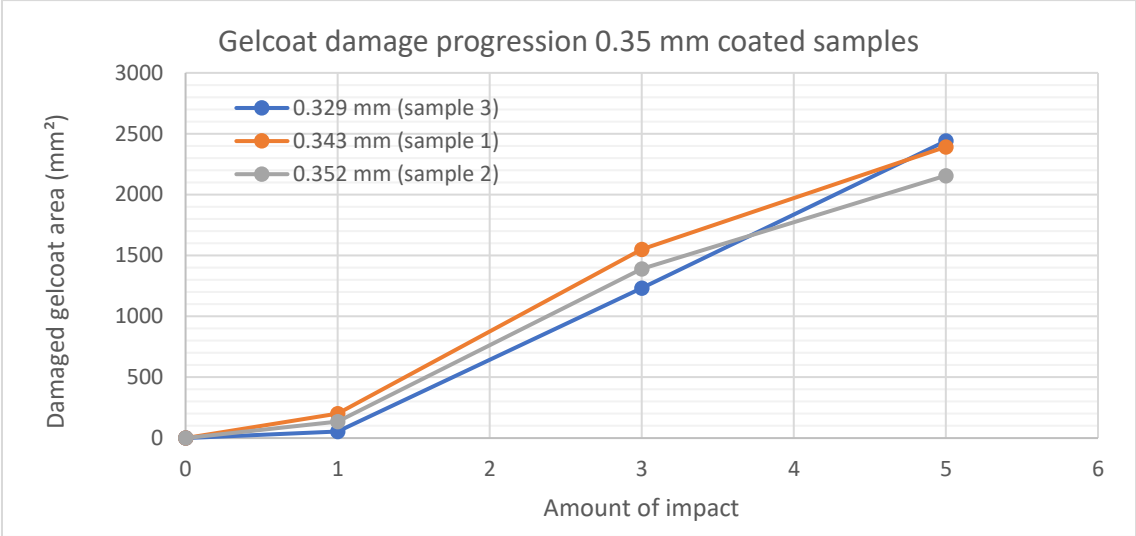


Figure 4.19: Damaged gelcoat area for individual samples of CG 0.35 mm impacted at 120 m/s.

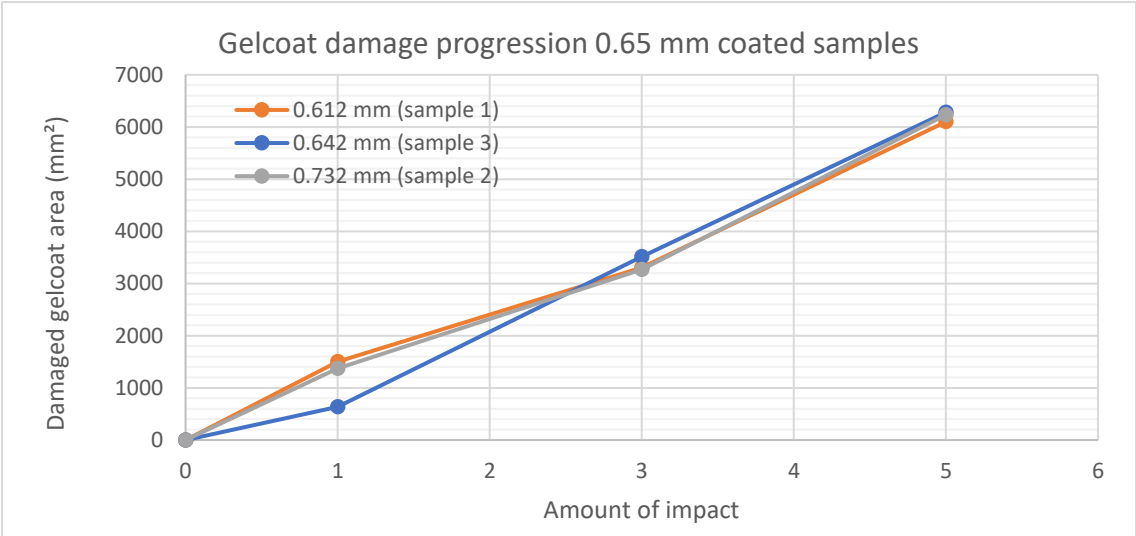


Figure 4.20: Damaged gelcoat area for individual samples of CG 0.65 mm impacted at 120 m/s.

To elaborate further on the influence of kinetic energy on the damaged gelcoat area, it is less likely that a different accumulated kinetic energy among the samples tested with 120 m/s has an influence on the DGA. This argument is further substantiated with Figure 2.21, where the damaged gelcoat area is plotted against the available accumulated kinetic energy data. It can be seen that there is no relationship like the higher the accumulated kinetic energy, the higher the DGA, or vice versa.

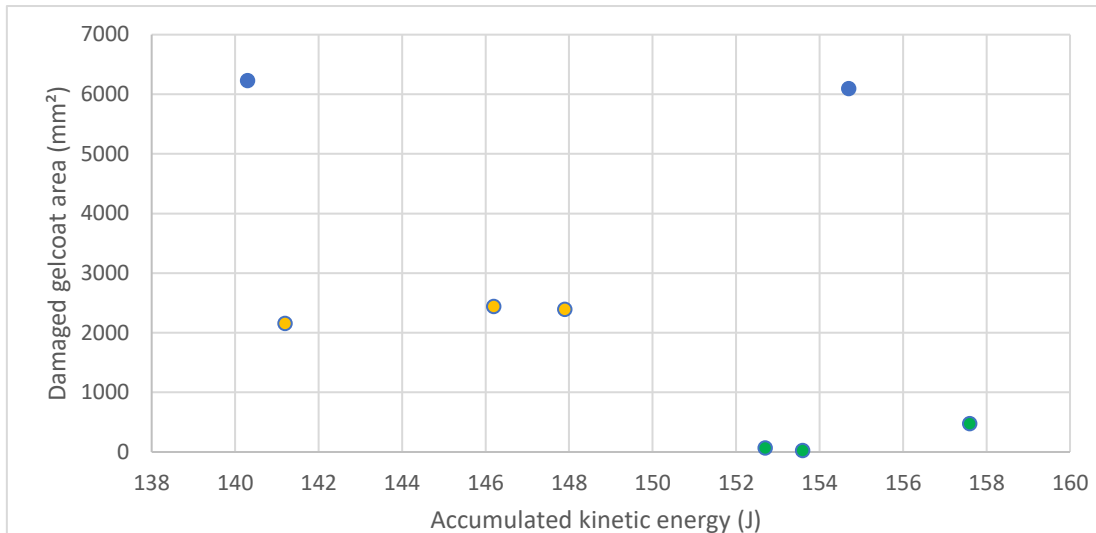


Figure 4.21: Accumulated kinetic energy effect on damaged gelcoat area for the samples tested at a velocity of 120 m/s, without sample 3 from CG 0.65 mm due to missing data. Green dots are a sample from CG 0.15 mm, orange dots from CG 0.35 mm and blue dots are from CG 0.65 mm.

The DGA is also plotted against the thickness of individual samples tested with a velocity of 120 m/s see Figure 4.22. The figure shows the ACT of the samples obtained from the laser confocal microscope on the x-axis, which is increasing in gelcoat thickness from left to right, but it is not linear. The general trend that a higher coating thickness has more gelcoat area removal can be seen in this figure for the three groups of coating thicknesses, 0.15 mm, 0.35 mm and 0.65 mm highlighted with a light grey, grey and dark grey background, respectively. However, if you look at the individual samples from the same CG it is difficult to judge, because the standard deviation of the thickness is overlapping see Table 4.2. The reason that thicker CGs have a higher DGA is because the thicker the coating is, the more brittle it becomes [49][50]. Brittle materials in general perform bad against impact compared to tough materials, which absorb impact better. Moreover, thin coating thicknesses tends to undercure [12], but the results from the DSC showed that the degree of cure was more or less the same for the three CGs. In conclusion, the individual samples in a CG are difficult to compare with each other, but if you look at the three CGs, it can be said that a 0.15 mm thick coating is the coating thickness to have the least amount of DGA.

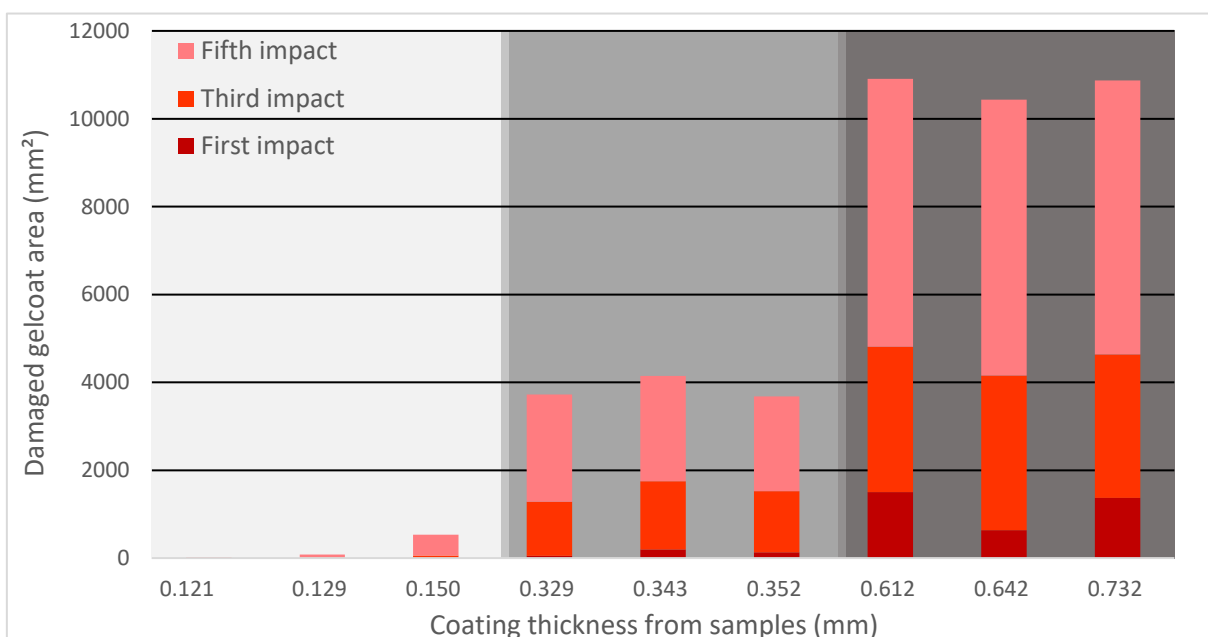


Figure 4.22: Bart chart of the damaged gelcoat area and all the samples tested with a velocity of 120 m/s.

From the images taken from the back side of the samples with the optical microscope and smartphone camera, no form of fibre fracture could be seen. The images from the cross-section of the sample taken with the laser confocal microscope were looked at to determine if fibre fracture can be found. Matrix cracking and delamination on the other hand is clearly visible. What can be noticed is that all the matrix cracking occurs along the fibres at the bottom side. The samples tested with 90 m/s and 100 m/s showed matrix cracking for all impacts see Table 4.3, except for sample 8 for the first impact. For the samples tested with 120 m/s, CG 0.15 mm is one that showed in the beginning matrix cracking, but after more impacts, the matrix cracking turned to delamination. The other two CGs (0.35 mm and 0.65 mm) had already delamination after the first impact.

Velocity	Samples	Damage after one impact	Damage after three impacts	Damage after five impacts
120 m/s	Sample 1 of 0.65 mm	Delamination	Delamination	Delamination
	Sample 2 of 0.65 mm	Delamination	Delamination	Delamination
	Sample 3 of 0.65 mm	Delamination	Delamination	Delamination
	Sample 1 of 0.35 mm	Delamination	Delamination	Delamination
	Sample 2 of 0.35 mm	Delamination	Delamination	Delamination
	Sample 3 of 0.35 mm	Delamination	Delamination	Delamination
	Sample 1 of 0.15 mm	Matrix cracking	Matrix cracking	Delamination
	Sample 2 of 0.15 mm	Matrix cracking	Delamination	Delamination
	Sample 3 of 0.15 mm	Matrix cracking	Delamination	Delamination
100 m/s	Sample 5 of 0.15 mm	Matrix cracking	Matrix cracking	Matrix cracking
	Sample 6 of 0.15 mm	Matrix cracking	Matrix cracking	Matrix cracking
	Sample 7 of 0.15 mm	Matrix cracking	Matrix cracking	Matrix cracking
90 m/s	Sample 8 of 0.15 mm	No damage	Matrix cracking	Matrix cracking
	Sample 9 of 0.15 mm	Matrix cracking	Matrix cracking	Matrix cracking
	Sample 10 of 0.15 mm	Matrix cracking	Matrix cracking	Matrix cracking

Table 4.3: All samples divided in three damage conditions, no damage, matrix cracking and delamination.

It is difficult to quantify the matrix cracking for all samples, especially for the same impact, because the amount of matrix cracking is difficult to count and the size of these cracks are not the same. A significant difference in the severity of matrix cracking can be seen for first impact and fifth impact for the samples tested with a velocity 100 m/s.

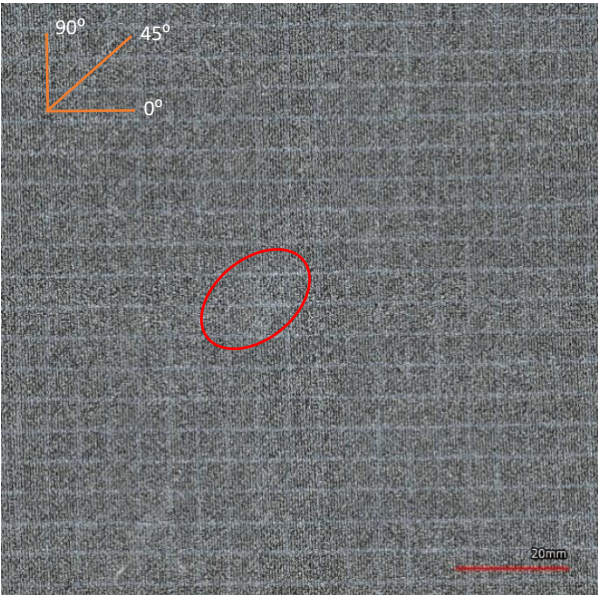


Figure 4.23: Minor matrix cracking in sample 5 of CG 0.15 mm after one impact.

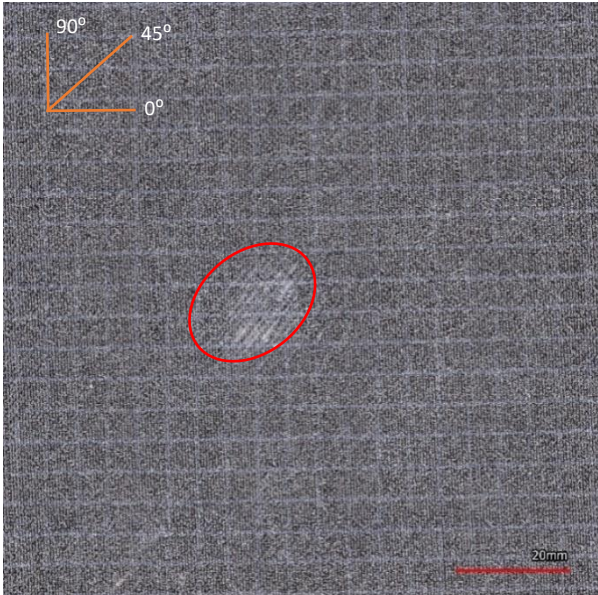


Figure 4.24: Major matrix cracking in sample 5 of CG 0.15 mm after five impacts.

See Figure 4.23 for an optical image of the back side of sample 5 in CG 0.15 mm after the first impact. The matrix cracks are difficult to see, because of their small size. The matrix cracking is encircled with a red oval marking. The same sample after the fifth impact can be seen in Figure 4.24. In addition, the samples tested with a velocity of 90 m/s showed after 5 impacts a similar amount of matrix cracking for a sample tested with 100 m/s after 1 impact. More images from the back and the front side of the samples can be found in Appendix G.

Quantification of delamination on the other hand is less difficult by looking at the delamination area. The results of this are shown in the next section. From the samples showing delamination in Table 4.3, it can be noticed that most of the samples show delamination at two locations, see Figure 4.25. Delamination is recognizable by the whitening of the matrix material. The shiny substance around the delamination is Vaseline. Delamination at two locations seems to be strange because the impact is focused on one point, the centre of the sample. However, from literature it is found that a ‘peanut’ shape appears often in composite plates after impact [51][52][53][54][55]. According to Lu X. and Liu D. [56] delamination should narrow down at the impact point and the elongated part should be aligned with the fibre direction of the first layer at the back side of the interface see Figure 4.26. In Figure 4.25 it can be seen that the centre of the ‘peanut’ shape doesn’t contain delamination, but the delamination appears to align with the fibre direction. In literature it is found that the space between the two halves of the ‘peanut’ shape can be a clear area of non-delamination [57][58].

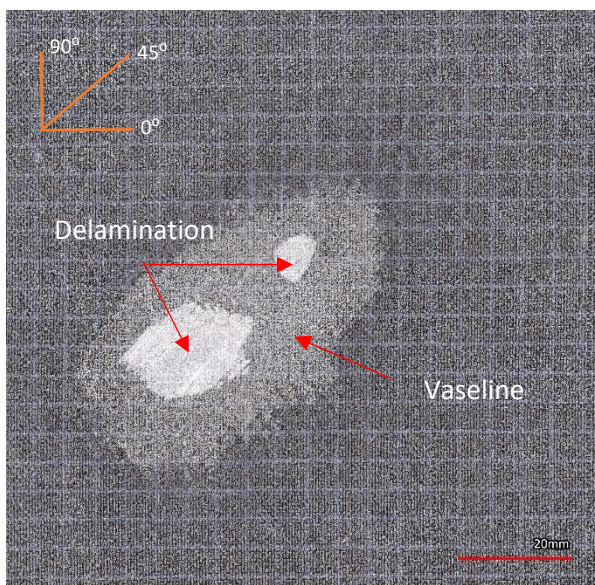


Figure 4.25: Delamination after 5 impacts on sample 2 of CG 0.15 mm.

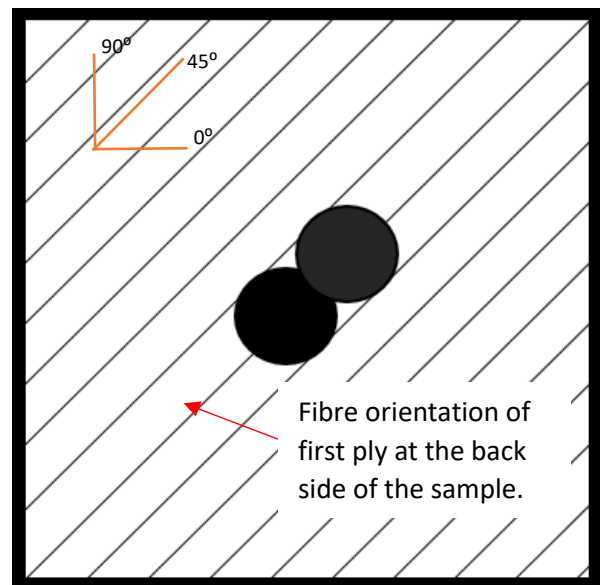


Figure 4.26: Schematic picture of ‘peanut’ shaped delamination, based on [56].



### 4.3 C-SCAN

This section consist of a subsection 'before impact' and 'damage progression'. The first mentioned subsection shows results of the C-scan before impact. In the second one, the delamination area is compared between the CGs and in the CG itself. In addition, a discussion is made whether the obtained results are correct or if there is an influence of factors.

#### 4.3.1 Before impact

All samples are scanned before the impact to check for porosity and delamination in the composite. A typical C-scan can be seen in Figures 4.27 and 4.28, which is from sample number one with from CG 0.65 mm and sample number one from CG 0.35 mm, respectively. From the c-scan taken for each sample before impact (see Appendix H for all C-scan images), it can be seen that there is no delamination and no accumulation of air bubbles in one spot. If this would happen, then there would be an orange or red colour in the composite.

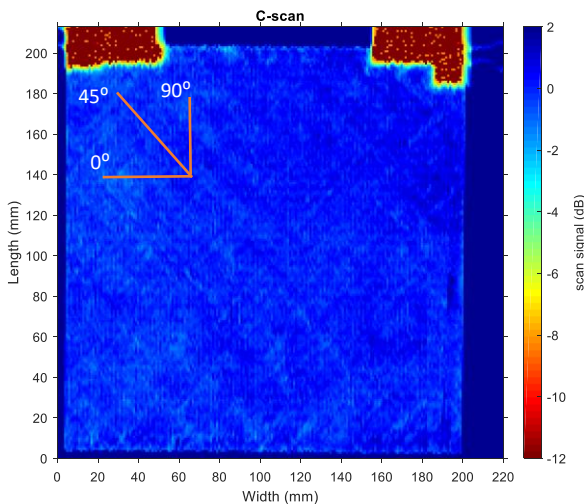


Figure 4.27: C-scan from sample 1 of CG 0.65 mm before impact.

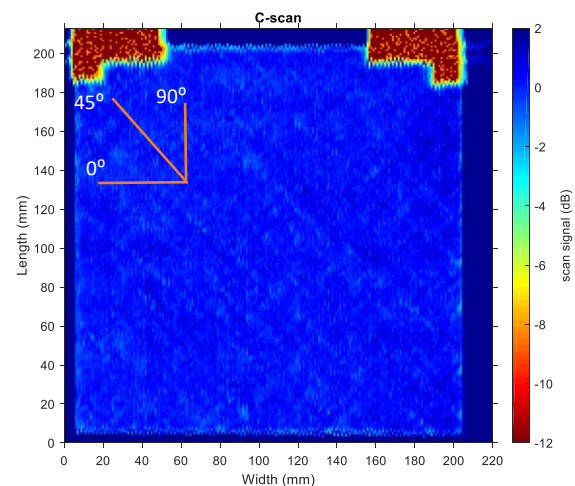


Figure 4.28: C-scan from sample 1 of CG 0.35 mm before impact.

#### 4.3.2 Damage progression

The results show that the samples with a 0.15 mm thick coating tested with impact velocities of 90 and 100 m/s did not have a delamination. All samples tested with a higher velocity (120 m/s) showed delamination after one impact, except the 0.15 mm coated samples. For the third impact of this CG, only sample one with a 0.15 mm thick coating showed no delamination. And after five impacts, all the samples impacted with a velocity of 120 m/s showed delamination see Appendix I.

The progress in the delamination area has been plotted for all the samples impacted with a velocity of 120 m/s see Figure 4.29. The average of the delamination area is shown since there are multiple samples with the same coating thickness. The error bar is also included, which shows the minimum and maximum value of the delamination area for all samples from the same coating thickness group for each impact session.

In Figure 4.29, it can be seen that a 0.35 mm coated sample has the highest average delamination area for impact one till impact five. This is followed by the 0.65 mm coated sample and the lowest amount of average delamination area has the 0.15 mm coated sample. For the first and third impact it can be noticed that the error bars are overlapping each other. This indicates that the before mentioned order in delamination area is not always like that, for instance, a 0.65 mm coated sample could have a higher delamination area than a 0.35 mm coated sample. For the fifth impact, a clearer significance can be observed with higher delamination area for CG 0.35 mm and the lowest for CG 0.15 mm. The CG 0.65 mm and 0.35 mm have more or less a linear slope, while the CG 0.3 mm show flattening of the curve after the third impact.

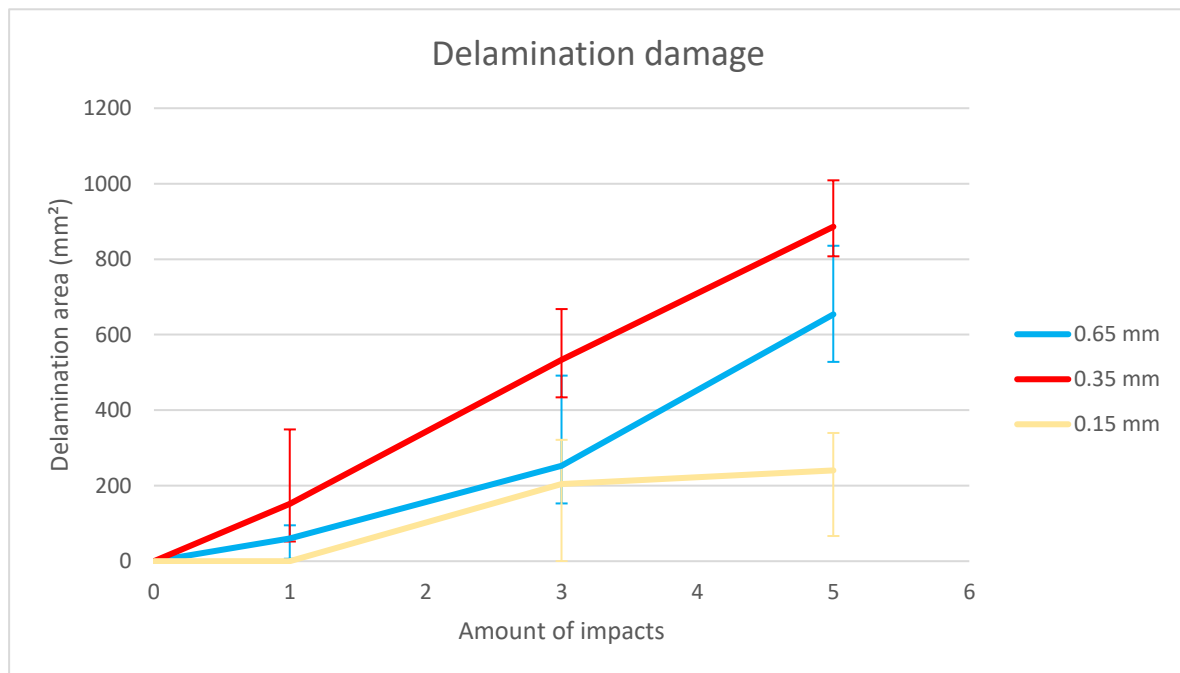


Figure 4.29: Average delamination area (mm<sup>2</sup>) for the three coating groups per impact session.

The individual samples of the CGs are analysed to find more information. In Figure 4.30, Individual samples of coating group 0.65 mm can be seen. The graphs are separated, especially at the second and third impacts. Sample 1 has 10 % higher accumulated kinetic energy than sample 2 and shows nearly for every impact a higher kinetic energy. Sample 1 was expected to have a higher delamination area, but it turned out the other way. Unfortunately, sample three could not be compared, because of missing data. Effect of dry spots was not the reason, because there is none.

Looking further at Figure 4.31, shows that sample 2 is an outlier of the CG 0.35 mm. The AKC is about 4 % lower than the other two samples. Looking at the standard deviation of AKC brings an overlapping of the AKC values. Further, sample 2 had also some dry spots, which is shown in Figure 4.6. So, that might also be a cause for the higher amount of delamination.

Furthermore, Sample 1 of CG 0.15 mm showed a significant difference between to other two panels in this group, see Figure 4.32. The AKC is 3 % higher than the other two panels, the difference is a small percentage, hence the possibility that the AKC values might be the same for all three panels due to the standard deviation. These panels did not have any dry spots, so the influence is invalid.

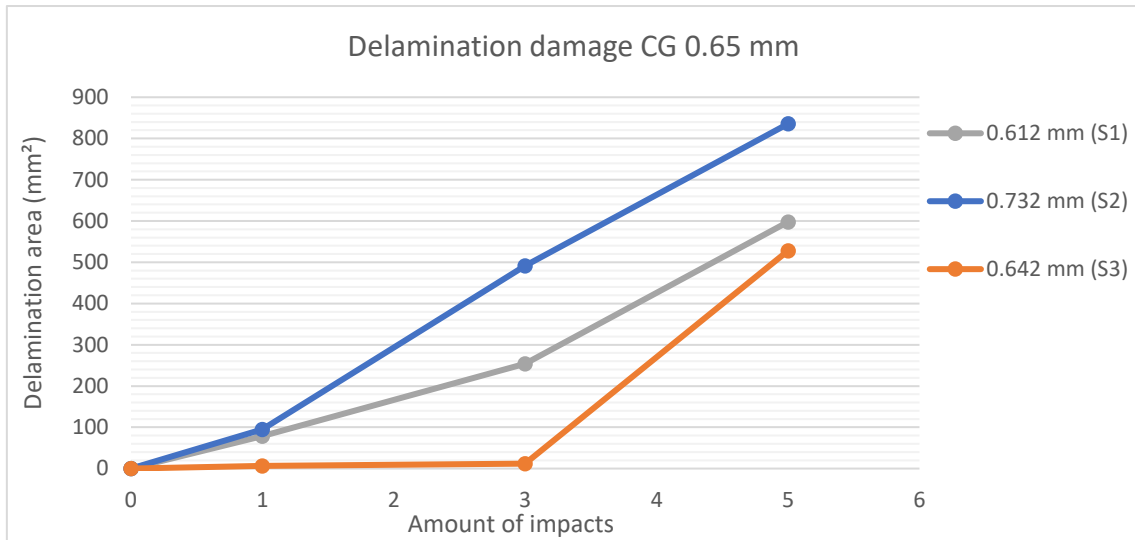


Figure 4.30: Delamination area (mm<sup>2</sup>) for samples from CG 0.65 mm per impact session.

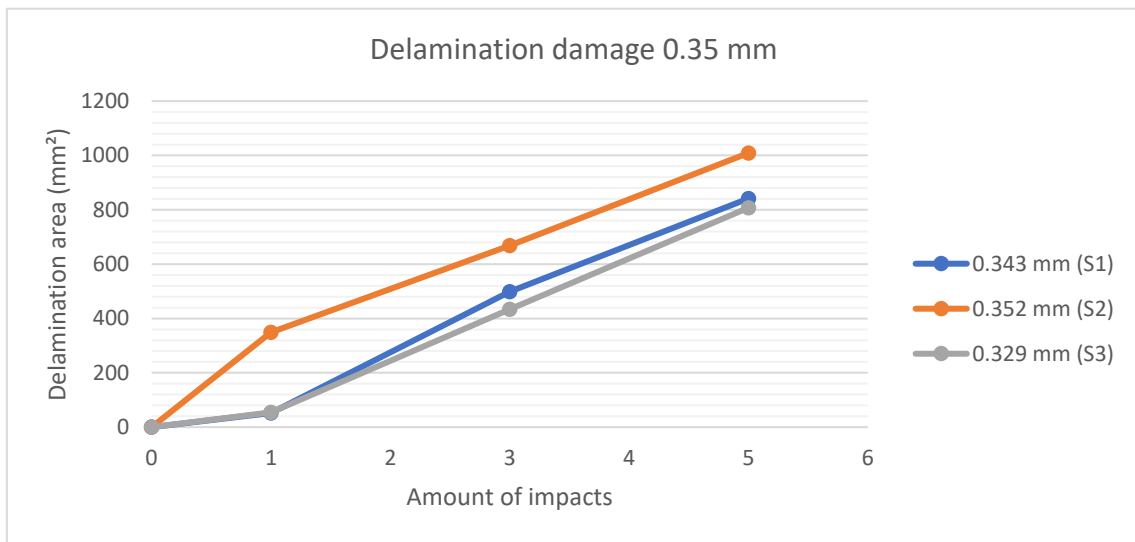


Figure 4.31: Delamination area (mm<sup>2</sup>) for samples from CG 0.35 mm per impact session.

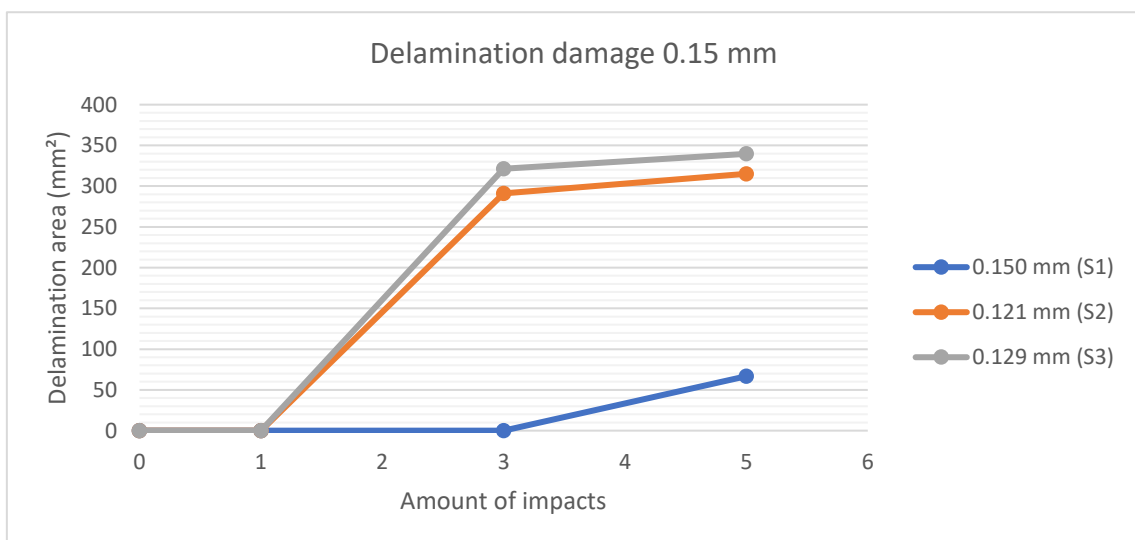


Figure 4.32: Delamination area (mm<sup>2</sup>) for samples from CG 0.15 mm per impact session.

It is observed that the AKE could have an influence on the delamination area. So, a plot is made with the delamination area of the samples tested with 120 m/s for the fifth impact on the y-axis and their AKE on the x-axis, see Figure 4.33 for the plot. Sample 3 of CG 0.65 mm is excluded due to lacking results of the AKE. The blue dot indicates the value of one sample for the two quantities. The blue line is a trendline added to show the relationship between the delamination area and AKE. It can be seen that the higher the AKE is the lower the delamination area is. This is true if a high AKE is only due to a higher impact velocity and for a certain velocity range, because with low velocities the damage mode is different for example, matrix cracking was observed for low velocities from the optical images. For high impact velocities, a lower delamination area is observed for a higher AKE possibly due to a change in damage mode from delamination to fibre fracture. This change in damage mode due to increasing velocity/kinetic energy is observed by Kim H. & Kedward K. T. [33].

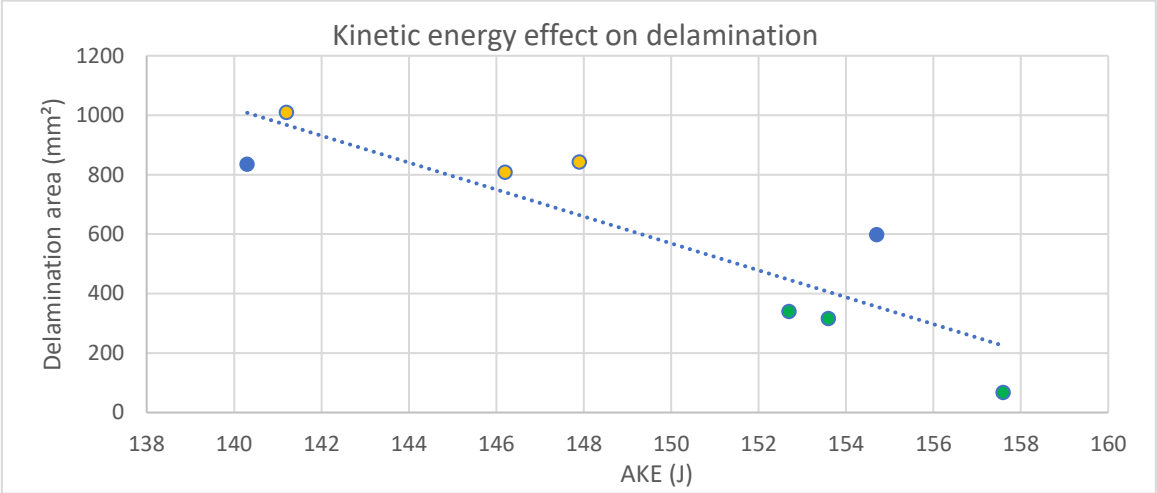


Figure 4.33: Delamination area (mm<sup>2</sup>) plotted against the accumulated kinetic energy for samples tested at 120 m/s, without sample 3 from CG 0.65 mm due to missing data. Green dots are a sample from CG 0.15 mm, orange dots from CG 0.35 mm and blue dots are from CG 0.65 mm.

In Figure 4.34, an overview is given of the 9 samples with their ACT and delamination area. No clear trend could be observed. The reason why CG 0.35 mm has one of the highest delamination areas is due to a lower AKE in general.

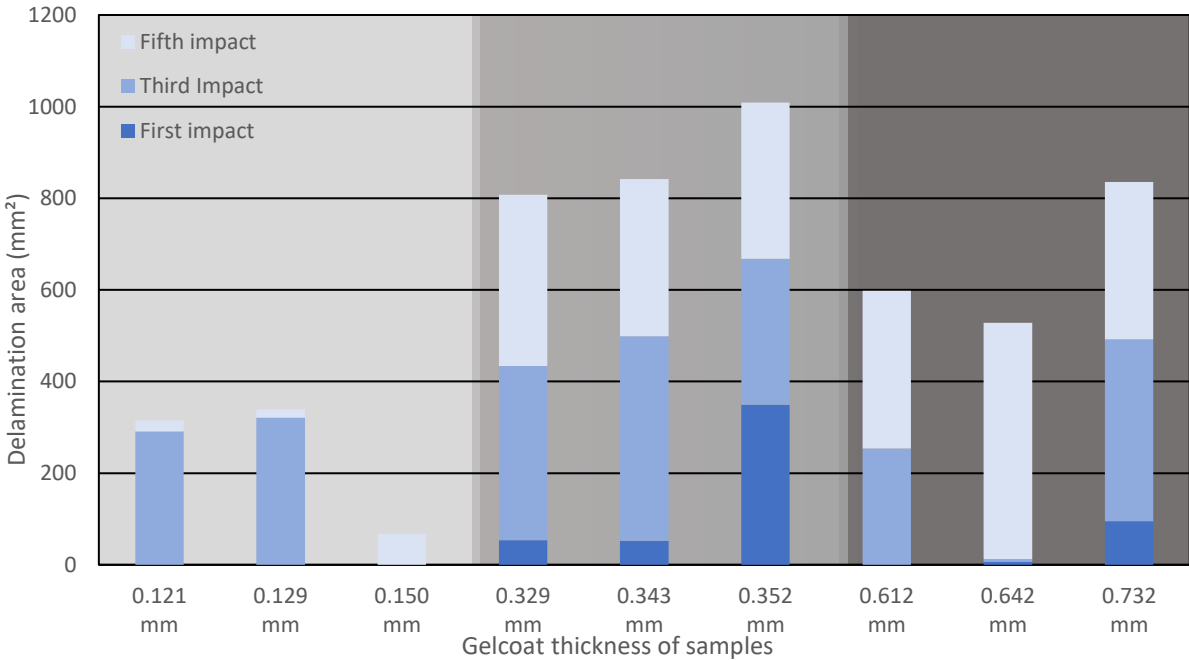


Figure 4.34: Overview of the 9 samples tested at 120 m/s and their delamination area (mm<sup>2</sup>).

#### 4.4 LASER CONFOCAL MICROSCOPE

All samples are assessed on the damaged found and only delamination and matrix cracking are found. It could be that the impact energy level is too low since high impact energy is required to get fibre breakage [59]. Overall, the samples shot with the same velocity showed similar damage. The samples shot with a velocity of 120 m/s do have an (interlaminar) delamination and (interlaminar and interlaminar) matrix cracking. An example of how that damage looks is given with sample 1 of CG 0.65 mm see Figure 4.35.

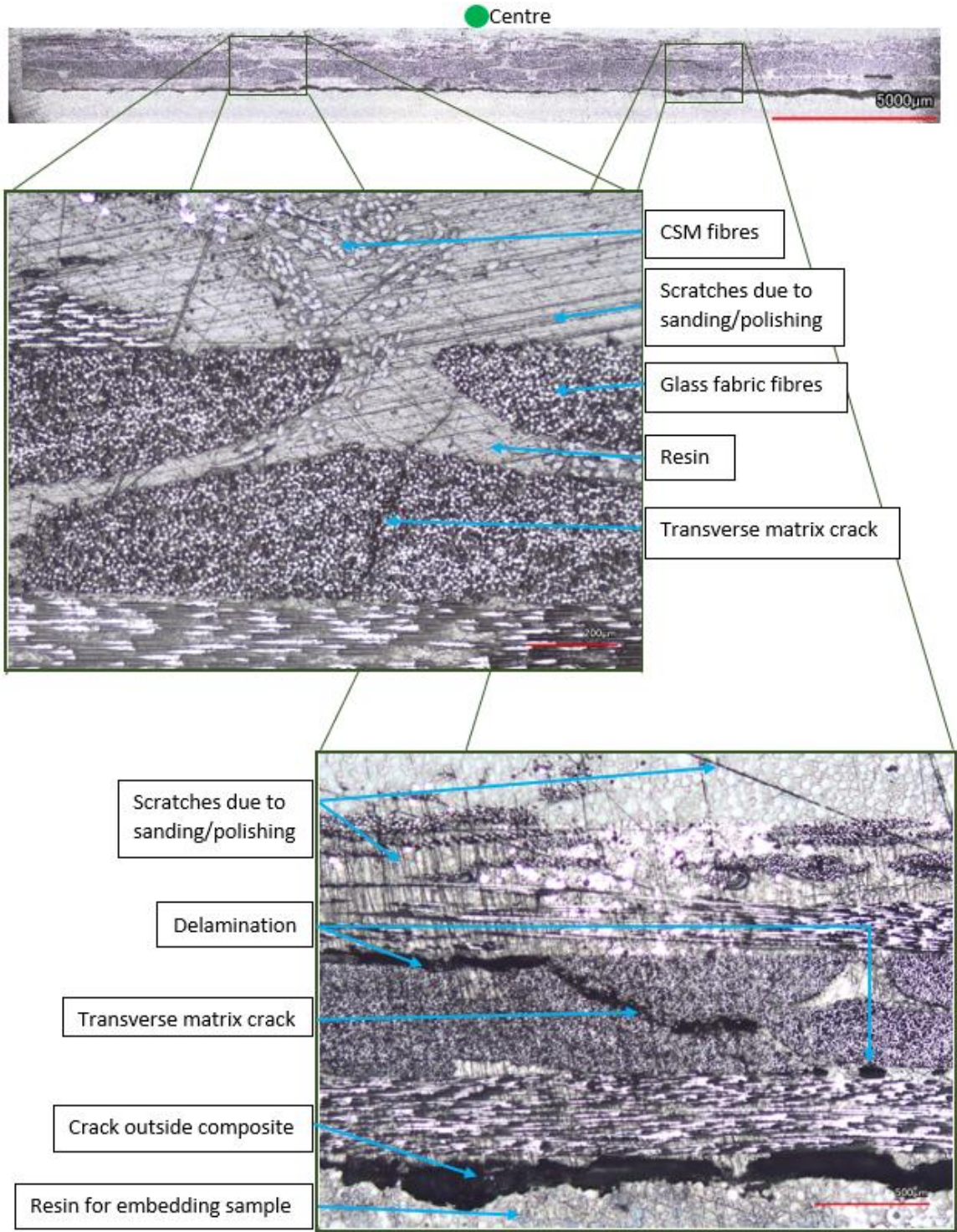


Figure 4.35: Cross-section of sample 1 from CG 0.65 mm after 5 impacts at a velocity of 120 m/s.

The figure shows a full scan of the cross-section with images stitched with a 10x lens, where the centre is highlighted with a green circle. Due to the stitching, the quality is automatically lowered. To see more details, local images are taken to show a close-up of damage, one with a 10x lens (top left) and one with a 5x lens (bottom right). The image on the top left shows a transverse matrix crack in layers 2 and 3. The image on the bottom right shows delamination between layers 1 and 2 (filled with a little bit of embedding resin), which is connected via a transverse matrix crack to another delamination between layers 3 and 4. Another crack can be seen below layer 1 (on the outside of the composite sample). This is due to the shrinkage of the resin used for embedding samples.

The samples shot with a velocity of 100 m/s showed only (interlaminar and intralaminar) matrix cracks, see sample 6 of CG 0.35 mm after 5 impacts in Figure 4.36. The matrix crack in the detailed image (20x) is changing direction, this crack could be an initiation for a delamination since it is propagating between layer 1 and layer 2.

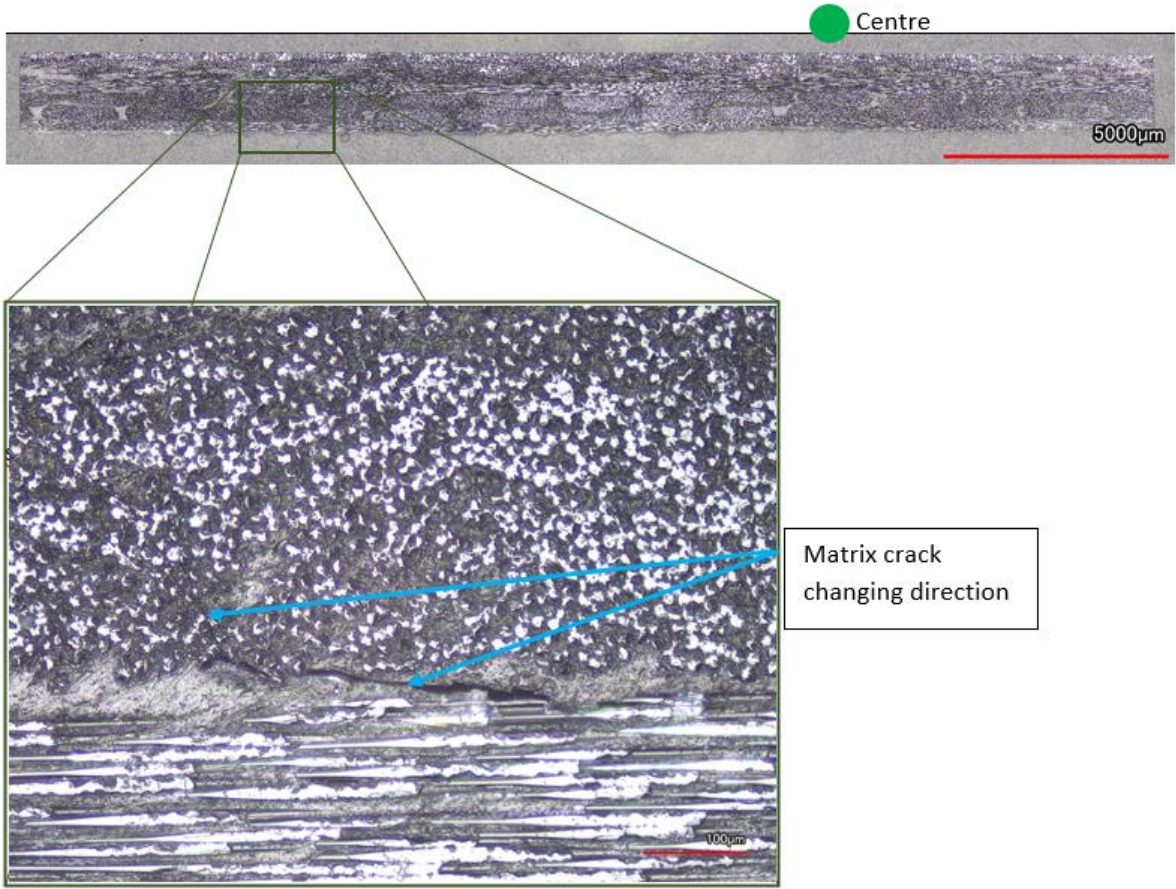


Figure 4.36: Cross-section of sample 6 from CG 0.35 mm after 5 impacts at a velocity of 100 m/s.

Samples shot with a velocity of 90 m/s showed even smaller cracks see Figure 4.37. The detailed image is from sample 9 of CG 0.15 mm after 5 impacts. An arrow points to a possible transverse matrix crack in layer 3, it is small and dark, making it difficult to judge if it is a transverse matrix crack. Furthermore, no matrix cracks are visible for sample 8 of the same CG, which is also the case from the optical microscope see Table 4.3. There might be a crack in layers 1 and 4, but this could not be seen to a trade-off explained earlier.

From the images of the cross-section, it can be noticed that the matrix cracks and delamination are not exactly beneath the centre where the impact should have happened, especially at the layers on the bottom. According to O'Brien T. and Elber W., it is due to the high transverse shear stresses in the event of an impact [60].

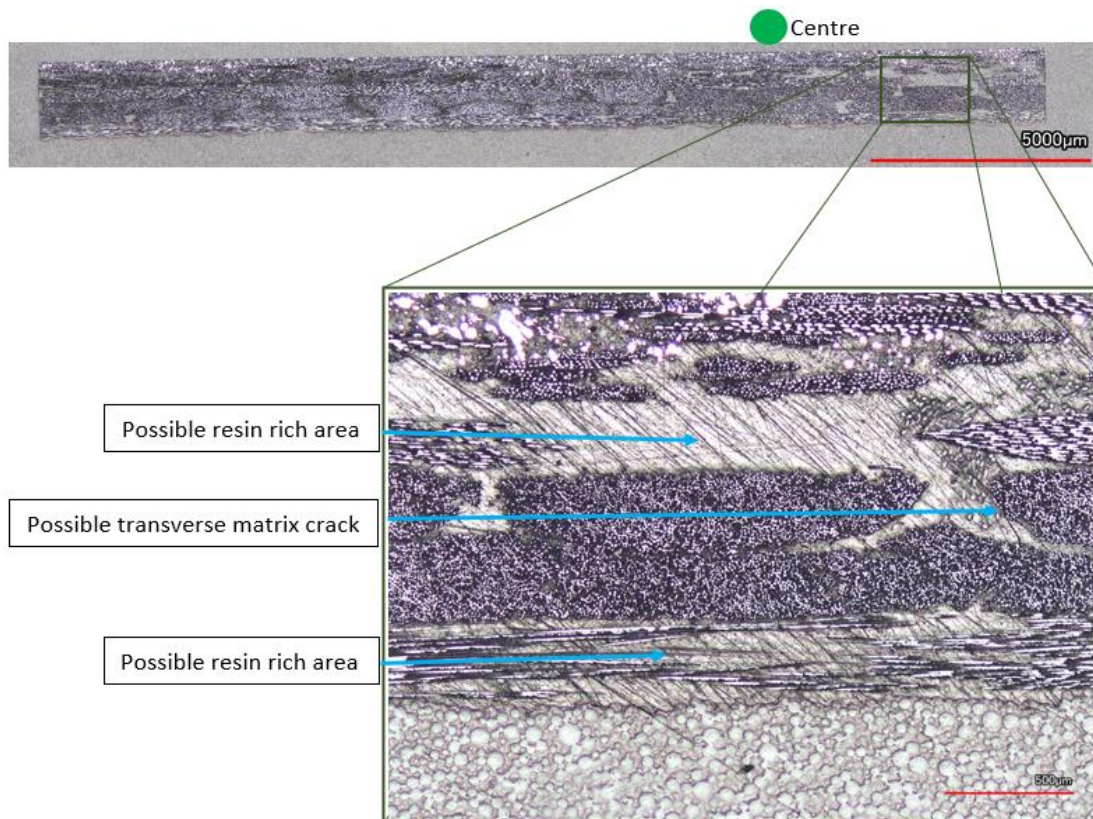


Figure 4.37: Cross-section of sample 9 from CG 0.15 mm after 5 impacts at a velocity of 90 m/s.

A comparison of the three methods used to analyse damage confirms that the analyses have been carried out well. From the optical images, the samples tested at 90 m/s showed matrix cracking except for sample 8, which had no damage for the first impact. This is similar to what is found from the LCM. Increasing the velocity to 100 m/s led to more severe matrix cracking. The optical images showed a larger area with matrix cracks and the LCM images showed more and bigger cracks. At an impact speed of 120 m/s, the damage mode shifted to delamination between the glass fabric layers and between the glass fabric layer and CSM. This could be seen by whitening of the matrix material from the optical images, the C-scan showed a reduction in signal strength resulting in a red area for delamination and the LCM showed that the delamination occurs between glass fabric layer 1 and 2 and switches to delamination between glass fabric layer 3 and 4 at a certain point. The variation in kinetic energy for velocities tested at 120 m/s showed that especially delamination (between glass fibre layers and CSM) is very sensitive to velocity/kinetic energy. According to Kim H. & Kedward, K. T. [33], a certain high velocity/kinetic energy can lead to reduction in delamination area and initiation of fibre fracture. The reduction in delamination area was observed, but no fibre fracture could be seen with LSM.

## 5 CONCLUSION AND RECOMMENDATION

---

In the last chapter, important findings from the thesis regarding the research question and sub questions are concluded. In addition, recommendations are formulated about further improvement of the performed test and other interesting tests that could be performed to provide useful information to the wind turbine community.

### 5.1 CONCLUSION

It was decided to perform SHI impact on a gelcoated glass fibre samples with varying coating thicknesses (0.65 mm, 0,35 mm and 0.15 mm). A SHI with a diameter of 20 mm was shot at 120 m/s to these samples. The size and velocities are based on what is found in literature. On one coating thickness (0.15 mm) is tested at different velocities (120 m/s, 100 m/s and 90 m/s) to gain more knowledge about the effect of velocity. The challenging and most important part of the project was to make the gas cannon ready to shoot a hailstone with a high velocity impact, because of melting and fracture problems with the SHI. A solution was found, which made It possible to continue with this topic for the master thesis. The research question and sub question(s) were answered based on the results found from the optical microscope, C-scan, laser confocal microscope, and velocity and mass measurement. The results were then discussed by checking if other factors could have influenced it, such as gelcoat undercure, kinetic energy, dry spots and difference of coating thickness in the individual samples from the same CG. A conclusion can be drawn for the research question and sub questions, these are listed below:

- **What are the effects of a varying gelcoat thickness on damage resistance of leading edge gelcoated glass fibre composites subjected to hailstone impact?**

First of all, it is interesting to know what the hypothesis for the research question was: a thicker coating will have less damage in the substrate and interface, because the energy will be transferred better due to the thick coating, while the surface damage will be the same for both a thin or thick coating, since this is more material dependent. The elaborate more on the last part, the same amount of coating will be removed for both a thin and thick coating. Meaning that the thicker coating will last longer since it will take more time to degrade the surface.

The experimental results showed that the effect of coating thickness is: the thicker the gelcoat is, the more damaged gelcoat area is observed, at least from the three tested CGs: 0.65 mm, 0.35 mm and 0.15 mm. The reason is that thick applied coatings become more brittle, than when a thin layer of coating is applied [49][50], because thin coating thicknesses tends to undercure [12], but from the DSC results it was found that there is no major difference in the degree of cure between the three varying gelcoat thicknesses.

The same samples showed also damage between glass fibre layers and CSM as delamination and matrix cracking (interlaminar as well as intralaminar). Both types of damage are sensitive to the kinetic energy of the impact, especially delamination. Due to a small variation in the (accumulated) kinetic energy between the samples, it is difficult to conclude whether the coating thickness influences damage between and in the glass fibre layers and CSM. The gelcoat is less sensitive to this factor.



- How could a hailstone be shot with the available gas cannon in the lab of the university?**

Three concepts were made in order to shoot a SHI without melting and fracturing in the barrel. The first concept was found in literature, where a SHI is put in a sabot (casing around SHI) , these two were put in the barrel together. The idea was to shoot the SHI on a composite, while the sabot is stopped at the tip of the barrel. The concept worked for low velocities, for higher velocities thorough adjustments were needed and the shooting became dangerous. So, another concept was tried, which is the same as a test standard, where a sabot consists out of two parts. The SHI is in the centre of the two halves and when the sabot is shot, the two parts are separating, while the path of the SHI doesn't change. The separation of the two parts was not sufficient enough, which lead to trying of concept three. This concept was placed as the last try since it was believed difficult to realize and there were doubts about whether the SHI is going to be intact by using this concept. For this concept, a plastic tube is put in the barrel that has an inner diameter close to the SHI and an outer diameter close to the inner diameter of the barrel. A special structure was made to hold the plastic tube in place, while the SHI could be shot. The concept worked, which was important in order to answer the research question and sub questions.
- What is the main governing damage mode in the composite: delamination, matrix cracks on the gelcoat, matrix cracks in the substrate or fibre breakage?**

It was expected that gelcoat damage would be the main governing damage mode for all 15 samples, but there was no general main governing damage mode in the composite. This was dependent on the velocity of the impact, gelcoat thickness, size of the SHI and the amount of repeated impacts. Therefore, it could not be answered, but the sub questions of this sub question could be answered.

- How does the main governing damage mode change for different velocities?**

Three velocities (90 m/s, 100 m/s and 120 m/s) are tested on samples of CG 0.15 mm. The main governing damage mode was delamination for the highest velocity. By reducing the velocity, it was observed that the main governing damage mode changed from delamination to matrix cracking.
- How will the main governing damage mode change for different coating thickness?**

Three different coating thicknesses (0.15 mm, 0.35 mm and 0.65 mm) are tested under the same velocity (120 m/s). At this velocity, mainly delamination and gelcoat damaged happened and they are compared in area to decide which one is the main governing damage mode. In general, the samples from CG 0.15 mm have delamination as the main governing damage mode. The samples from a thicker CG showed gelcoat damage as the main governing damage mode.

## 5.2 RECOMMENDATION

The gas cannon works fine with concept three and the modification by mounting a velocity sensor with a hinge to the tip of the barrel makes it suitable for repeated impacts tests. After finishing shooting, it is recommended to remove the plastic tube and dry the inside of the barrel by moving a towel inside to prevent any corrosion inside the barrel. Another option would be redesigning the plastic tube, such that water from the SHI cannot pour in the barrel.

The impact test performed in the thesis is with the idea in mind to form a basis. Making sure that the available gas cannon could be used to shoot a SHI with the required basic measurements, such as the velocity and mass of the SHI. It is recommended to perform a test on a curved panel to make it more realistic since wind turbine blades are also curved. A special mould needs to be made for this. The challenging part is to apply a coating on a curved mould with a roller. It is advised to use an automated spray gun depending on the coating used. The reason for using a spray gun is the minor thickness difference in the coating over the mould that could be achieved. Moreover, the kinetic energy is measured to have an idea about the input energy on the panel. On top of this measurement, it could be useful to measure the contact force and deflection of the sample to gain information about the absorbed energy in the panel.

Another object that could be improved is the SHI, it is made in one filling session, but a natural hailstone consists out of multiple spherical layers of ice. This layered structure is making the hailstone tougher than a SHI made in one filling session. It is recommended to make spherical layered SHI to make the test more realistic and also to gain more information about the difference between a SHI made in one filling session and one that is made spherically layered.

Besides, it is also interesting to see a hail impact test in combination with rain droplet impact test. This makes the test more realistic, because in real life both precipitation of hail and rain will occur during the lifetime of a wind turbine blade. They both can influence the optimum coating thickness in different ways.

## REFERENCES

---

- [1] Macdonald, H., Nash, D., & Stack, M. M. (2019). Repeated impact of simulated hail ice on glass fibre composite materials. *Wear*, 432-433, 102926. doi:10.1016/j.wear.2019.06.001.
- [2] Herring, R., Dyer, K., Martin, F., & Ward, C. (2019). The increasing importance of leading edge erosion and a review of existing protection solutions. *Renewable and Sustainable Energy Reviews*, 115, 109382.
- [3] Sareen, A., Sapre, C. A., & Selig, M. S. (2013). Effects of leading edge erosion on wind turbine blade performance. *Wind Energy*, 17(10), 1531–1542. doi:10.1002/we.1649.
- [4] Nash, D., Keegan, M.K., Stack, M. (2014). "wind turbine blade leading edge erosion: An investigation of rain droplet and hailstone impact induced damage mechanisms.". PhD diss. University of Strathclyde.
- [5] Macdonald, H. (2017). The influence of hail on wind turbine blade leading edge erosion and damage (Doctoral dissertation, University of Strathclyde).
- [6] Emami, S. (2017). Development of Probabilistic Models for Long Term Reliability of Sandwich Composites in Saline Freeze/Thaw Environment for Civil Engineering Applications. Available from: [https://www.researchgate.net/publication/322373749\\_Development\\_of\\_Probabilistic\\_Models\\_for\\_Long\\_Term\\_Reliability\\_of\\_Sandwich\\_Composites\\_in\\_Saline\\_FreezeThaw\\_Environment\\_for\\_Civil\\_Engineering\\_Applications](https://www.researchgate.net/publication/322373749_Development_of_Probabilistic_Models_for_Long_Term_Reliability_of_Sandwich_Composites_in_Saline_FreezeThaw_Environment_for_Civil_Engineering_Applications) [accessed Sep 21 2020].
- [7] Yang, J., Peng, C., Xiao, J., Zeng, J., Xing, S., Jin, J., & Deng, H. (2013). Structural investigation of composite wind turbine blade considering structural collapse in full-scale static tests. *Composite Structures*, 97, 15–29.
- [8] Thomsen, O. T. (2009). Sandwich Materials for Wind Turbine Blades — Present and Future. *Journal of Sandwich Structures & Materials*, 11(1), 7–26.
- [9] Ciang, C. C., Lee, J.-R., & Bang, H.-J. (2008). Structural health monitoring for a wind turbine system: a review of damage detection methods. *Measurement Science and Technology*, 19(12), 122001.
- [10] Sareen, A., Sapre, C. A., & Selig, M. S. (2012). Effects of Leading-Edge Protection Tape on Wind Turbine Blade Performance. *Wind Engineering*, 36(5), 525–534.
- [11] Kjærside Storm, B. (2013). Surface protection and coatings for wind turbine rotor blades. *Advances in Wind Turbine Blade Design and Materials*, 387–412. doi:10.1533/9780857097286.3.387.
- [12] Saltz, W.T. (2009). Bay area air quality management district. Bay Area 2005 Ozone Strategy Control Measure SS-4BAAQMD Regulation 8, Rule 50: Polyester Resin Operations.
- [13] DNVGL-ST-0376 standard (2015). Rotor blades for wind turbines. P 70. Retrieved from: <https://rules.dnvgl.com/docs/pdf/DNVGL/ST/2015-12/DNVGL-ST-0376.pdf>.
- [14] Yuhazri, M. Y., Haeryip, S., Zaimi, Z. A. M., & Nilson, G. C. H. (2015). A review on gelcoat used in laminated composite structure. *Int. J. Res. Eng. Technol*, 4, 49-58.

- [15] Stephan N. (2020). SYSWE rotor blade inspection. Retrieved from: <https://www.syswe.de/en/windenergie-rotorblattinspektion>.
- [16] Verma, Amrit Shankar; Castro, Saullo G.P.; Jiang, Zhiyu; Teuwen, Julie J.E. (2020). Numerical investigation of rain droplet impact on offshore wind turbine blades under different rainfall conditions: A parametric study. *Composite Structures*, 241(), 112096– . doi:10.1016/j.compstruct.2020.112096.
- [17] Cortés, Enrique; Sánchez, Fernando; O’Carroll, Anthony; Madramany, Borja; Hardiman, Mark; Young, Trevor (2017). On the Material Characterisation of Wind Turbine Blade Coatings: The Effect of Interphase Coating–Laminate Adhesion on Rain Erosion Performance. *Materials*, 10(10), 1146– . doi:10.3390/ma10101146.
- [18] Dong, C. (2009). Liquid resin and polymer solution processing. *Advances in Polymer Processing*, 289–311. doi:10.1533/9781845696429.3.289.
- [19] BUFA Gelcoat Plus Corp. (2008). Technical information: working with OLDOPAL-Gelcoats, BUFA Gelcoat Plus GmbH & Co. KG.
- [20] Shadaksharappa, S. G., & Veerappa, A. K. (2020, May). Methods and process parameters of gel coating on laminated composites-A review. In *AIP Conference Proceedings* (Vol. 2236, No. 1, p. 040004). AIP Publishing LLC.
- [21] Field P.R., Hand W., Cappelluti G., McMillan A., Foreman A., Stubbs D. and Willows M. (2009). Hail threat standardisation final report for EASA. Link: [https://www.easa.europa.eu/sites/default/files/dfu/EASA\\_REP\\_RESEA\\_2008\\_5.pdf](https://www.easa.europa.eu/sites/default/files/dfu/EASA_REP_RESEA_2008_5.pdf).
- [22] Abrate, S., Castanié, B., & Rajapakse, Y. D. (Eds.). (2012). *Dynamic failure of composite and sandwich structures* (Vol. 192). Springer Science & Business Media.
- [23] Fluck, E. (2017). Hail statistics for European countries, PhD thesis, Institute of Meteorology and Climate Research (IMK), Karlsruhe Institute of Technologie (KIT), Karlsruhe, Germany.
- [24] Púčik, T., C. Castellano, P. Groenemeijer, T. Kühne, A. T. Rädler, B. Antonescu, and E. Faust, 2019: Large Hail Incidence and Its Economic and Societal Impacts across Europe. *Mon. Wea. Rev.*, 147, 3901–3916.
- [25] B. Xie, Q. Zhang, and Y. Wang, “Observed Characteristics of Hail Size in Four Regions in China during 1980-2005.” *J. Clim.*, vol. 23, no. 18, pp. 4973–4982, 2010.
- [26] Phelps M.B. et al (2019). Evaluating the compressive strength of hail and its relationship to freezer iceballs.
- [27] Gunn, R., & Kinzer, G. D. (1949). The terminal velocity of fall for water droplets in stagnant air. *Journal of Meteorology*, 6(4), 243–248. doi:10.1175/1520-0469(1949)0062.0.co;2.
- [28] Keegan, M. H., Nash, D. H., & Stack, M. M. (2013). On erosion issues associated with the leading edge of wind turbine blades. *Journal of Physics D: Applied Physics*, 46(38), 383001. doi:10.1088/0022-3727/46/38/383001
- [29] Kessler, E. (1982). *Thunderstorm morphology and dynamics* (Vol. 2). US Department of Commerce, National Oceanic and Atmospheric Administration, Environmental Research Laboratories.

- [30] Heymsfield, Andrew J.; Giammanco, Ian M.; Wright, Robert (2014). Terminal velocities and kinetic energies of natural hailstones. *Geophysical Research Letters*, 41(23), 8666– 8672. doi:10.1002/2014GL062324.
- [31] Schulson, E.M (1990). The brittle compressive fracture of ice. *Acta Metallurgica et Materialia*, 38(10), 1963–1976. doi:10.1016/0956-7151(90)90308-4.
- [32] Juntikka, R., & Olsson, R. (2009, July). Experimental and modelling study of hail impact on composite plates. In *Proceedings of The 17th International Conference of Composite Materials* (pp. 27-31).
- [33] Kim, H., & Kedward, K. T. (2000). Modeling Hail Ice Impacts and Predicting Impact Damage Initiation in Composite Structures. *AIAA Journal*, 38(7), 1278–1288. doi:10.2514/2.1099.
- [34] ASTM F320-05, 2005. Standard Test Method for Hail Impact Resistance of Aerospace Transparent Enclosures.
- [35] Fiore, G., Camarinha Fujiwara, G. E., & Selig, M. S. (2015). A damage assessment for wind turbine blades from heavy atmospheric particles. In *53rd AIAA Aerospace Sciences Meeting* (p. 1495).
- [36] Tang, Z., Hang, C., Suo, T., Wang, Y., Dai, L., Zhang, Y., & Li, Y. (2017). Numerical and experimental investigation on hail impact on composite panels. *International Journal of Impact Engineering*, 105, 102–108. doi:10.1016/j.ijimpeng.2016.05.016.
- [37] P. J., & Dahini, G. (2011). On the response of two commercially important CFRP structures to multiple ice impacts. *Composite Structures*, 93(10), 2619– 2627. doi:10.1016/j.compstruct.2011.04.029.
- [38] Mahinfalah, M., & Skordahl, R. A. (1998). The effects of hail damage on the fatigue strength of a graphite/epoxy composite laminate. *Composite Structures*, 42(2), 101–106. doi:10.1016/s0263-8223(98)00056-7.
- [39] Azouaoui, K. (2001). Modelling of damage and failure of glass/epoxy composite plates subject to impact fatigue. *International Journal of Fatigue*, 23(10), 877–885. doi:10.1016/s0142-1123(01)00050-0.
- [40] Hyung Yun Choi, ; Chang, F.-K. (1992). A Model for Predicting Damage in Graphite/Epoxy Laminated Composites Resulting from Low-Velocity Point Impact. *Journal of Composite Materials*, 26(14), 2134–2169. doi:10.1177/002199839202601408.
- [41] Guo, Z., Li, Z., Zhu, H., Cui, J., Li, D., Li, Y., & Luan, Y. (2020). Numerical simulation of bolted joint composite laminates under low-velocity impact. *Materials Today Communications*, 23, 100891. doi:10.1016/j.mtcomm.2020.100891.
- [42] Carroll D. (1962). Rainwater as a chemical agent of Geologic processes. *Chemistry of water*.
- [43] waterkwaliteit drinkwater Amsterdam. (2021, 1 juni). Waternet. Retrieved from: <https://www.waternet.nl/service-en-contact/drinkwater/waterkwaliteit/>.
- [44] Tobin, E.F.; Rohr, O.; Raps, D.; Willemse, W.; Norman, P.; Young, T.M. (2015). Surface topography parameters as a correlation factor for liquid droplet erosion test facilities. *Wear*, 328-329(), 318–328. doi:10.1016/j.wear.2015.02.054.
- [45] Atas, C., Icten, B. M., & Küçük, M. (2013). Thickness effect on repeated impact response of woven fabric composite plates. *Composites Part B: Engineering*, Pages 80-85.

- [46] Dolati, S., Fereidoon, A., & Sabet, A. (2013). Hail impact damage behaviors of glass fiber reinforced epoxy filled with nanoclay. *Journal of Composite Materials*, 48(10), 1241– 1249. doi:10.1177/0021998313484950.
- [47] Tawk, I., Aubry, J., Navarro, P., Ferrero, J.-F., Marguet, S., Rivallant, S., ... Rauch, P. (2012). Study of impact on helicopter blade. *Engineering Failure Analysis*, 24, 38– 45. doi:10.1016/j.engfailanal.2012.03.005.
- [48] Keegan, M. H., Nash, D., & Stack, M. (2013). Numerical modelling of hailstone impact on the leading edge of a wind turbine blade. EWEA Annual Wind Energy Event 2013.
- [49] Yuhazri, M. Y., Amirhafizan, M. H., Nilson, G. C. H., Sihombing, H., Kamarul, A. M., & Nirmal, U. (2018). Effects of gelcoat thickness on mechanical properties of woven glass/polyester laminated composite. *Journal of Mechanical Engineering and Sciences*, 12(1), 3370.
- [50] Yuhazri, M. Y., Nilson, G. C. H., Sihombing, H., & Abd Manaf, M. E. (2016). Mechanical Properties and Failure Analysis of Laminated Glass Reinforced Composite with Various Gelcoat Thickness. *Key Engineering Materials*, 694, 8–12. <https://doi.org/10.4028/www.scientific.net/kem.694.8>
- [51] Marulo F. (2016). Numerical-experimental investigation on the biomechanical performances of an aeronautical seat. University of Naples 'Federico II', Italy.
- [52] Dienel, C. P. (2019). *Damage Assessment for Composite Structures based on Individual Residual Strength Prediction* (Doctoral dissertation, Institut für Faserverbundleichtbau und Adaptronik).
- [53] Van Hoof, J. (2000). *Modelling of impact induced delamination in composite materials* (Doctoral dissertation, Carleton University).
- [54] Hitchen, S. A., & Kemp, R. M. J. (1995). *The effect of stacking sequence on impact damage in a carbon fibre/epoxy composite*. *Composites*, 26(3), 207–214. doi:10.1016/0010-4361(95)91384-h
- [55] Fuoss, E., Straznicky, P. V., & Poon, C. (1998). *Effects of stacking sequence on the impact resistance in composite laminates — Part 1: parametric study*. *Composite Structures*, 41(1), 67–77. doi:10.1016/s0263-8223(98)00036-1
- [56] Lu, X., & Liu, D. (1991). Finite element analysis of strain energy release rate at delamination front. *Journal of reinforced plastics and composites*, 10(3), 279-292.
- [57] Luo, R. K., Green, E. R., & Morrison, C. J. (1999). *Impact damage analysis of composite plates*. *International Journal of Impact Engineering*, 22(4), 435–447. doi:10.1016/s0734-743x(98)00056-6
- [58] Wang, H., & Vu-Khanh, T. (1994). Damage extension in carbon fiber/PEEK crossply laminates under low velocity impact. *Journal of Composite Materials*, 28(8), 684-707.
- [59] Kreculj, D., & Rasuo, B. (2018). *Impact damage modeling in laminated composite aircraft structures*. *Sustainable Composites for Aerospace Applications*, 125–153. doi:10.1016/b978-0-08-102131-6.00007-4
- [60] O'Brien T. & Elber W. (1993). Delamination and fatigue in composite materials: a review. Proceedings of the 9<sup>th</sup> international conference on composite materials, pp 2.1-2.11.

# APPENDICES

---

## APPENDIX A

	IR measurement 1			HSC measurement 1	
	Pressure (bar)	Velocity (m/s)		Pressure (bar)	Velocity (m/s)
	1	0		1	0
	2.14	24,3		2.14	22,7
	3.14	50,67		3.14	55,6
	4.14	76,4		4.14	71,4
	4,64	80,2		5.14	88,3
	5.14	90,6		6.14	96,7
	6.14	105,3		7.14	103,4
	8,64	121,5		8.14	111,1
				8,64	117,4
	IR measurement 2			HSC measurement 2	
	Pressure (bar)	Velocity (m/s)		Pressure (bar)	Velocity (m/s)
	1	0		1	0
	2.14	22,8		2.14	22,27
	3.14	56,3		3.14	47,62
	4.14	73,5		4.14	69,78
	5.14	89,5		5.14	76,92
	6.14	102,4		6.14	93,72
	7.14	107,4		7.14	96,71
	8.14	115,1		8.14	111,1
	8,64	119,2		8.64	117,4

## APPENDIX B

Making of the 0.15 mm CG samples	
Begin applying gelcoat session 1 and 2 <ul style="list-style-type: none"> <li>• Date: 31-3-2021</li> <li>• Time: 9:07</li> <li>• Temperature: 21,9 °C</li> <li>• Humidity: 34 %</li> </ul>	End applying gelcoat session 1 and 2 <ul style="list-style-type: none"> <li>• Date: 31-3-2021</li> <li>• Time: 13:40</li> <li>• Temperature: 21,8 °C</li> <li>• Humidity: 34 %</li> </ul>

Gelcoat Thickness measurement during manufacturing										
	Smooth surface measurement (mm)					Rough surface measurement (mm)				
Samples	Top	Bottom	Left	Right	Average	Top	Bottom	Left	Right	Average
1, 0.15 mm	0.35	0.4	0.35	0.3	0.35	0.3	0.3	0.35	0.3	0.313
2, 0.15 mm	0.3	0.35	0.3	0.3	0.313	0.2	0.2	0.2	0.2	0.2
3, 0.15 mm	0.3	0.35	0.3	0.3	0.313	0.275	0.275	0.175	0.175	0.225
4, 0.15 mm	0.35	0.35	0.3	0.3	0.325	0.275	0.225	0.2	0.2	0.225
5, 0.15 mm	0.35	0.4	0.35	0.4	0.375	0.2	0.3	0.225	0.2	0.231
6, 0.15 mm	0.35	0.35	0.3	0.3	0.325	0.275	0.25	0.225	0.2	0.238
7, 0.15 mm	0.35	0.35	0.3	0.3	0.325	0.2	0.25	0.2	0.2	0.213
8, 0.15 mm	0.45	0.45	0.35	0.35	0.4	0.225	0.2	0.2	0.275	0.225
9, 0.15 mm	0.4	0.35	0.3	0.3	0.338	0.25	0.225	0.175	0.225	0.219
10, 0.15 mm	0.4	0.4	0.35	0.25	0.35	0.3	0.225	0.225	0.225	0.244

Making of the 0.35 mm and 0.65 mm CG samples	
Begin applying gelcoat session 3 and 4 <ul style="list-style-type: none"> <li>• Date: 7-4-2021</li> <li>• Time: 10:00</li> <li>• Temperature: 20,7 °C</li> <li>• Humidity: 34 %</li> </ul>	End applying gelcoat session 3 and 4 <ul style="list-style-type: none"> <li>• Date: 7-4-2021</li> <li>• Time: 15:45</li> <li>• Temperature: 20,9 °C</li> <li>• Humidity: 33 %</li> </ul>

Gelcoat thickness measurement during manufacturing										
	surface measurement with process 'raken' (mm)					Final surface measurement (mm)				
Samples	Top	Bottom	Left	Right	Average	Top	Bottom	Left	Right	Average
1, 0.65 mm	0.85	0.85	0.75	0.85	0.825	0.7	0.65	0.7	0.7	0.688
2, 0.65mm	1.0	0.9	1.0	0.9	0.95	0.75	0.9	0.8	0.7	0.788
3, 0.65 mm	0.9	0.9	0.9	0.9	0.9	0.75	0.85	0.8	0.8	0.8
4, 0.65 mm	1.0	0.9	0.85	0.9	0.913	0.8	0.9	0.75	0.7	0.788
1, 0.35 mm	0.65	0.55	0.55	0.5	0.563	0.45	0.45	0.45	0.4	0.438
2, 0.35 mm	0.65	0.6	0.55	0.6	0.6	0.55	0.45	0.45	0.4	0.463
3, 0.35 mm	0.55	0.6	0.55	0.5	0.55	0.4	0.45	0.5	0.4	0.438
4, 0.35 mm	0.6	0.6	0.5	0.5	0.55	0.5	0.65	0.5	0.4	0.513



Start information Vacuum infusion session 1 and 2 <ul style="list-style-type: none"> <li>• Date: 1-4-2021</li> <li>• Time: 14:03</li> <li>• Temperature: 22.8 °C</li> <li>• Humidity: 35 %</li> </ul>	Start information Vacuum infusion session 3 and 4 <ul style="list-style-type: none"> <li>• Date: 8-4-2021</li> <li>• Time: 15:01</li> <li>• Temperature: 21.6 °C</li> <li>• Humidity: 33 %</li> </ul>
---	---

Desired length and width of the samples: 20 cm		
Samples	Width of the sample	Length of the sample
1, 0.6 mm	19,9 cm	20 cm
2, 0.6 mm	20 cm	20 cm
3, 0.6 mm	20 cm	20 cm
4, 0.6 mm	20 cm	19,9 cm
1, 0.45 mm	20 cm	20 cm
2, 0,45 mm	20 cm	20 cm
3, 0.45 mm	19,9 cm	20 cm
4, 0.45 mm	20 cm	19,8 cm
1, 0.3 mm	20 cm	20,2 cm
2, 0,3 mm	20 cm	20 cm
3, 0.3 mm	19,9 cm	19,9 cm
4, 0.3 mm	20 cm	20 cm
5, 0.3 mm	20 cm	20,2 cm
6, 0.3 mm	19,9 cm	20 cm
7, 0.3 mm	20 cm	20,1 cm
8, 0.3 mm	19,9 cm	20 cm
9, 0.3 mm	19,9 cm	20 cm
10, 0.3 mm	20 cm	20,1 cm
Maximum deviation of 1 %		

Thickness of the samples measured with a caliper				
Samples	Top	Bottom	Left	Right
1, 0.65 mm	2.49 mm	2.40 mm	2.45 mm	2.44 mm
2, 0.65 mm	2.52 mm	2.50 mm	2.64 mm	2.46 mm
3, 0.65 mm	2.55 mm	2.56 mm	2.53 mm	2.47 mm
4, 0.65 mm	2.42 mm	2.50 mm	2.43 mm	2.37 mm
1, 0.35 mm	2.25 mm	2.08 mm	2.19 mm	2.11 mm
2, 0,35 mm	2.06 mm	2.12 mm	2.08 mm	2.08 mm
3, 0.35 mm	2.13 mm	2.08 mm	2.02 mm	2.04 mm
4, 0.35 mm	2.21 mm	2.11 mm	1.97 mm	2.09 mm
1, 0.15 mm	1.94 mm	1.88 mm	1.91 mm	1.91 mm
2, 0,15 mm	1.90 mm	1.75 mm	1.83 mm	1.84 mm
3, 0,15 mm	1.91 mm	1.86 mm	1.90 mm	1.90 mm
4, 0.15 mm	1.91 mm	1.87 mm	1.82 mm	1.92 mm
5, 0.15 mm	1.88 mm	2.01 mm	1.96 mm	1.95 mm
6, 0.15 mm	1.93 mm	1.90 mm	1.82 mm	1.88 mm
7, 0.15 mm	1.92 mm	1.97 mm	1.89 mm	1.90 mm
8, 0.15 mm	2.08 mm	1.95 mm	1.97 mm	1.93 mm
9, 0.15 mm	1.91 mm	2.01 mm	1.91 mm	1.94 mm
10, 0.15 mm	1.90 mm	1.91 mm	1.91 mm	1.93 mm

## APPENDIX C

```
B=Afterfiveimpactsagainniew0(:,:); % variable for the
name of imported data

xx1=13; % start point of the image at x-axis
yy1=18; % start point of image at y axis
C=table2array(B); % converting table to homogeneous array
D=C(1+xx1:230,1+yy1:230); % range of data
q=size(D); % determining the maximum amount of rows and
columns

x1=115-xx1; % coordinate on x-axis
y1=205-yy1; % coordinate on y-axis
x2=x1; % coordinate on x-axis
y2=40-yy1; % Coordinate on y-axis
% These coordinate are in the composite close to the edge
E=D; % Giving the matrix D another name
F=E-
((E(x1,y1)+E(x1+5,y1)+E(x1+10,y1)+E(x1+15,y1)+E(x2+20,y1)+
E(x2,y2)+E(x2+15,y2)+E(x2+10,y2)+E(x2+5,y2)+E(x2+20,y2))/
10);
% the average dB of then coordinates are substructed from
the whole matrix E and the new matrix is called F

G=F'; % the transpose of the matrix F is taken and is now
called G
imshow(G, [-12 2]); % Showing an image based on the db
values from matrix G
xlabel('Width (mm)', 'FontSize',12) % Name of the x-axis
ylabel('Length (mm)', 'FontSize',12) % Name of the y-axis
title('C-scan', 'FontSize',12) % Title name of the
graph
ax = gca; % current axis
ax.YDir = 'normal' % y-axis starting from zero
ax.XDir= 'normal' % x-axis starting from zero
axis([0 q(1) 0 q(2)]) % reach of the axis specified
axis on
h=colormap (jet); % specifying the colour of the plor
y2 = colorbar; % including a colour bar
colormap( flipud(h) ); % reversing/flipping the colours in
the plot

ylabel(y2 , 'scan signal (dB)', 'FontSize',12) % mentioning
the unit of the colour bar
set(y2, 'ylim' , [-12 2], 'FontSize',12) % setting the range
of the colourbar
```

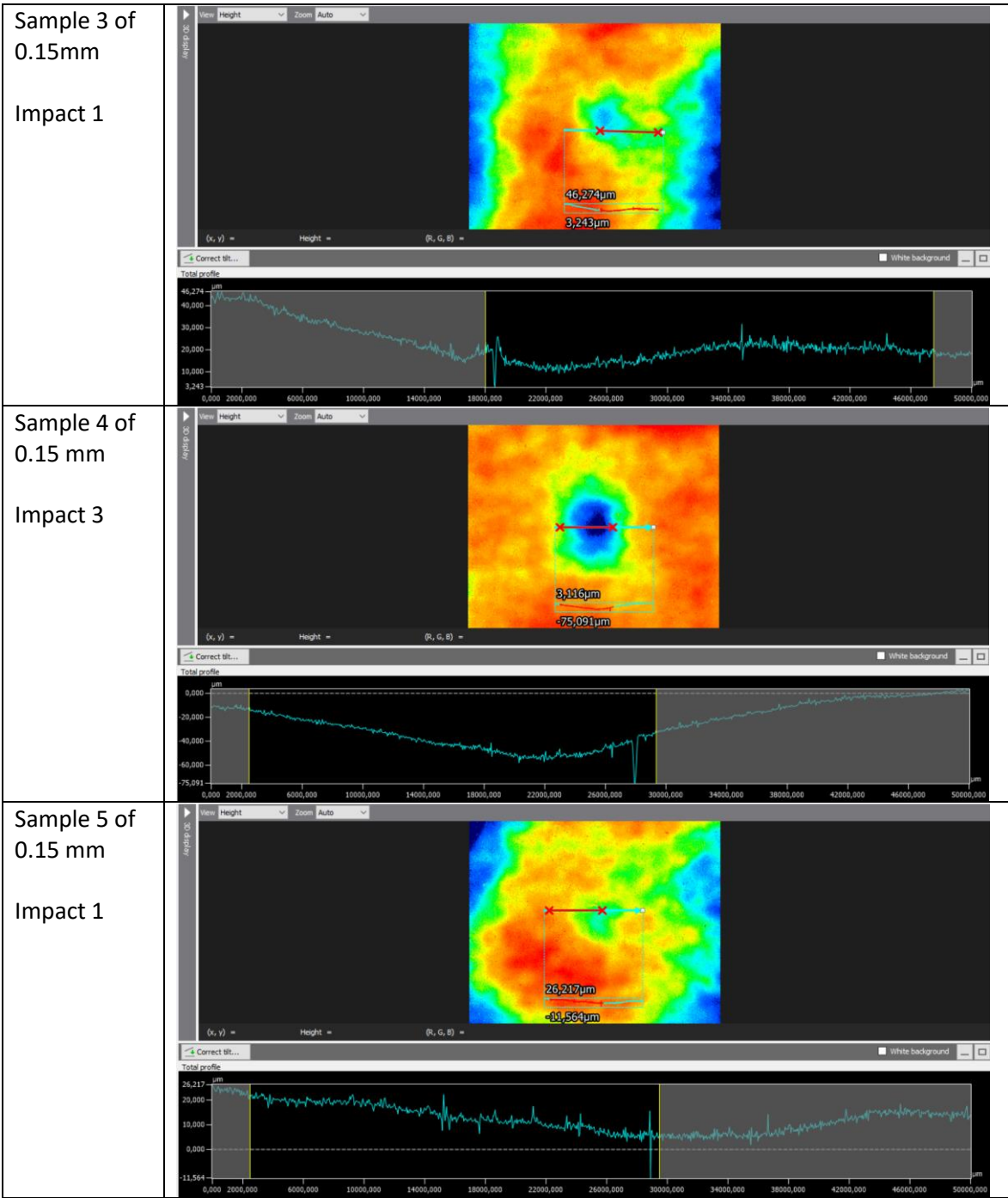
## APPENDIX D

Samples	First impact		Second impact		Third impact	
	Velocity	mass	Velocity	mass	Velocity	Mass
1, 0.65 mm	127.03 m/s	4.09 g	125.23 m/s	4.06 g	123.92 m/s	4.02 g
2, 0.65 mm	118.13 m/s	4.01 g	118.13 m/s	4.07 g	117.35 m/s	3.92 g
3, 0.65 mm	116.20 m/s	3.96 g	-	3.91 g	124.35 m/s	4.02 g
4, 0.65 mm	116.96 m/s	4.09 g	126.57 m/s	3.94 g	125.68 m/s	3.86 g
1, 0.35 mm	121.37 m/s	4.05 g	118.13 m/s	4.17 g	118.92 m/s	4.11 g
2, 0,35 mm	114.69 m/s	3.96 g	115.82 m/s	4.01 g	124.79 m/s	3.93 g
3, 0.35 mm	122.63 m/s	3.91 g	124.79 m/s	3.94 g	121.26 m/s	3.83 g
4, 0.35 mm	122.21 m/s	3.96 g	115.07 m/s	3.99 g	-	4.03 g
1, 0.15 mm	130.78 m/s	4.05 g	128.41 m/s	3.93 g	122.63 m/s	3.87 g
2, 0.15 mm	129.82 m/s	3.90 g	123.92 m/s	4.08 g	123.06 m/s	3.90 g
3, 0.15 mm	126.57 m/s	3.94 g	123.06 m/s	3.95 g	127.03 m/s	3.92 g
4, 0.15 mm	123.92 m/s	4.05 g	124.79 m/s	3.87 g	121.37 m/s	3.88 g
5, 0.15 mm	96.83 m/s	4.03 g	100.11 m/s	4.00 g	89.50 m/s	3.83 g
6, 0.15 mm	107.07 m/s	4.09 g	-	4.03 g	107.70 m/s	3.97 g
7, 0.15 mm	105.48 m/s	3.91 g	108.05 m/s	3.89 g	104.24 m/s	3.92 g
8, 0.15 mm	88.60 m/s	3.96 g	91.34 m/s	3.97 g	92.29 m/s	4.08 g
9, 0.15 mm	81.28 m/s	4.07 g	90.87 m/s	4.00 g	92.78 m/s	4.00 g
10, 0.15 mm	95.01 m/s	4.06 g	91.81 m/s	3.97 g	92.29 m/s	3.99 g

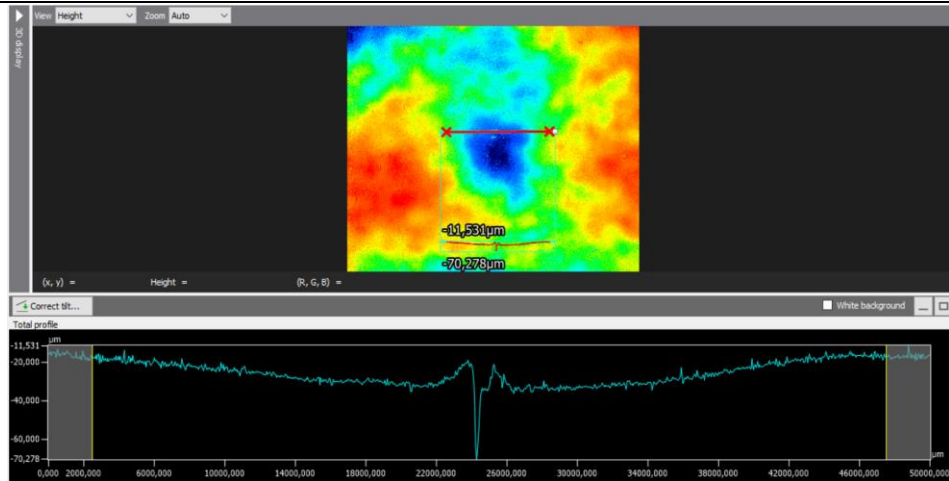
	Fourth impact		Fifth impact		Sixth impact	
	Velocity	mass	Velocity	mass	Velocity	mass
1, 0.65 mm	121.37 m/s	3.94 g	123.48 m/s	3.93 g		
2, 0.65 mm	123.48 m/s	3.81 g	118.85 m/s	3.93 g		
3, 0.65 mm	119.73 m/s	3.96 g	119.73 m/s	3.80 g		
4, 0.65 mm	123.06 m/s	4.00 g	124.79 m/s	3.97 g		
1, 0.35 mm	123.06 m/s	3.96 g	123.48 m/s	3.92 g		
2, 0,35 mm	124.35 m/s	3.80 g	121.37 m/s	3.84 g		
3, 0.35 mm	120.96 m/s	3.92 g	122.21 m/s	3.92 g		
4, 0.35 mm	120.96 m/s	3.86 g	118.92 m/s	3.85 g		
1, 0.15 mm	124.79 m/s	3.99 g	123.48 m/s	3.99 g		
2, 0.15 mm	118.92 m/s	4.01 g	11.30 m/s	3.90 g	123.92 m/s	4.07 g
3, 0.15 mm	123.48 m/s	3.81 g	124.35 m/s	3.95 g		
4, 0.15 mm	123.06 m/s	3.89 g	124.35 m/s	4.03 g		
5, 0.15 mm	104.24 m/s	3.93 g	104.85 m/s	3.93 g		
6, 0.15 mm	104.85 m/s	4.06 g	105.48 m/s	4.04 g		
7, 0.15 mm	106.43 m/s	3.90 g	101.55 m/s	4.08 g		
8, 0.15 mm	89.72 m/s	4.04 g	91.97 m/s	3.98 g		
9, 0.15 mm	92.29 m/s	4.01 g	88.82 m/s	4.05 g		
10, 0.15 mm	90.41 m/s	4.11 g	87.51 m/s	4.00 g		

# APPENDIX E

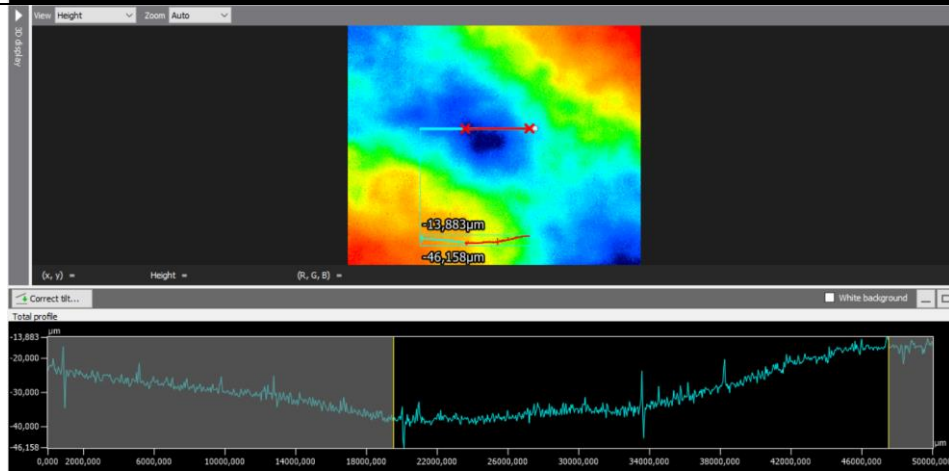
Roughness plot of cracks after impact	
<p>Sample 1 of 0.15 mm</p> <p>Impact 1</p>	
<p>Sample 2 of 0.15 mm</p> <p>Impact 1</p>	
<p>Sample 2 of 0.15 mm</p> <p>Impact 3</p>	



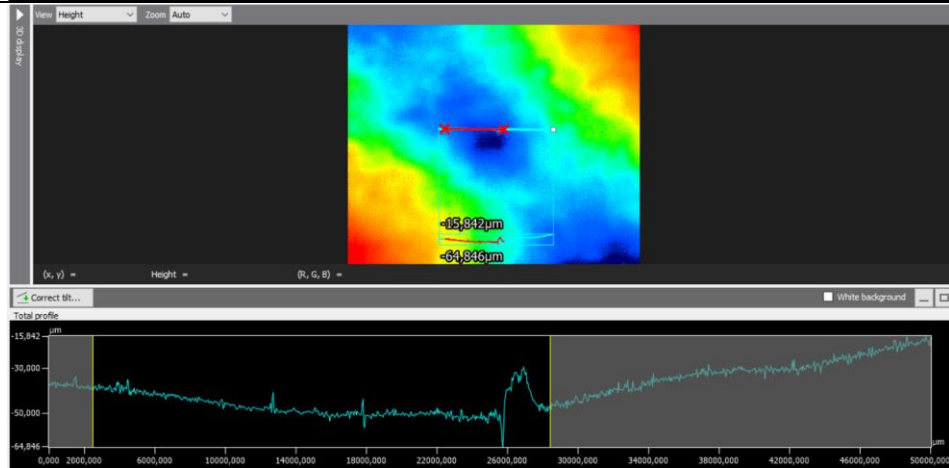
Sample 5 of  
0.15 mm  
Impact 3

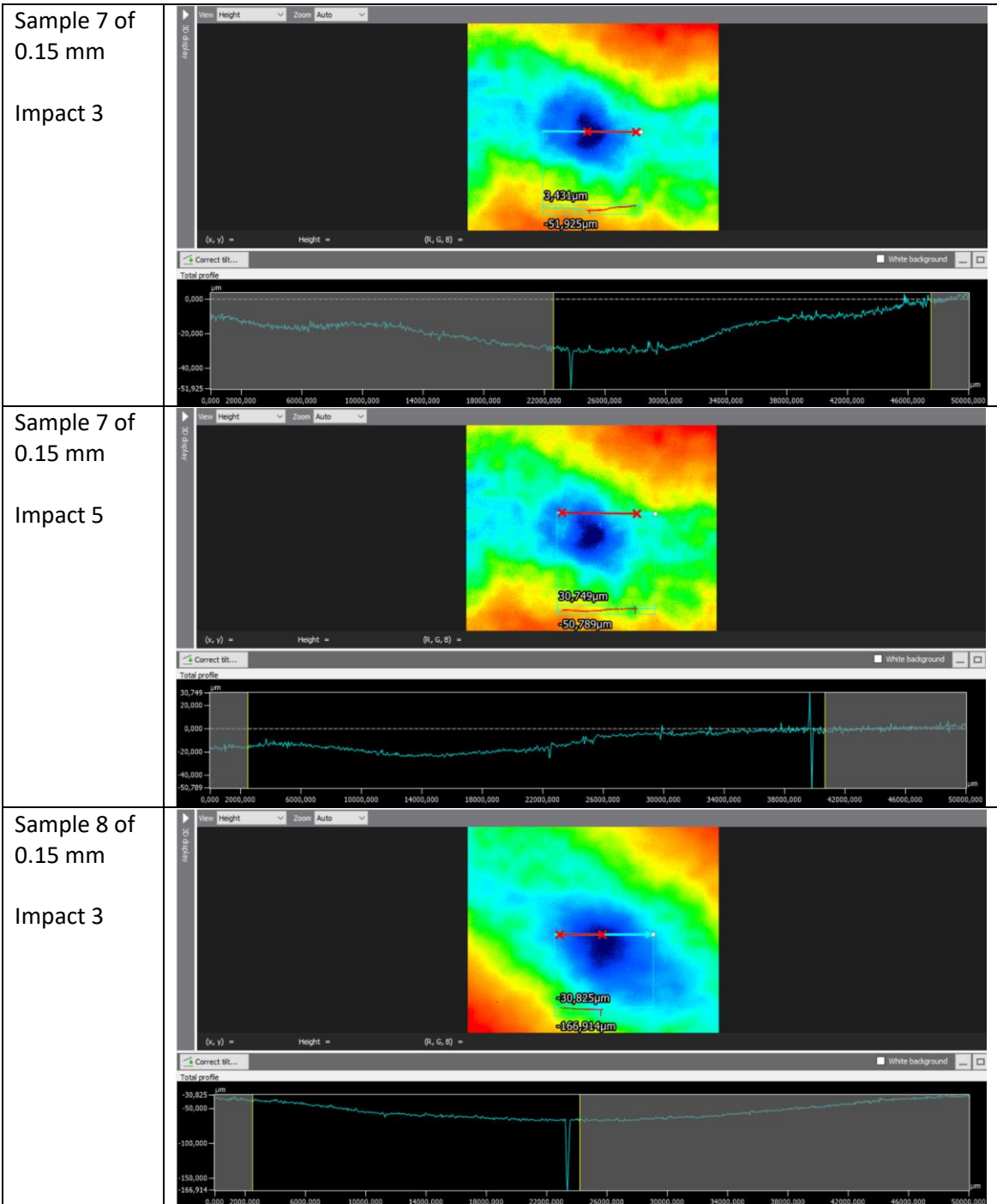


Sample 6 of  
0.15 mm  
Impact 3



Sample 6 of  
0.15 mm  
Impact 5



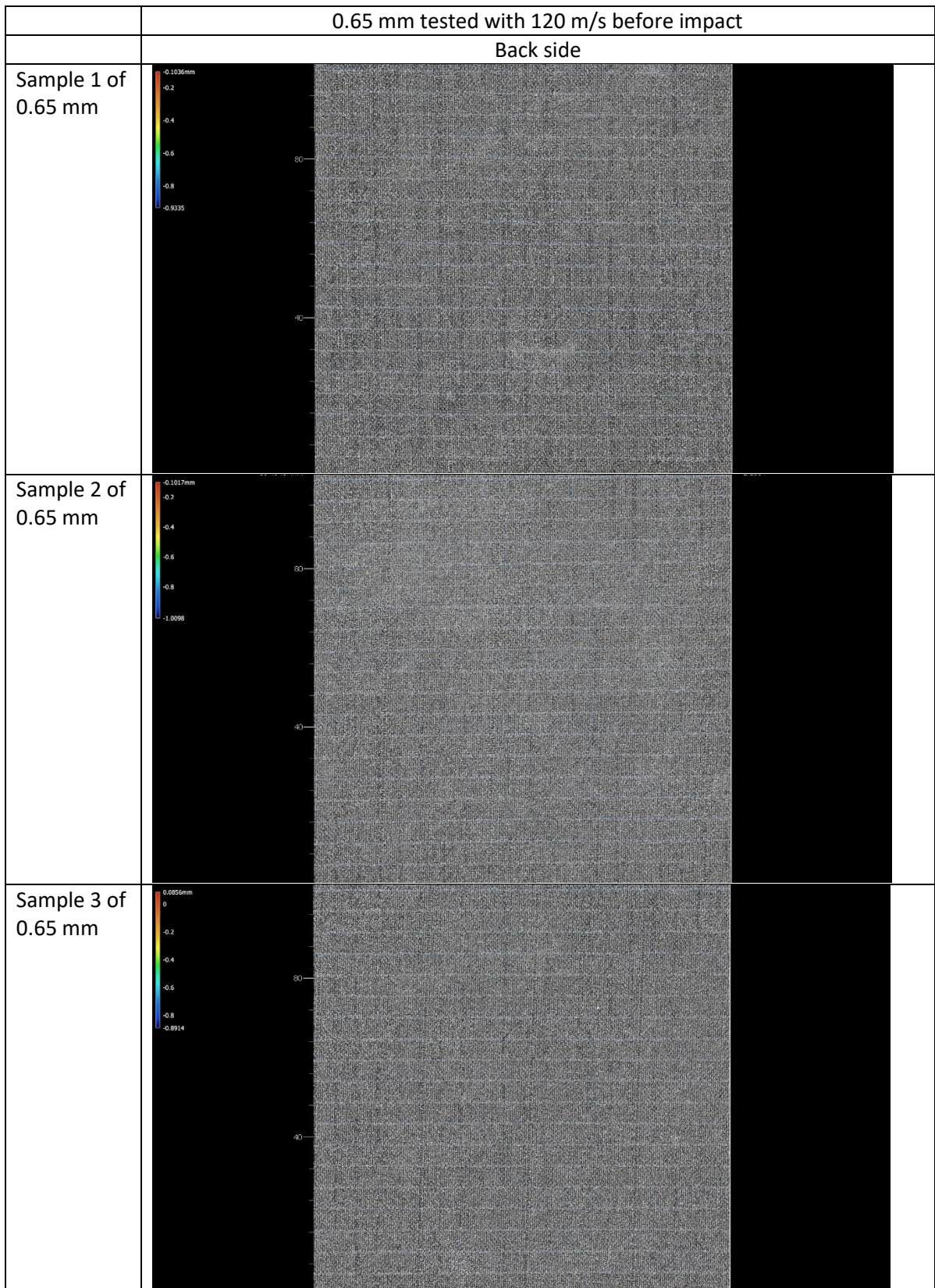


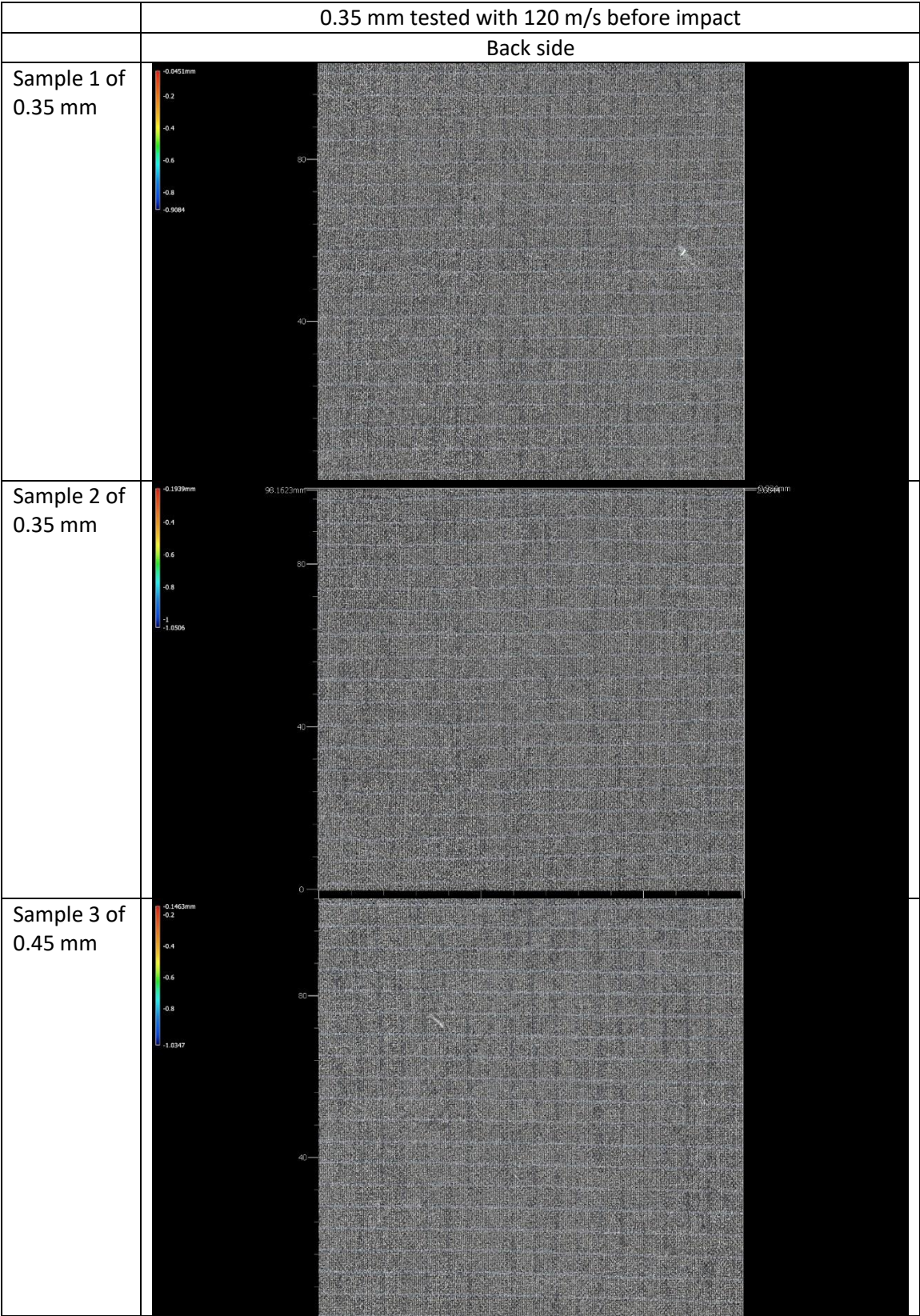
## APPENDIX F

Velocity	Samples	Damaged area after one impact	Damaged area after three impacts	Damage area after five impacts
120 m/s	Sample 1 of 0.65 mm	1498.79 mm <sup>2</sup>	3307.53 mm <sup>2</sup>	6100.10 mm <sup>2</sup>
	Sample 2 of 0.65 mm	1369.91 mm <sup>2</sup>	3266.74 mm <sup>2</sup>	6234.29 mm <sup>2</sup>
	Sample 3 of 0.65 mm	637.78 mm <sup>2</sup>	3515.11 mm <sup>2</sup>	6282.18 mm <sup>2</sup>
	Sample 1 of 0.35 mm	200.64 mm <sup>2</sup>	1550.41 mm <sup>2</sup>	2392.45 mm <sup>2</sup>
	Sample 2 of 0.35 mm	135.30 mm <sup>2</sup>	1390.63 mm <sup>2</sup>	2156.29 mm <sup>2</sup>
	Sample 3 of 0.35 mm	53.36 mm <sup>2</sup>	1233.20 mm <sup>2</sup>	2440.41 mm <sup>2</sup>
	Sample 1 of 0.15 mm	Cracks	57.56 mm <sup>2</sup>	475.11 mm <sup>2</sup>
	Sample 2 of 0.15 mm	Cracks	Cracks	20.24 mm <sup>2</sup>
	Sample 3 of 0.15 mm	Cracks	18.44 mm <sup>2</sup>	65.47 mm <sup>2</sup>
100 m/s	Sample 5 of 0.15 mm	Cracks	Cracks	14.28 mm <sup>2</sup>
	Sample 6 of 0.15 mm	No damage	Cracks	Cracks
	Sample 7 of 0.15 mm	No damage	Cracks	Cracks
90 m/s	Sample 8 of 0.15 mm	No damage	No damage	Cracks
	Sample 9 of 0.15 mm	No damage	No damage	No damage
	Sample 10 of 0.15 mm	No damage	No damage	No damage



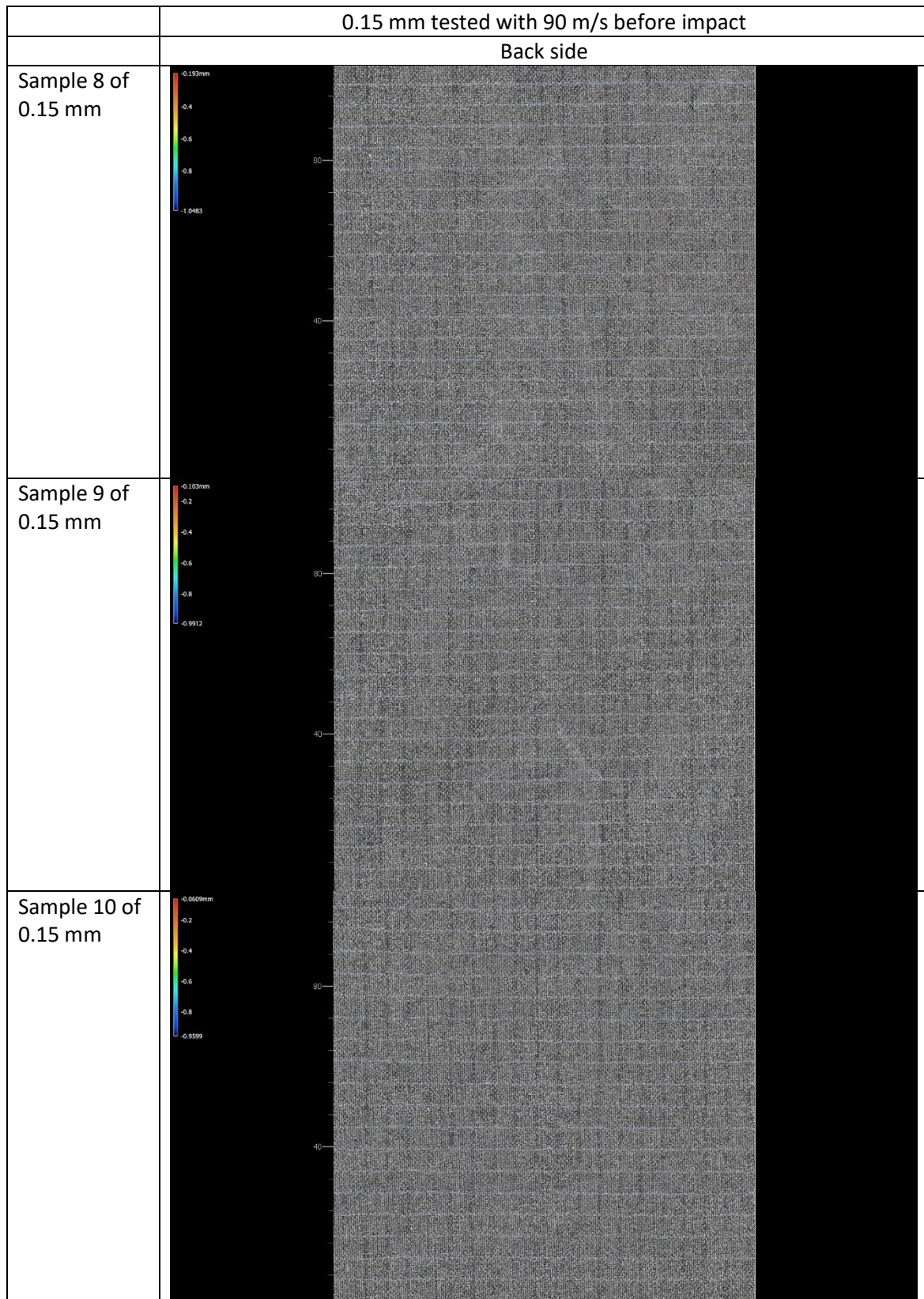
# APPENDIX G



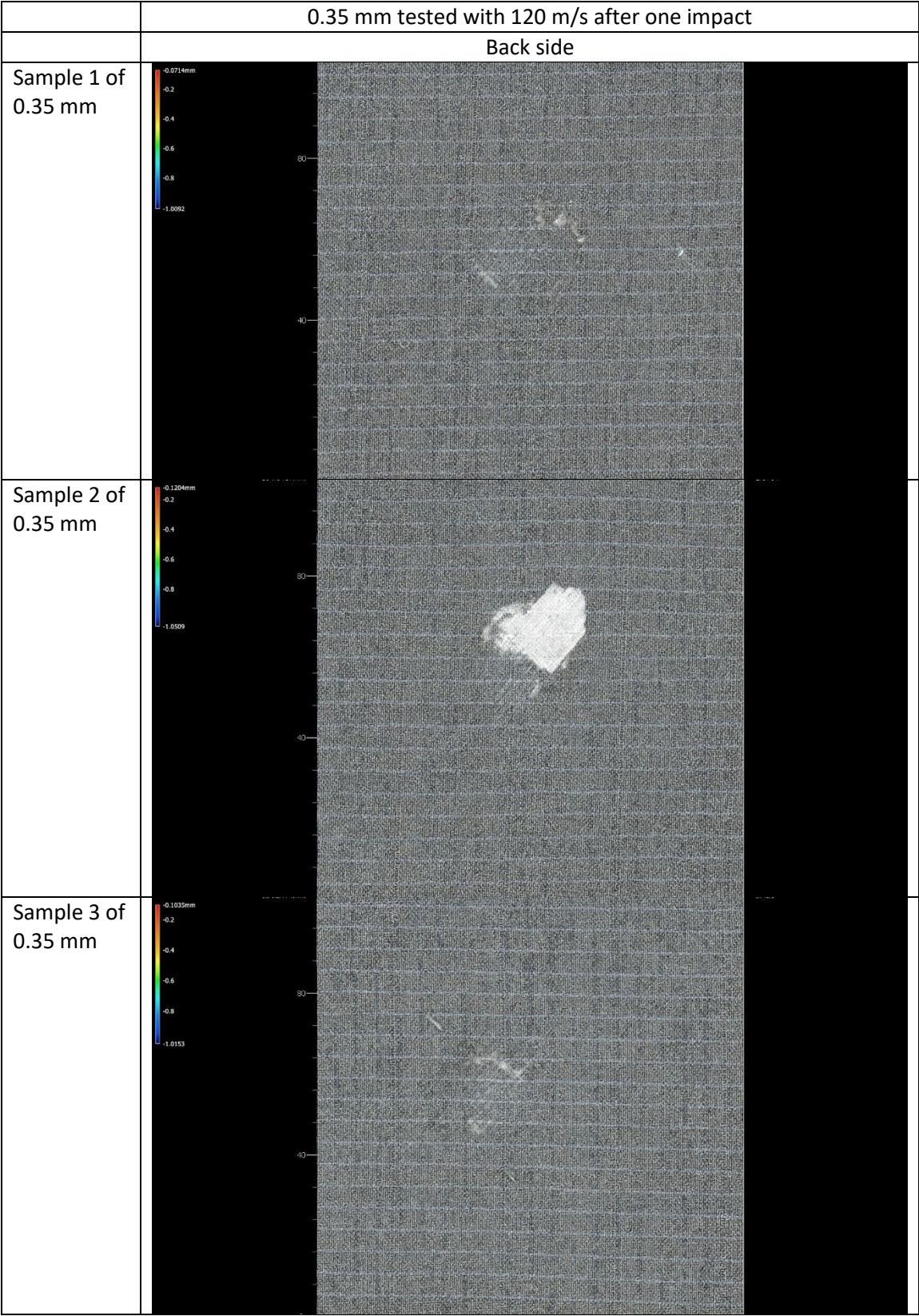


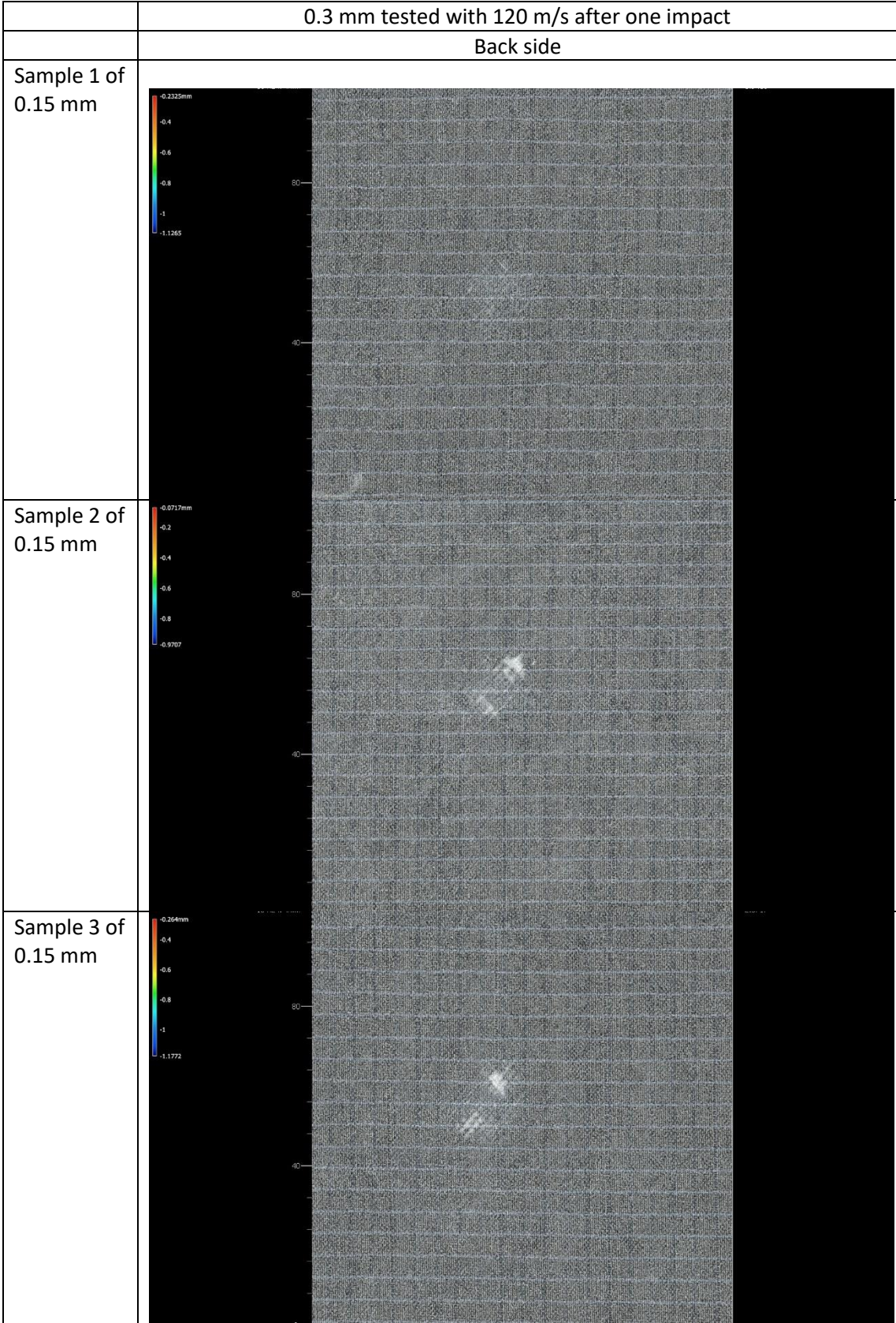
0.15 mm tested with 120 m/s before impact	
Back side	
Sample 1 of 0.15 mm	
Sample 2 of 0.15 mm	
Sample 3 of 0.15 mm	

0.15 mm tested with 100 m/s before impact	
Back side	
Sample 5 of 0.15 mm	<p>DIC image of Sample 5 back side. The image shows a grid pattern on a dark background. A color scale on the left indicates displacement values from -0.0233mm (red) to -0.8993mm (blue). The grid is slightly distorted, indicating deformation. The x-axis is labeled '0mm', '40', and '80'. The y-axis is labeled '0', '40', and '80'. There are also labels '104.4932mm' and '1.8188mm' at the top corners.</p>
Sample 6 of 0.15 mm	<p>DIC image of Sample 6 back side. The image shows a grid pattern on a dark background. A color scale on the left indicates displacement values from -0.0938mm (red) to -0.9642mm (blue). The grid is significantly distorted, indicating deformation. The x-axis is labeled '0mm', '40', and '80'. The y-axis is labeled '0', '40', and '80'.</p>
Sample 7 of 0.15 mm	<p>DIC image of Sample 7 back side. The image shows a grid pattern on a dark background. A color scale on the left indicates displacement values from -0.0288mm (red) to -0.9086mm (blue). The grid is significantly distorted, indicating deformation. The x-axis is labeled '0mm', '40', and '80'. The y-axis is labeled '0', '40', and '80'.</p>

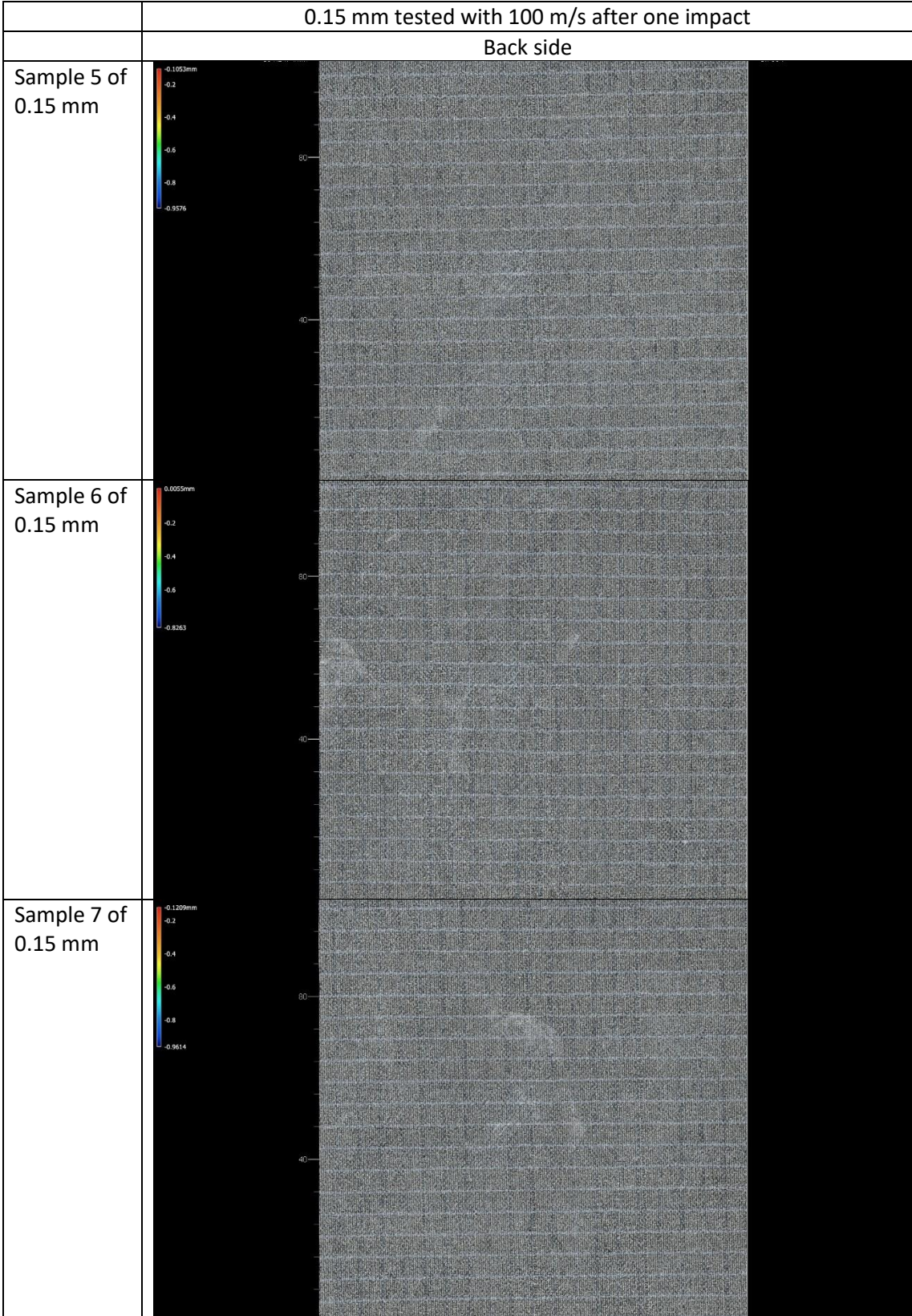


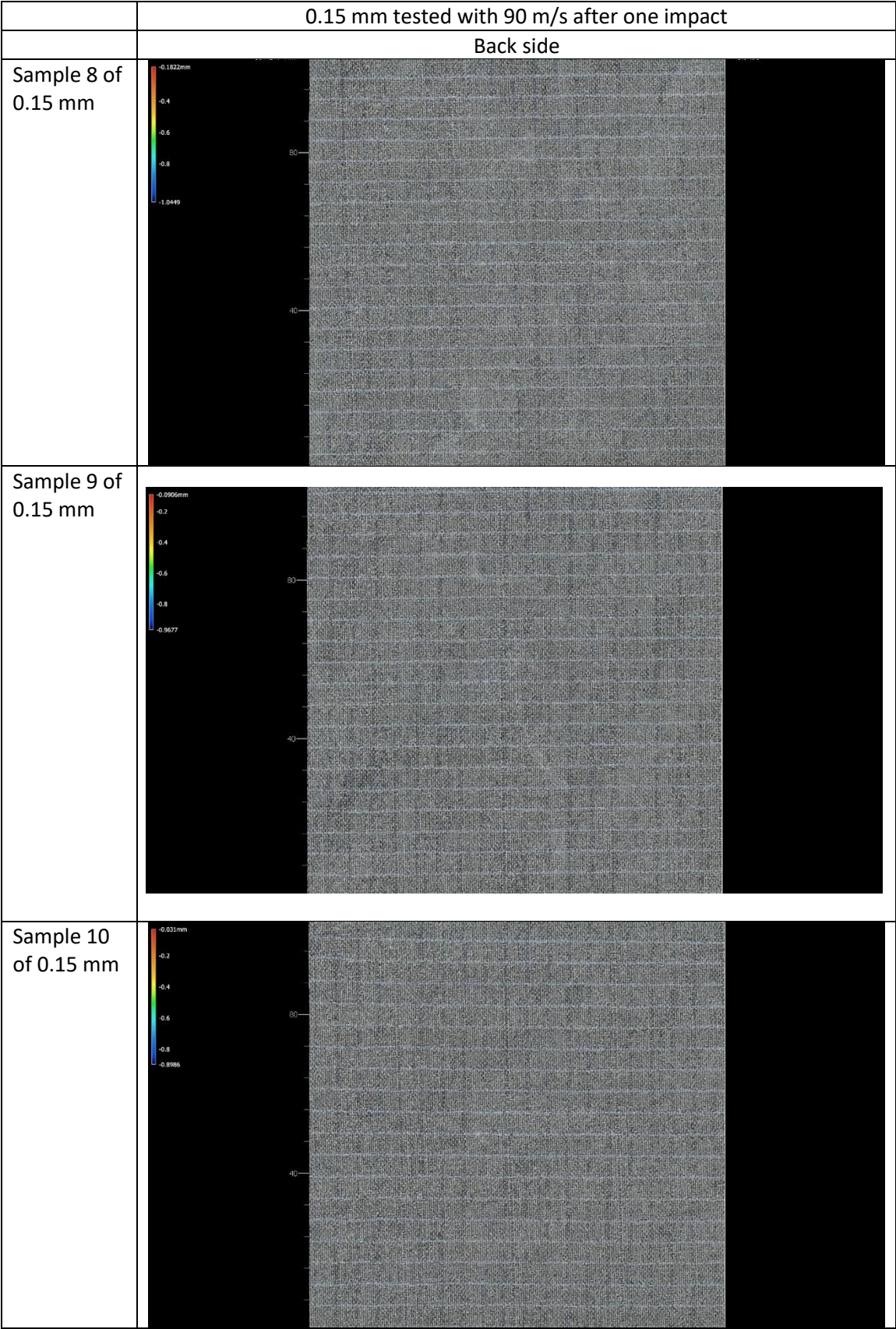
0.65 mm tested with 120 m/s after one impact	
Back side	
Sample 1 of 0.65 mm	
Sample 2 of 0.65 mm	
Sample 3 of 0.65 mm	

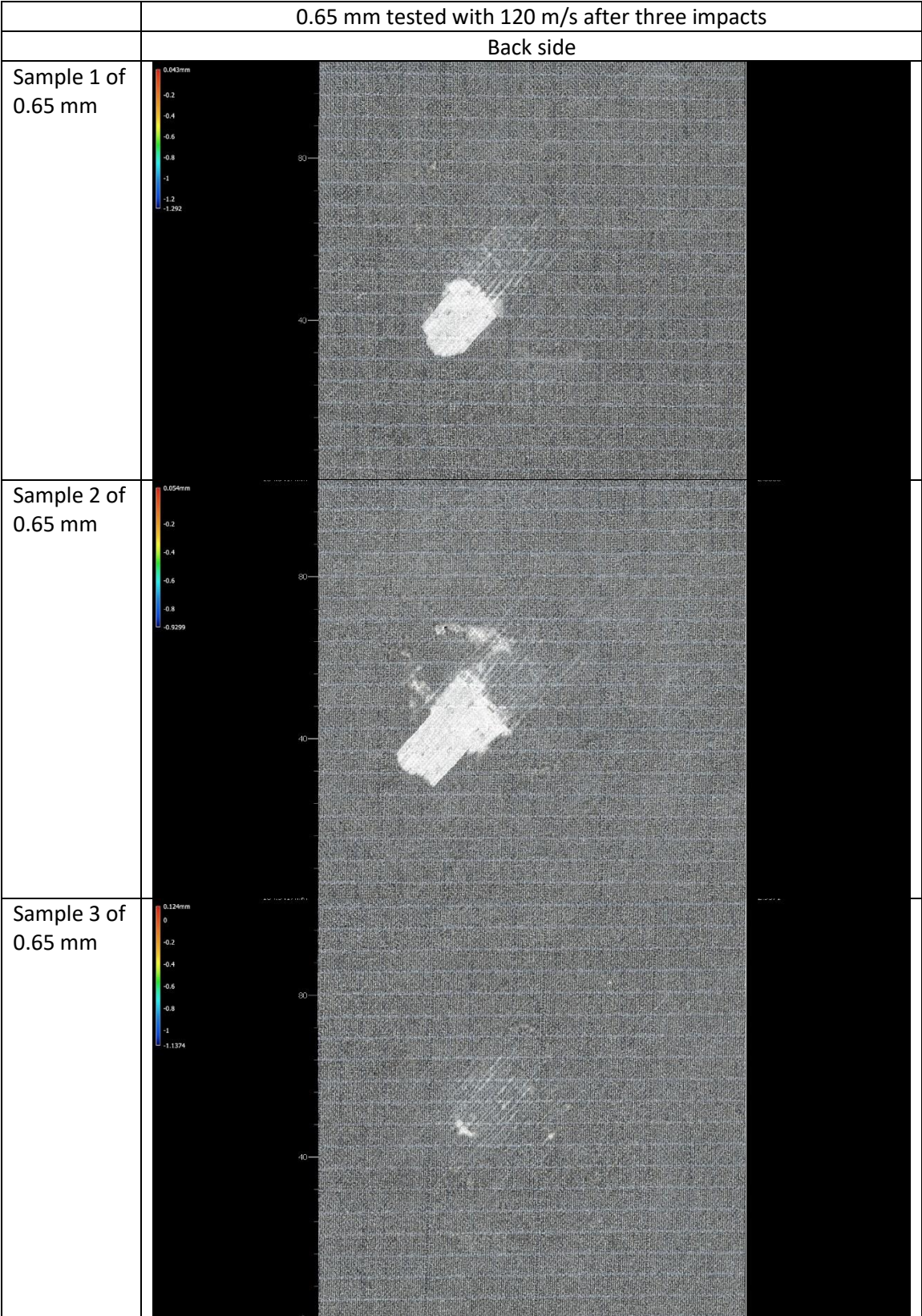


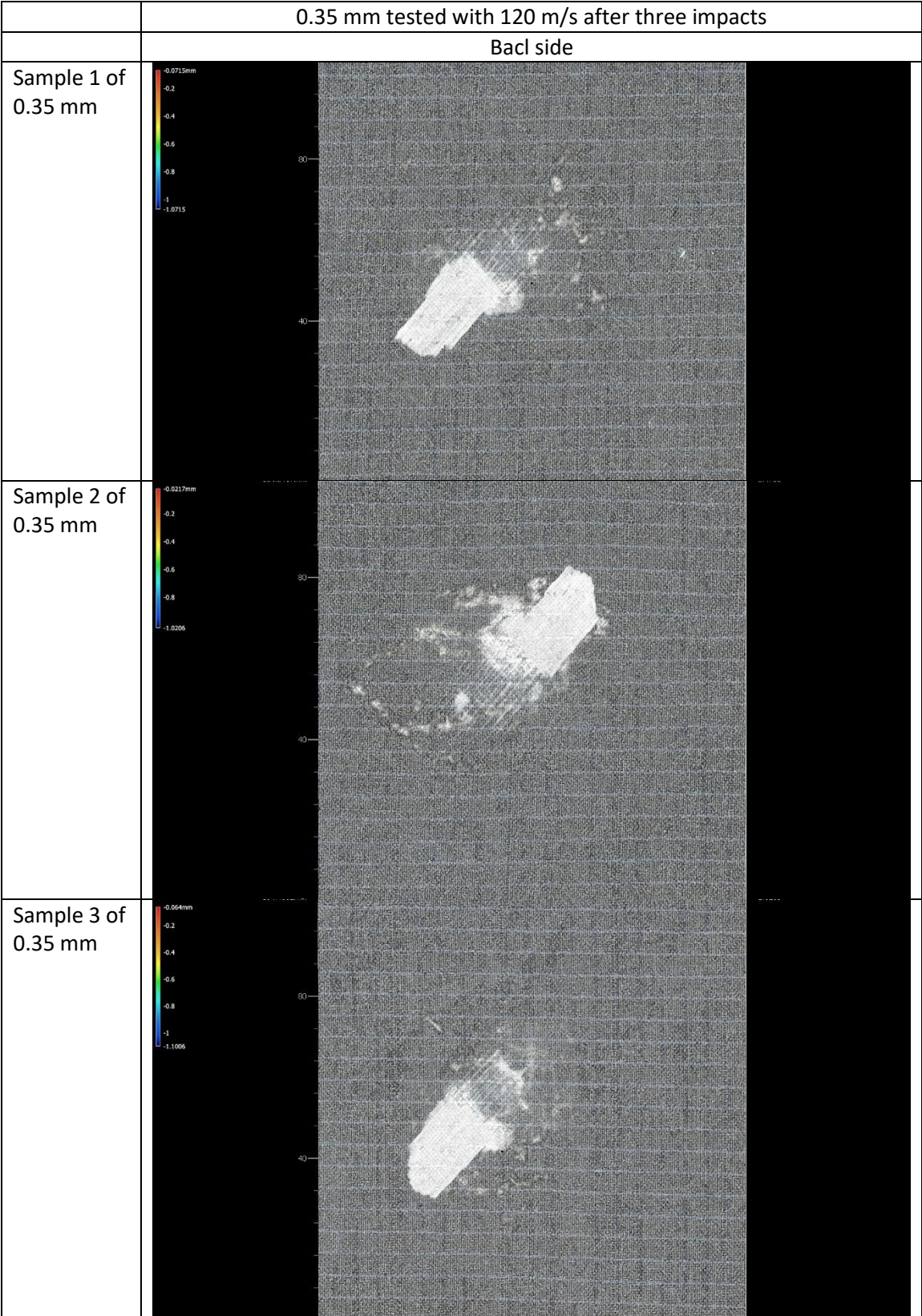


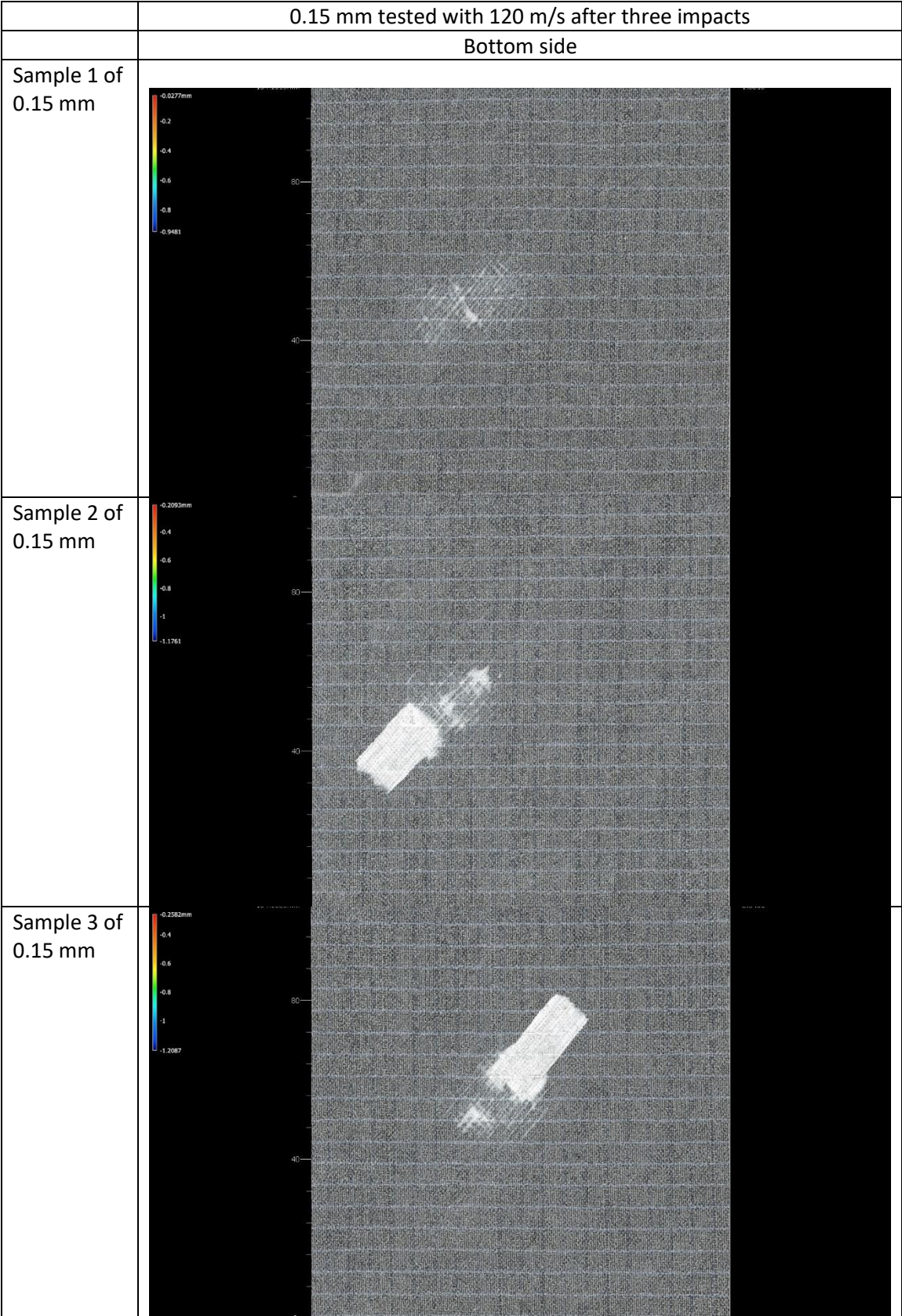


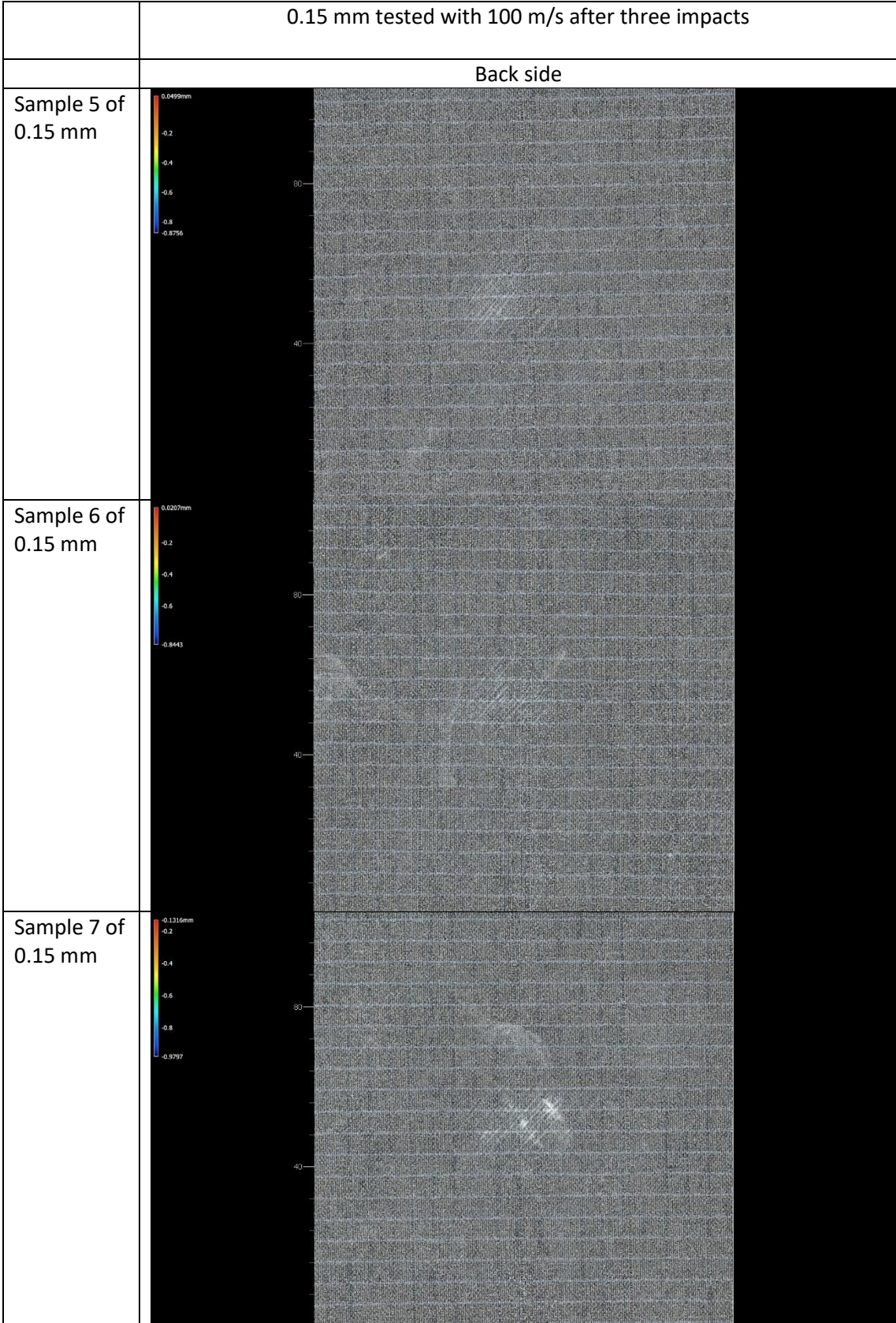


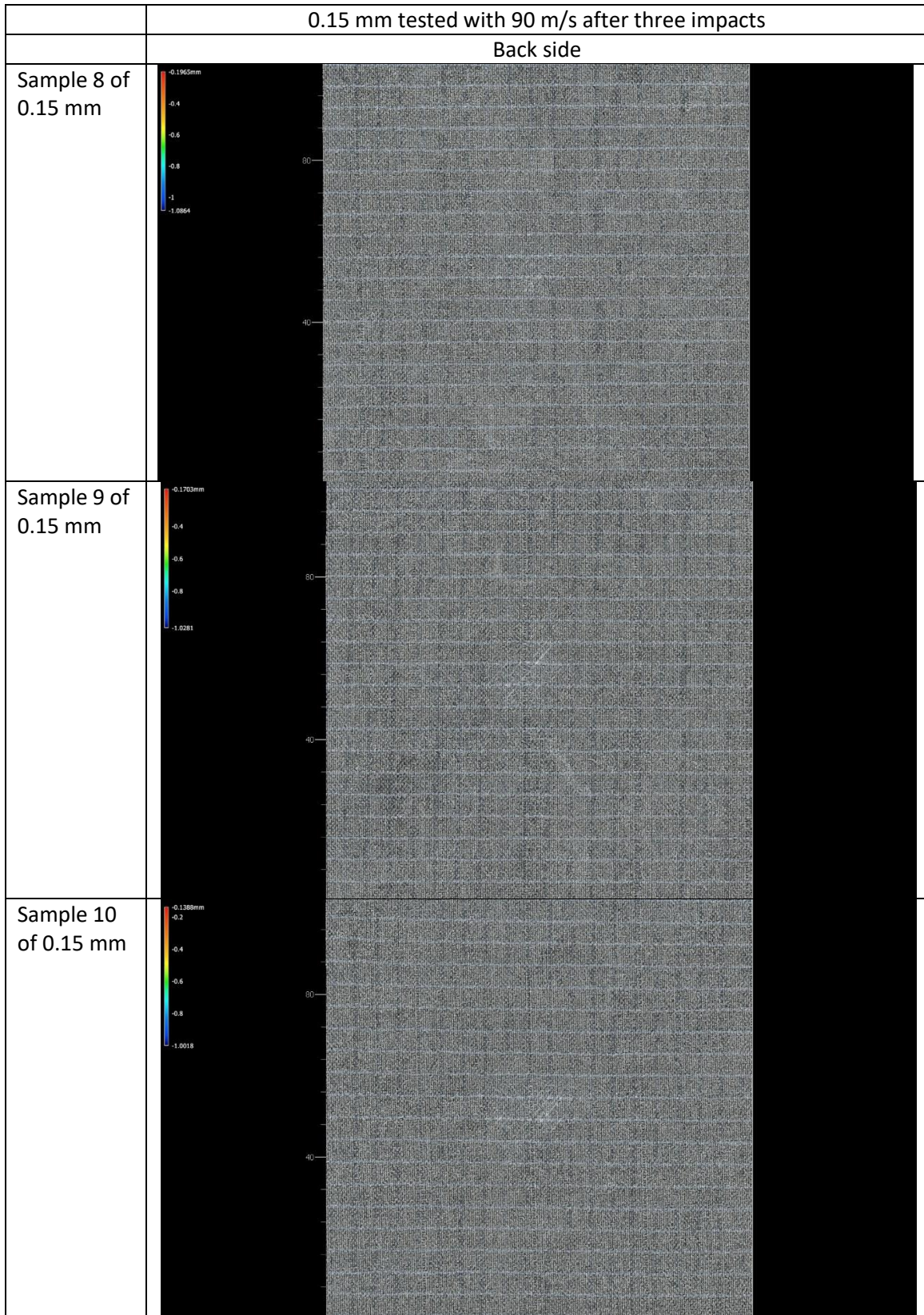










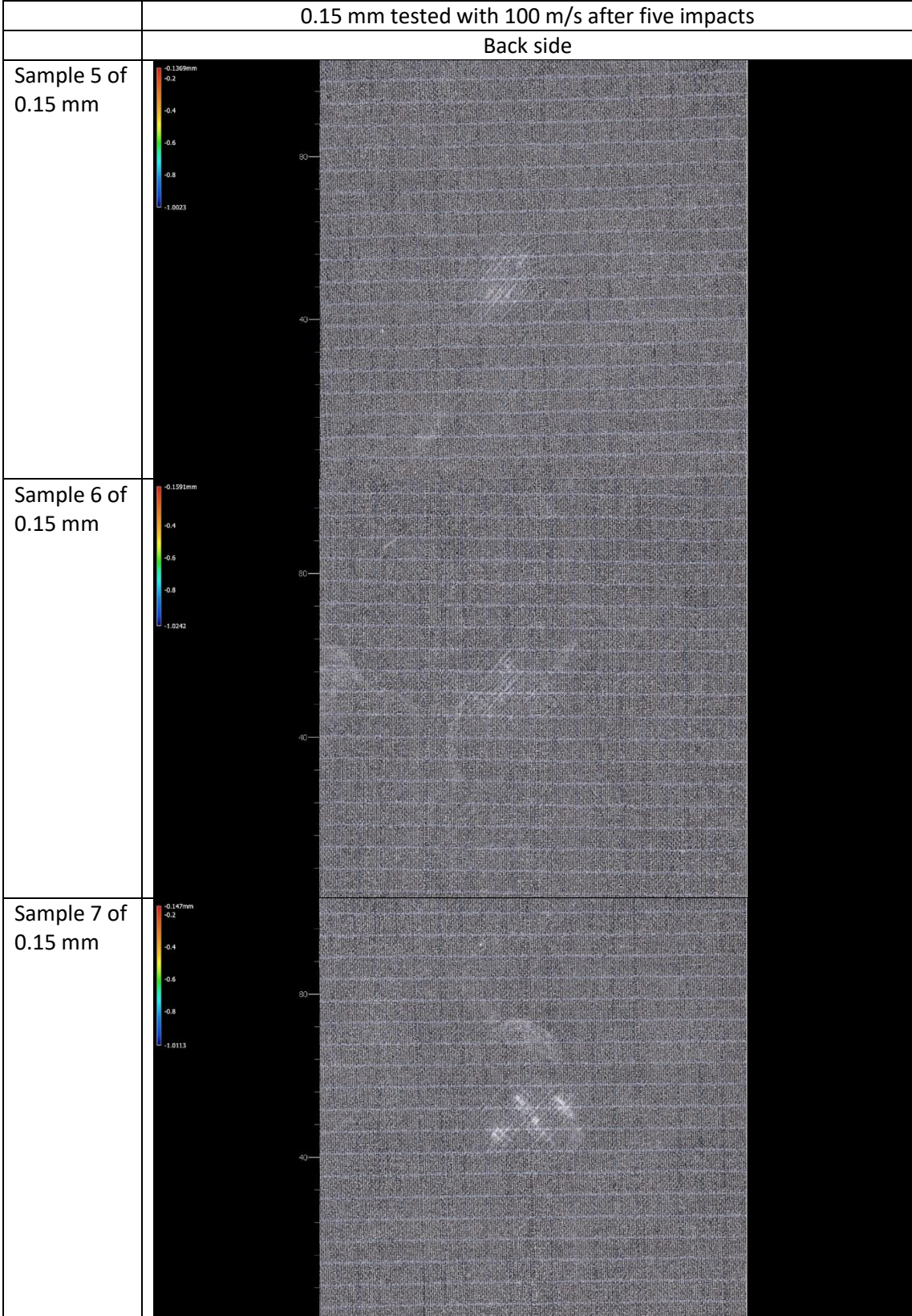


0.65 mm tested with 120 m/s after five impacts	
Back side	
Sample 1 of 0.65 mm	
Sample 2 of 0.65 mm	
Sample 3 of 0.65 mm	



0.35 mm tested with 120 m/s after five impacts	
Back side	
Sample 1 of 0.35 mm	
Sample 2 of 0.35 mm	
Sample 3 of 0.35 mm	

0.15 mm tested with 120 m/s after five impacts	
Back side	
Sample 1 of 0.15 mm	
Sample 2 of 0.15 mm	
Sample 3 of 0.15 mm	



0.15 mm tested with 90 m/s after five impacts	
Back side	
Sample 8 of 0.15 mm	
Sample 9 of 0.15 mm	
Sample 10 of 0.15 mm	

0.65 mm tested with 120 m/s before impact	
Front side	
Sample 1 of 0.65 mm	<p>0.2221mm 0.1 0 -0.1 -0.2 -0.3 -0.3823</p>
Sample 2 of 0.65 mm	<p>-0.01mm -0.05 -0.1 -0.15 -0.2 -0.25 -0.3153</p>
Sample 3 of 0.65 mm	<p>0.0273mm 0 -0.08 -0.16 -0.24 -0.32 -0.3623</p>

0.35 mm tested with 120 m/s before impact	
Front side	
Sample 1 of 0.35 mm	
Sample 2 of 0.35 mm	
Sample 3 of 0.35 mm	

0.15 mm tested with 120 m/s before impact	
Front side	
Sample 1 of 0.15 mm	<p>Micrograph of Sample 1 showing a circular ring. A color scale on the left indicates values from -0.2115mm (red) to -0.3358mm (blue).</p>
Sample 2 of 0.15 mm	<p>Micrograph of Sample 2 showing a circular ring. A color scale on the left indicates values from -0.0281mm (red) to -0.1929mm (blue).</p>
Sample 3 of 0.15 mm	<p>Micrograph of Sample 3 showing a circular ring. A color scale on the left indicates values from 0.0365mm (red) to -0.1984mm (blue).</p>

0.15 mm tested with 100 m/s before impact	
Front side	
Sample 5 of 0.15 mm	<p>A circular ring-shaped micrograph of Sample 5. The ring is dark against a lighter background. A color scale on the left indicates depth or displacement, ranging from -0.0469mm (red) to -0.2462mm (blue).</p>
Sample 6 of 0.15 mm	<p>A circular ring-shaped micrograph of Sample 6. The ring is dark against a lighter background. A color scale on the left indicates depth or displacement, ranging from -0.0226mm (red) to -0.2617mm (blue).</p>
Sample 7 of 0.15 mm	<p>A circular ring-shaped micrograph of Sample 7. The ring is dark against a lighter background. A color scale on the left indicates depth or displacement, ranging from -0.0427mm (red) to -0.169mm (blue).</p>



0.15 mm tested with 90 m/s before impact	
Front side	
Sample 8 of 0.15 mm	<p>0.0145mm 0 -0.05 -0.1 -0.15 -0.2 -0.2205</p>
Sample 9 of 0.15 mm	<p>-0.0539mm -0.06 -0.08 -0.1 -0.12 -0.1393</p>
Sample 10 of 0.15 mm	<p>-0.0312mm -0.08 -0.12 -0.16 -0.1906</p>

0.65 mm tested with 120 m/s after one impact	
Front side	
Sample 1 of 0.65 mm	
Sample 2 of 0.65 mm	
Sample 3 of 0.65 mm	

0.35 mm tested with 120 m/s after one impact	
Front side	
Sample 1 of 0.35 mm	
Sample 2 of 0.35 mm	
Sample 3 of 0.35 mm	

0.15 mm tested with 120 m/s after one impact	
Front side	
Sample 1 of 0.15 mm	<p>Micrograph of Sample 1 showing a circular impact ring. The color scale ranges from -0.1881mm (red) to -0.2472mm (blue). The ring is relatively uniform in thickness and color.</p>
Sample 2 of 0.15 mm	<p>Micrograph of Sample 2 showing a circular impact ring. The color scale ranges from -0.1317mm (red) to -0.2363mm (blue). The ring shows some non-uniformity in thickness and color.</p>
Sample 3 of 0.15 mm	<p>Micrograph of Sample 3 showing a circular impact ring. The color scale ranges from -0.1228mm (red) to -0.26mm (blue). The ring shows significant non-uniformity in thickness and color, with some areas appearing much thicker and more reddish.</p>

0.15 mm tested with 100 m/s after one impact	
Front side	
Sample 5 of 0.15 mm	<p>Micrograph of Sample 5 showing a circular impact crater. The depth scale ranges from -0.154mm (red) to -0.2305mm (blue). The crater diameter is approximately 100mm. The impact location is marked at 104.3889mm and 0.0833mm.</p>
Sample 6 of 0.15 mm	<p>Micrograph of Sample 6 showing a circular impact crater. The depth scale ranges from -0.3704mm (red) to -0.5592mm (blue). The crater diameter is approximately 100mm. The impact location is marked at 104.4361mm and 0.5099mm.</p>
Sample 7 of 0.15 mm	<p>Micrograph of Sample 7 showing a circular impact crater. The depth scale ranges from 0.1144mm (red) to -0.0687mm (blue). The crater diameter is approximately 100mm. The impact location is marked at 104.4832mm and 0.0284mm.</p>

0.315 mm tested with 90 m/s after one impact	
Front side	
Sample 8 of 0.15 mm	
Sample 9 of 0.15 mm	
Sample 10 of 0.15 mm	

0.65 mm tested with 120 m/s after three impacts	
Front side	
Sample 1 of 0.65 mm	<p>3.4769mm 3 2 1 0 -1 -1.3441</p> <p>104.4832mm 6.7253mm 2.7975</p> <p>50</p> <p>0mm 50 100 127.1724</p>
Sample 2 of 0.65 mm	<p>4.5279mm 4 3 2 1 0 -1.0034</p> <p>104.4832mm 11.4961mm 2.5996</p> <p>50</p> <p>0mm 50 100 127.1724</p>
Sample 3 of 0.65 mm	<p>3.1653mm 2.4 1.6 0.8 0 -0.905</p> <p>104.4361mm 6.6589mm 2.948</p> <p>50</p> <p>0mm 50 100 127.1724</p>

0.35 mm tested with 120 m/s after three impacts	
Front side	
Sample 1 of 0.35 mm	
Sample 2 of 0.35 mm	
Sample 3 of 0.35 mm	



0.15 mm tested with 120 m/s after three impacts	
Front side	
Sample 1 of 0.15 mm	<p>Micrograph of Sample 1 showing a circular impact pattern. The color scale ranges from -0.1363mm (red) to -0.3928mm (blue). The impact is centered at approximately (50, 50) on a 100x100 mm scale. The circular boundary is clearly visible, with a diameter of approximately 100 mm. The impact depth is approximately 0.15 mm.</p>
Sample 2 of 0.15 mm	<p>Micrograph of Sample 2 showing a circular impact pattern. The color scale ranges from -0.1336mm (red) to -0.3676mm (blue). The impact is centered at approximately (50, 50) on a 100x100 mm scale. The circular boundary is clearly visible, with a diameter of approximately 100 mm. The impact depth is approximately 0.15 mm.</p>
Sample 3 of 0.15 mm	<p>Micrograph of Sample 3 showing a circular impact pattern. The color scale ranges from -0.0942mm (red) to -0.2155mm (blue). The impact is centered at approximately (50, 50) on a 100x100 mm scale. The circular boundary is clearly visible, with a diameter of approximately 100 mm. The impact depth is approximately 0.15 mm.</p>

0.15 mm tested with 100 m/s after three impacts	
Front side	
Sample 5 of 0.15 mm	<p>Micrograph of Sample 5 showing a circular impact crater. The color scale ranges from -0.1896mm (red) to -0.2385mm (blue). The crater is approximately 100mm in diameter. The x-axis is labeled from 0mm to 127.1724mm, and the y-axis is labeled from 0 to 104.4832mm.</p>
Sample 6 of 0.15 mm	<p>Micrograph of Sample 6 showing a circular impact crater. The color scale ranges from -0.0402mm (red) to -0.2261mm (blue). The crater is approximately 100mm in diameter. The x-axis is labeled from 0mm to 127.1724mm, and the y-axis is labeled from 0 to 104.4832mm.</p>
Sample 7 of 0.15 mm	<p>Micrograph of Sample 7 showing a circular impact crater. The color scale ranges from -0.0504mm (red) to -0.1681mm (blue). The crater is approximately 100mm in diameter. The x-axis is labeled from 0mm to 127.1724mm, and the y-axis is labeled from 0 to 104.4832mm.</p>

0.15 mm tested with 90 m/s after three impacts	
Front side	
Sample 8 of 0.15 mm	
Sample 9 of 0.15 mm	
Sample 10 of 0.15 mm	

0.65 mm tested with 120 m/s after five impacts	
Front side	
Sample 1 of 0.65 mm	<p>4.0145mm 3 2 1 0 -0.6606</p> <p>104.4832mm 14.1029mm 2.9483</p> <p>50 0 0mm 50 100 127.1724</p>
Sample 2 of 0.65 mm	<p>3.6171mm 3 2 1 0 -0.792</p> <p>104.4361mm 12.5051mm 2.7295</p> <p>50 0 0mm 50 100 127.1724</p>
Sample 3 of 0.65 mm	<p>3.6851mm 3 2 1 0 -1.0996</p> <p>104.4361mm 11.9551mm 2.3138</p> <p>50 0 0mm 50 100 127.1724</p>

0.35 mm tested with 120 m/s after five impacts	
Front side	
Sample 1 of 0.35 mm	
Sample 2 of 0.35 mm	
Sample 3 of 0.35 mm	

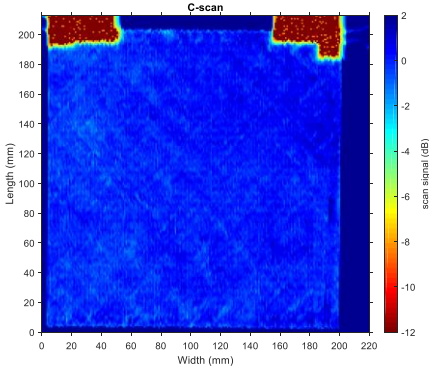
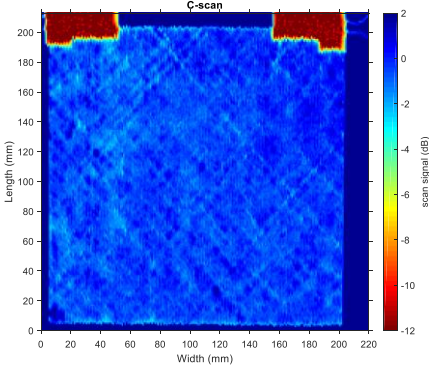
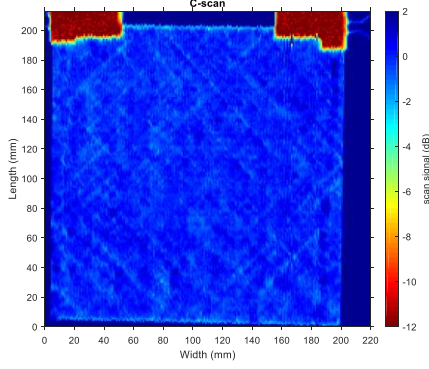
0.15 mm tested with 120 m/s after five impacts	
Front side	
Sample 1 of 0.15 mm	
Sample 2 of 0.15 mm	
Sample 3 of 0.15 mm	

0.15 mm tested with 100 m/s after five impacts	
Front side	
Sample 5 of 0.15 mm	<p>Micrograph of Sample 5 showing a circular impact zone. The color scale ranges from -0.1799mm (red) to -0.2412mm (blue). The impact zone is centered around 50mm on the x-axis. The y-axis ranges from 0 to 104.4361mm. The x-axis ranges from 0 to 127.1724mm.</p>
Sample 6 of 0.15 mm	<p>Micrograph of Sample 6 showing a circular impact zone. The color scale ranges from -0.078mm (red) to -0.2872mm (blue). The impact zone is centered around 50mm on the x-axis. The y-axis ranges from 0 to 104.4832mm. The x-axis ranges from 0 to 127.1724mm.</p>
Sample 7 of 0.15 mm	<p>Micrograph of Sample 7 showing a circular impact zone. The color scale ranges from -0.1257mm (red) to -0.2329mm (blue). The impact zone is centered around 50mm on the x-axis. The y-axis ranges from 0 to 104.3889mm. The x-axis ranges from 0 to 127.1724mm.</p>

0.15 mm tested with 90 m/s after five impacts	
Front side	
Sample 8 of 0.15 mm	<p>Micrograph showing the front side of Sample 8. The image displays a circular impact pattern on a light-colored surface. A color scale on the left indicates depth values ranging from -0.0722mm (red) to -0.2838mm (blue). The circular pattern is centered around a diameter of approximately 100mm. The x-axis is labeled from 0mm to 127.1724mm, and the y-axis is labeled from 0 to 104.4361mm.</p>
Sample 9 of 0.15 mm	<p>Micrograph showing the front side of Sample 9. The image displays a circular impact pattern on a light-colored surface. A color scale on the left indicates depth values ranging from -0.2105mm (red) to -0.3108mm (blue). The circular pattern is centered around a diameter of approximately 100mm. The x-axis is labeled from 0mm to 127.1724mm, and the y-axis is labeled from 0 to 104.4361mm.</p>
Sample 10 of 0.15 mm	<p>Micrograph showing the front side of Sample 10. The image displays a circular impact pattern on a light-colored surface. A color scale on the left indicates depth values ranging from -0.1781mm (red) to -0.3731mm (blue). The circular pattern is centered around a diameter of approximately 100mm. The x-axis is labeled from 0mm to 127.1724mm, and the y-axis is labeled from 0 to 104.4832mm.</p>



# APPENDIX H

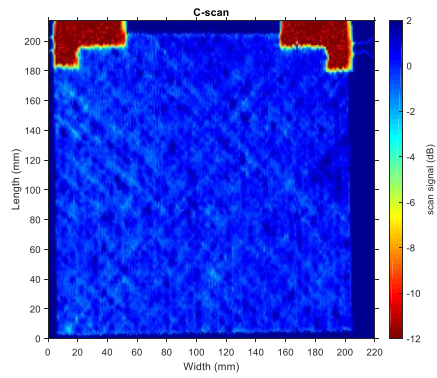
0.65 mm tested with 120 m/s before impact	
Sample 1 of 0.65 mm	
Sample 2 of 0.65 mm	
Sample 3 of 0.65 mm	

0.35 mm tested with 120 m/s before impact	
Sample 1 of 0.35 mm	<p>The C-scan plot for Sample 1 shows a square area with Width (mm) on the x-axis (0 to 220) and Length (mm) on the y-axis (0 to 200). The color scale represents scan signal in dB, ranging from -12 (dark blue) to 2 (dark red). The plot shows a blue field with high signal (red/yellow) at the top corners, indicating a defect or high signal region.</p>
Sample 2 of 0.35 mm	<p>The C-scan plot for Sample 2 shows a square area with Width (mm) on the x-axis (0 to 220) and Length (mm) on the y-axis (0 to 200). The color scale represents scan signal in dB, ranging from -12 (dark blue) to 2 (dark red). The plot shows a blue field with high signal (red/yellow) at the top corners, indicating a defect or high signal region.</p>
Sample 3 of 0.35 mm	<p>The C-scan plot for Sample 3 shows a square area with Width (mm) on the x-axis (0 to 220) and Length (mm) on the y-axis (0 to 200). The color scale represents scan signal in dB, ranging from -12 (dark blue) to 2 (dark red). The plot shows a blue field with high signal (red/yellow) at the top corners, indicating a defect or high signal region.</p>

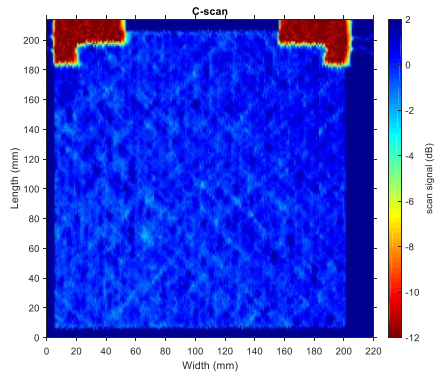
0.15 mm tested with 120 m/s before impact	
Sample 1 of 0.15 mm	<p>C-scan</p> <p>Length (mm)</p> <p>Width (mm)</p> <p>scan signal (dB)</p>
Sample 2 of 0.15 mm	<p>C-scan</p> <p>Length (mm)</p> <p>Width (mm)</p> <p>scan signal (dB)</p>
Sample 3 of 0.15 mm	<p>C-scan</p> <p>Length (mm)</p> <p>Width (mm)</p> <p>scan signal (dB)</p>

0.15 mm tested with 100 m/s before impact

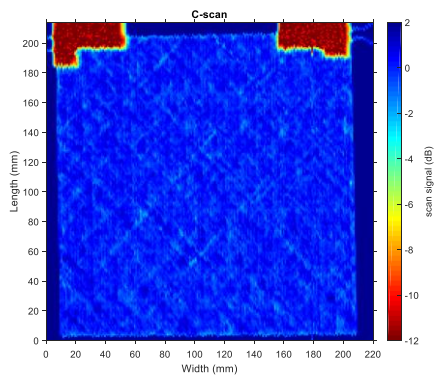
Sample 5 of 0.15 mm



Sample 6 of 0.15 mm



Sample 7 of 0.15 mm

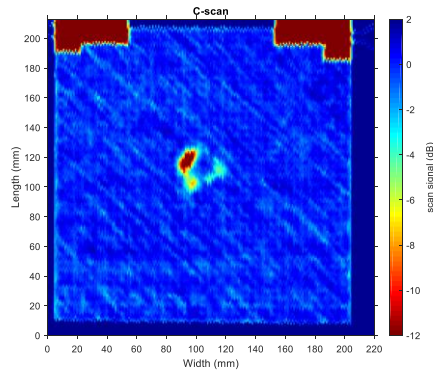


0.15 mm tested with 90 m/s before impact	
Sample 8 of 0.15 mm	<p style="text-align: center;">C-scan</p> <p style="text-align: center;">scan signal (dB)</p> <p style="text-align: center;">Length (mm)</p> <p style="text-align: center;">Width (mm)</p>
Sample 9 of 0.15 mm	<p style="text-align: center;">C-scan</p> <p style="text-align: center;">scan signal (dB)</p> <p style="text-align: center;">Length (mm)</p> <p style="text-align: center;">Width (mm)</p>
Sample 10 of 0.15 mm	<p style="text-align: center;">C-scan</p> <p style="text-align: center;">scan signal (dB)</p> <p style="text-align: center;">Length (mm)</p> <p style="text-align: center;">Width (mm)</p>

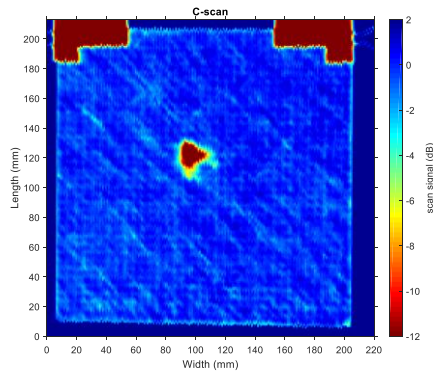
0.65 mm tested with 120 m/s after one impact	
Sample 1 of 0.65 mm	
Sample 2 of 0.65 mm	
Sample 3 of 0.65 mm	

0.35 mm tested with 120 m/s after one impact

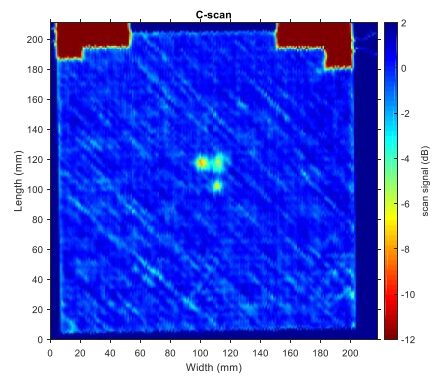
Sample 1 of 0.35 mm



Sample 2 of 0.35 mm



Sample 3 of 0.35 mm



0.15 mm tested with 120 m/s after one impact	
Sample 1 of 0.15 mm	<p>A C-scan plot for Sample 1. The x-axis is labeled 'Width (mm)' and ranges from 0 to 200. The y-axis is labeled 'Length (mm)' and ranges from 0 to 200. A color scale on the right indicates 'scan signal (dB)' from -12 (dark blue) to 2 (dark red). The plot shows a blue field with high signal (red/yellow) at the top corners, indicating damage or high signal intensity.</p>
Sample 2 of 0.15 mm	<p>A C-scan plot for Sample 2. The x-axis is labeled 'Width (mm)' and ranges from 0 to 200. The y-axis is labeled 'Length (mm)' and ranges from 0 to 200. A color scale on the right indicates 'scan signal (dB)' from -12 (dark blue) to 2 (dark red). The plot shows a blue field with high signal (red/yellow) at the top corners, indicating damage or high signal intensity.</p>
Sample 3 of 0.15 mm	<p>A C-scan plot for Sample 3. The x-axis is labeled 'Width (mm)' and ranges from 0 to 200. The y-axis is labeled 'Length (mm)' and ranges from 0 to 200. A color scale on the right indicates 'scan signal (dB)' from -12 (dark blue) to 2 (dark red). The plot shows a blue field with high signal (red/yellow) at the top corners, indicating damage or high signal intensity.</p>

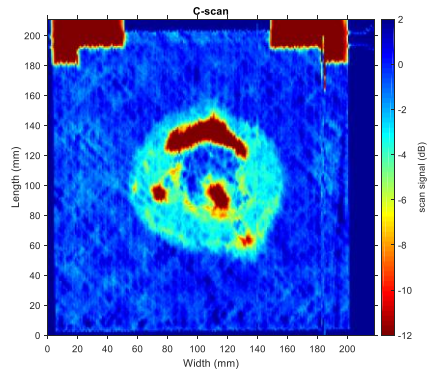


0.15 mm tested with 100 m/s after one impact	
Sample 5 of 0.15 mm	<p>A C-scan plot for Sample 5. The x-axis is labeled 'Width (mm)' and ranges from 0 to 200 with major ticks every 20 units. The y-axis is labeled 'Length (mm)' and ranges from 0 to 200 with major ticks every 20 units. A color scale on the right indicates 'scan signal (dB)' from -12 (dark blue) to 2 (dark red). The plot shows a mostly uniform blue field with some red/orange artifacts at the top corners, indicating higher signal intensity in those regions.</p>
Sample 6 of 0.15 mm	<p>A C-scan plot for Sample 6. The x-axis is labeled 'Width (mm)' and ranges from 0 to 200 with major ticks every 20 units. The y-axis is labeled 'Length (mm)' and ranges from 0 to 200 with major ticks every 20 units. A color scale on the right indicates 'scan signal (dB)' from -12 (dark blue) to 2 (dark red). The plot shows a mostly uniform blue field with some red/orange artifacts at the top corners, indicating higher signal intensity in those regions.</p>
Sample 7 of 0.15 mm	<p>A C-scan plot for Sample 7. The x-axis is labeled 'Width (mm)' and ranges from 0 to 200 with major ticks every 20 units. The y-axis is labeled 'Length (mm)' and ranges from 0 to 200 with major ticks every 20 units. A color scale on the right indicates 'scan signal (dB)' from -12 (dark blue) to 2 (dark red). The plot shows a mostly uniform blue field with some red/orange artifacts at the top corners, indicating higher signal intensity in those regions.</p>

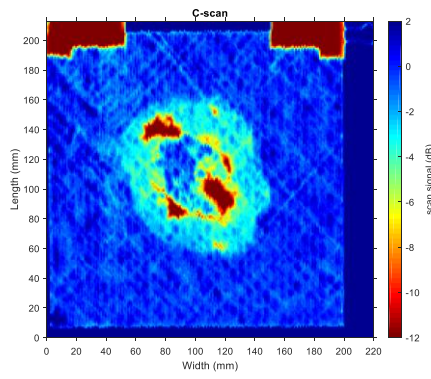
0.15 mm tested with 90 m/s after one impact	
Sample 8 of 0.15 mm	<p style="text-align: center;">C-scan</p> <p style="text-align: center;">scan signal (dB)</p> <p style="text-align: center;">Length (mm)</p> <p style="text-align: center;">Width (mm)</p>
Sample 9 of 0.15 mm	<p style="text-align: center;">C-scan</p> <p style="text-align: center;">scan signal (dB)</p> <p style="text-align: center;">Length (mm)</p> <p style="text-align: center;">Width (mm)</p>
Sample 10 of 0.15 mm	<p style="text-align: center;">C-scan</p> <p style="text-align: center;">scan signal (dB)</p> <p style="text-align: center;">Length (mm)</p> <p style="text-align: center;">Width (mm)</p>

0.65 mm tested with 120 m/s after three impact impacts

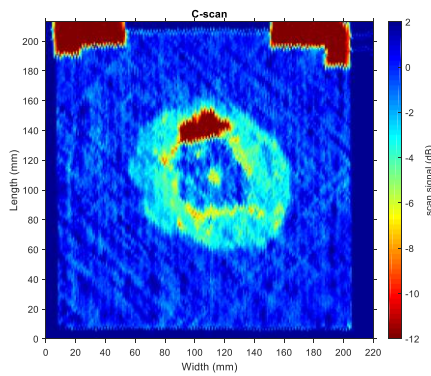
Sample 1 of 0.65 mm



Sample 2 of 0.65 mm

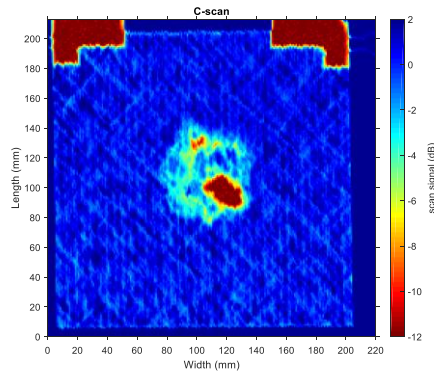


Sample 3 of 0.65 mm

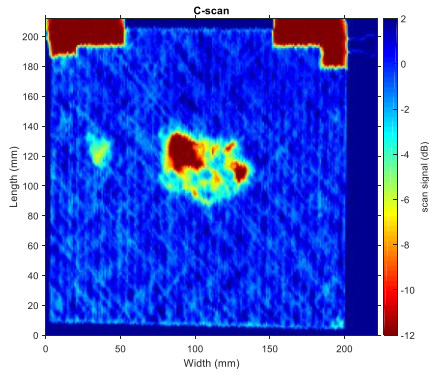


0.35 mm tested with 120 m/s after three impacts

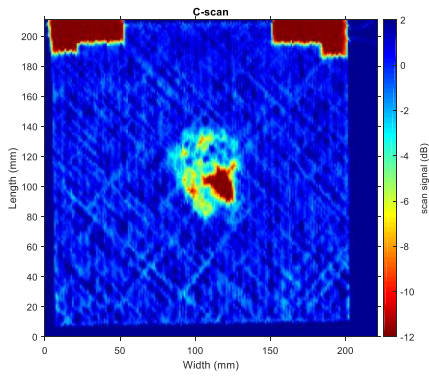
Sample 1 of 0.35 mm



Sample 2 of 0.35 mm

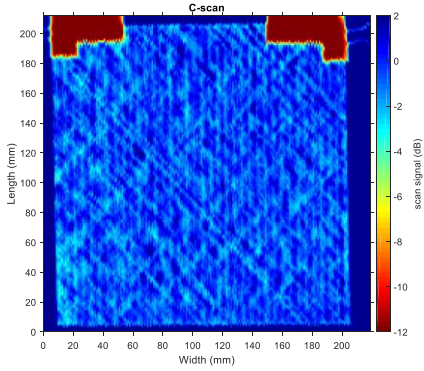
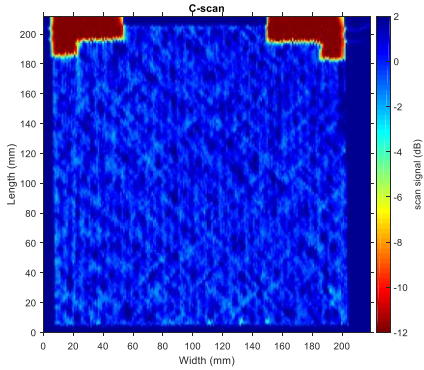
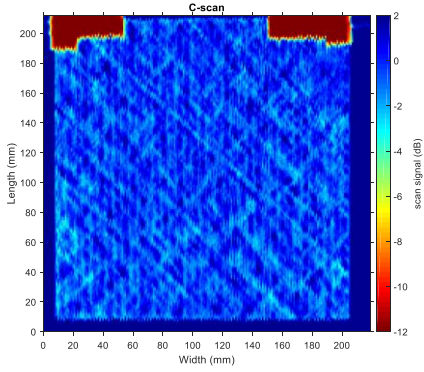


Sample 3 of 0.35 mm



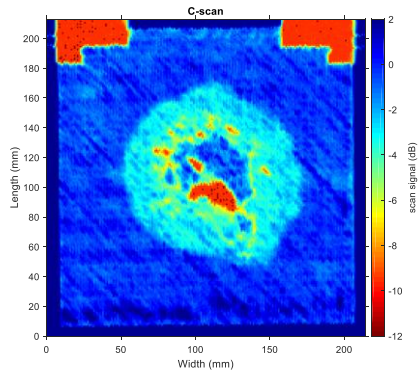
0.15 mm tested with 120 m/s after three impacts	
Sample 1 of 0.15 mm	<p>A C-scan image showing the scan signal (dB) for Sample 1. The x-axis is Width (mm) from 0 to 220, and the y-axis is Length (mm) from 0 to 200. The plot shows a square area with high signal (red/yellow) at the top corners and a noisy blue background. A color scale on the right indicates scan signal (dB) from -12 to 2.</p>
Sample 2 of 0.15 mm	<p>A C-scan image showing the scan signal (dB) for Sample 2. The x-axis is Width (mm) from 0 to 220, and the y-axis is Length (mm) from 0 to 200. The plot shows a square area with high signal (red/yellow) at the top corners and a central high-signal spot (red/yellow) at approximately (120, 100). A color scale on the right indicates scan signal (dB) from -12 to 2.</p>
Sample 3 of 0.15 mm	<p>A C-scan image showing the scan signal (dB) for Sample 3. The x-axis is Width (mm) from 0 to 200, and the y-axis is Length (mm) from 0 to 200. The plot shows a square area with high signal (red/yellow) at the top corners and a central high-signal spot (red/yellow) at approximately (120, 120). A color scale on the right indicates scan signal (dB) from -12 to 2.</p>

0.15 mm tested with 100 m/s after three impacts	
Sample 5 of 0.15 mm	<p style="text-align: center;">C-scan</p> <p style="text-align: center;">scan signal (dB)</p> <p style="text-align: center;">Width (mm)</p> <p style="text-align: center;">Length (mm)</p>
Sample 6 of 0.15 mm	<p style="text-align: center;">C-scan</p> <p style="text-align: center;">scan signal (dB)</p> <p style="text-align: center;">Width (mm)</p> <p style="text-align: center;">Length (mm)</p>
Sample 7 of 0.15 mm	<p style="text-align: center;">C-scan</p> <p style="text-align: center;">scan signal (dB)</p> <p style="text-align: center;">Width (mm)</p> <p style="text-align: center;">Length (mm)</p>

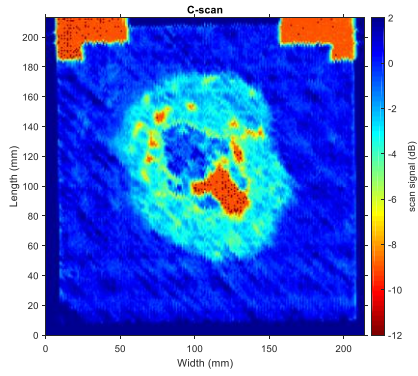
0.15 mm tested with 90 m/s after three impacts	
Sample 8 of 0.15 mm	 <p>C-scan plot for Sample 8. The x-axis is Width (mm) from 0 to 200, and the y-axis is Length (mm) from 0 to 200. The color scale represents scan signal (dB) from -12 to 2. High-signal regions (red/yellow) are visible at the top corners, indicating damage or impact sites.</p>
Sample 9 of 0.15 mm	 <p>C-scan plot for Sample 9. The x-axis is Width (mm) from 0 to 200, and the y-axis is Length (mm) from 0 to 200. The color scale represents scan signal (dB) from -12 to 2. High-signal regions (red/yellow) are visible at the top corners, indicating damage or impact sites.</p>
Sample 10 of 0.15 mm	 <p>C-scan plot for Sample 10. The x-axis is Width (mm) from 0 to 200, and the y-axis is Length (mm) from 0 to 200. The color scale represents scan signal (dB) from -12 to 2. High-signal regions (red/yellow) are visible at the top corners, indicating damage or impact sites.</p>

0.65 mm tested with 120 m/s after five impacts

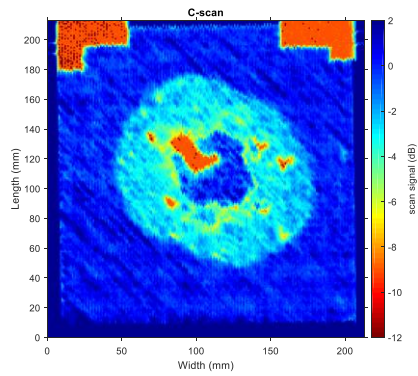
Sample 1 of 0.65 mm



Sample 2 of 0.65 mm



Sample 3 of 0.65 mm





0.35 mm tested with 120 m/s after five impacts	
Sample 1 of 0.35 mm	
Sample 2 of 0.35 mm	
Sample 3 of 0.35 mm	

0.15 mm tested with 120 m/s after five impacts	
Sample 1 of 0.15 mm	<p>C-scan plot for Sample 1. The plot shows a 200 mm by 200 mm area with Length (mm) on the y-axis and Width (mm) on the x-axis. A color scale on the right indicates scan signal intensity in dB, ranging from -12 (dark blue) to 2 (dark red). A small, localized high-signal region (yellow/red) is visible at approximately (100, 100) mm. The top corners of the plot show some orange/red noise.</p>
Sample 2 of 0.15 mm	<p>C-scan plot for Sample 2. The plot shows a 200 mm by 200 mm area with Length (mm) on the y-axis and Width (mm) on the x-axis. A color scale on the right indicates scan signal intensity in dB, ranging from -12 (dark blue) to 2 (dark red). A larger, more irregular high-signal region (yellow/red) is visible at approximately (100, 100) mm compared to Sample 1. The top corners of the plot show some orange/red noise.</p>
Sample 3 of 0.15 mm	<p>C-scan plot for Sample 3. The plot shows a 200 mm by 200 mm area with Length (mm) on the y-axis and Width (mm) on the x-axis. A color scale on the right indicates scan signal intensity in dB, ranging from -12 (dark blue) to 2 (dark red). A high-signal region (yellow/red) is visible at approximately (100, 100) mm, which is elongated and oriented diagonally. The top corners of the plot show some orange/red noise.</p>

0.15 mm tested with 100 m/s after five impacts	
Sample 5 of 0.15 mm	<p style="text-align: center;">C-scan</p> <p style="text-align: center;">Length (mm)</p> <p style="text-align: center;">Width (mm)</p> <p style="text-align: right;">scan signal (dB)</p>
Sample 6 of 0.15 mm	<p style="text-align: center;">C-scan</p> <p style="text-align: center;">Length (mm)</p> <p style="text-align: center;">Width (mm)</p> <p style="text-align: right;">scan signal (dB)</p>
Sample 7 of 0.15 mm	<p style="text-align: center;">C-scan</p> <p style="text-align: center;">Length (mm)</p> <p style="text-align: center;">Width (mm)</p> <p style="text-align: right;">scan signal (dB)</p>

0.15 mm tested with 90 m/s after five impacts	
Sample 8 of 0.15 mm	<p>C-scan plot for Sample 8. The x-axis is Width (mm) from 0 to 200, and the y-axis is Length (mm) from 0 to 200. The color scale represents scan signal (dB) from -12 to 2. High signal areas (orange/red) are visible at the top corners of the sample.</p>
Sample 9 of 0.15 mm	<p>C-scan plot for Sample 9. The x-axis is Width (mm) from 0 to 200, and the y-axis is Length (mm) from 0 to 200. The color scale represents scan signal (dB) from -12 to 2. High signal areas (orange/red) are visible at the top corners of the sample.</p>
Sample 10 of 0.15 mm	<p>C-scan plot for Sample 10. The x-axis is Width (mm) from 0 to 200, and the y-axis is Length (mm) from 0 to 200. The color scale represents scan signal (dB) from -12 to 2. High signal areas (orange/red) are visible at the top corners of the sample.</p>

## APPENDIX I

Velocity	Samples	Delamination area after one impact	Delamination area after three impacts	Delamination area after five impacts
120 m/s	Sample 1 of 0.65 mm	78.3 mm <sup>2</sup>	253.83 mm <sup>2</sup>	597.90 mm <sup>2</sup>
	Sample 2 of 0.65mm	95.06 mm <sup>2</sup>	491.60 mm <sup>2</sup>	835.60 mm <sup>2</sup>
	Sample 3 of 0.65 mm	6.43 mm <sup>2</sup>	12.24 mm <sup>2</sup>	528.02 mm <sup>2</sup>
	Sample 1 of 0.35 mm	52.14 mm <sup>2</sup>	498.96 mm <sup>2</sup>	841.61 mm <sup>2</sup>
	Sample 2 of 0.35 mm	349.03 mm <sup>2</sup>	667.93 mm <sup>2</sup>	1008.98 mm <sup>2</sup>
	Sample 3 of 0.35 mm	54.03 mm <sup>2</sup>	434.10 mm <sup>2</sup>	807.63 mm <sup>2</sup>
	Sample 1 of 0.15 mm	0 mm <sup>2</sup>	0 mm <sup>2</sup>	66.76 mm <sup>2</sup>
	Sample 2 of 0.15 mm	0 mm <sup>2</sup>	291.09 mm <sup>2</sup>	315.16 mm <sup>2</sup>
	Sample 3 of 0.15 mm	0 mm <sup>2</sup>	321.52 mm <sup>2</sup>	339.65 mm <sup>2</sup>
100 m/s	Sample 5 of 0.15 mm	0 mm <sup>2</sup>	0 mm <sup>2</sup>	0 mm <sup>2</sup>
	Sample 6 of 0.15 mm	0 mm <sup>2</sup>	0 mm <sup>2</sup>	0 mm <sup>2</sup>
	Sample 7 of 0.15 mm	0 mm <sup>2</sup>	0 mm <sup>2</sup>	0 mm <sup>2</sup>
90 m/s	Sample 8 of 0.15 mm	0 mm <sup>2</sup>	0 mm <sup>2</sup>	0 mm <sup>2</sup>
	Sample 9 of 0.15 mm	0 mm <sup>2</sup>	0 mm <sup>2</sup>	0 mm <sup>2</sup>
	Sample 10 of 0.15 mm	0 mm <sup>2</sup>	0 mm <sup>2</sup>	0 mm <sup>2</sup>

